

Dissertation zur Erlangung des Doktorgrades
der Fakultät für Chemie und Pharmazie
der Ludwig-Maximilians-Universität München

**Investigating the
causes and consequences of
altered subcellular spatial composition
in the immune system and beyond**

Niklas Arndt Schmacke

aus

Bonn

2023

Erklärung

Diese Dissertation wurde im Sinne von § 7 der Promotionsordnung vom 28. November 2011 von Herrn Prof. Dr. med. Veit Hornung betreut.

Eidesstattliche Versicherung

Diese Dissertation wurde eigenständig und ohne unerlaubte Hilfe erarbeitet.

Niklas Arndt Schmacke, München, 28.08.2023

Dissertation eingereicht am	31. August 2023
Erster Gutachter	Prof. Dr. med. Veit Hornung
Zweiter Gutachter	Prof. Dr. rer. nat. Lucas Jae
Mündliche Prüfung am	21. September 2023

Für

Karin & Martin

Die Vorbilder sind

Gundula

Die die Grundlage geschaffen hat

Sophia

Ohne die es nicht gegangen wäre

Contents

1	Introduction	1
1.1	The innate immune system	1
1.1.1	Sensing non-self	2
	Toll-like receptors	2
	RIG-I-like receptors	5
	NOD-like receptors	6
	cGAS-STING	7
	AIM2-like receptors	8
1.1.2	Relaying signals and eliminating threats	8
1.1.3	Emerging non-self sensing paradigms in innate immunity	10
1.1.4	Limitations of innate immune systems	11
1.2	The adaptive immune system	11
1.3	Evolution of immune systems	14
1.4	Cell death as the <i>ultima ratio</i> in host defense	14
1.4.1	Apoptosis	15
1.4.2	Necroptosis	16
1.4.3	Pyroptosis	17
1.4.4	Inflammasomes	19
	The NLRP3 inflammasome	20
1.5	Molecular genetics	22
1.5.1	The CRISPR era of genome editing	23
1.5.2	Genetic screening	25
2	Summary	28
2.1	NLRP3 priming by translocation	28
2.2	CRISPR screening for subcellular spatial phenotypes at genome scale	29

3 Publications	30
3.1 IKK β primes inflammasome formation by recruiting NLRP3 to the trans-Golgi network	30
3.2 SPARCS, a platform for genome-scale CRISPR screening for spatial cellular phenotypes	65
Acknowledgements	108
Bibliography	109

1 Introduction

Protecting their integrity is a core concern of all living things. In addition to physical damage, starvation and competition by rivals, among other dangers, most organisms are constantly threatened by pathogenic entities. To protect themselves, life forms ranging from single cell organisms such as bacteria to complex vertebrates have evolved diverse defense systems granting them immunity from pathogens through various mechanisms. These defenses, collectively termed an organism's "immune system" can take many forms: They can be located inside cells or on their membranes, or they can be secreted as a response to extracellular immunogens and work entirely independently of cells. They can be based on proteins, lipids, nucleic acids or small molecule second messengers (Takeuchi and Akira [2010](#); J. Chen and Z. J. Chen [2018](#); Shimizu [2009](#); Sorek et al. [2008](#); Zaver and Woodward [2020](#); Boehm and Swann [2014](#)). Nonetheless, at their root, all these systems share a common ability: They can distinguish between self and non-self structures (C. A. J. Janeway [1989](#)). A broad categorization of immune systems differentiates between two branches that work closely together in more complex organisms: innate and adaptive immunity.

1.1 The innate immune system

Many species protect themselves with passive barrier organs such as skin that generally keep most pathogens at bay (Murphy et al. [2012](#)). Internal threats and pathogens that have successfully crossed these barriers next face what is typically considered a host's first line of active defense: the innate immune system (C. A. J. Janeway [1989](#)). The primary tasks of this system are to sense the presence of non-self or altered-self-derived signatures and to then mount a tailored response to clear the corresponding threat. For both of these tasks innate immune systems have various tools at their disposal that in more complex multicellular organisms are often distributed across multiple cell types. Cells of the innate immune system can be found in almost all human

tissues, often developing an intricate relationship with a given tissue and contributing to its maintenance in the absence of pathogens (Meizlish et al. [2021](#); Kane and Lynch [2019](#)).

1.1.1 Sensing non-self

Diverse non-self derived motifs including lipids, nucleic acids and proteins are detected by a readily available repertoire of germline-encoded proteins called pattern recognition receptors (PRRs) (Medzhitov and C. A. Janeway [2002](#); Takeuchi and Akira [2010](#)). These sensors are expressed in specialized sentinel cells of the immune system and in some regular tissue cells. The specificity of PRRs is hard-coded into their amino acid sequence and has been evolutionarily selected to detect invariant microbe-associated molecular patterns (MAMPs, also referred to as pathogen-associated molecular patterns (PAMPs) (C. A. J. Janeway [1989](#); Koropatnick et al. [2004](#))) or host danger signals. They often surveil a “niche”, a spatially defined cellular or extracellular compartment. PRRs can be grouped into several families by their structural similarity and mechanism of action (Takeuchi and Akira [2010](#)).

Toll-like receptors

The transmembrane Toll-like receptor (TLR) proteins monitor the extracellular space from the plasma membrane and, following endocytosis of extracellular material, the membranes of the endolysosomal system (Medzhitov, Preston-Hurlburt, et al. [1997](#); Fitzgerald and Kagan [2020](#)). They are expressed on cells of the innate immune system such as macrophages and dendritic cells but also on non-professional immune cells such as fibroblasts and epithelial cells. All TLRs share a structure of extracellular leucine rich repeats (LRRs) that bind their respective ligands, a transmembrane domain, and an intracellular Toll-interleukin-1 receptor (TIR) domain to relay their activation status. Ten different TLRs have been identified in humans and twelve in mice. The *TLR10* gene is a non-coding type of genetic locus called a pseudogene in mice. Humans in contrast do not have coding genes for TLRs 11-13. TLRs 1, 2, 4, 5, 6 and 10 are localized on the plasma membrane while TLRs 3, 7, 8, 9, 11, 12 and 13 reside on the endosomal membrane. TLR4 can be localized on both the plasma membrane and the endosomal membrane. Upon ligand binding, TLRs form homo-, and, in case of some TLRs, heterodimers. The endosomal TLRs 3, 7, 8, 9 and 13 are activated by nucleic acids; a list of TLRs and their respective ligands is provided in table [1.1](#).

Table 1.1 | Human and mouse Toll-like receptors and their ligands. TLRs are membrane-bound pattern recognition receptors that dimerize upon ligand binding. Instead of homodimers, TLRs 1, 2 and 6 form the indicated heterodimers when they recognize their ligand. TLRs 11-13 are expressed in mice but not humans. *TLR10* is a pseudogene in mice.

TLR	Ligand	References
TLR1:TLR2	triacyl-lipopeptides	Takeuchi, Sato, et al. 2002 Takeuchi, Hoshino, et al. 1999
TLR2:TLR6	diacyl-lipopeptides	Takeuchi, Kawai, et al. 2001 Takeuchi, Hoshino, et al. 1999
TLR3	dsRNA	Alexopoulou et al. 2001
TLR4	Lipopolysaccharide (LPS)	Poltorak et al. 1998
TLR5	Flagellin	Hayashi et al. 2001 Gewirtz et al. 2001
TLR7	ssRNA	Diebold et al. 2004 Hemmi, Kaisho, et al. 2002 Heil et al. 2004
TLR8	ssRNA	Heil et al. 2004 Greulich et al. 2019
TLR9	CpG DNA	Hemmi, Takeuchi, et al. 2000
TLR10	inhibits TLR2?	Oosting et al. 2014
TLR11	Profilin	Yarovinsky et al. 2005
TLR12	Profilin	Koblansky et al. 2013 Andrade et al. 2013
TLR13	13nt sequence from ribosomal ssRNA	Oldenburg et al. 2012 X.-D. Li and Z. J. Chen 2012 Hidmark et al. 2012

The endosomal TLRs are regulated to be activated at their destination directly or indirectly by the trafficking adaptor UNC93B1 (Kim et al. [2008](#); B. L. Lee et al. [2013](#); Pelka et al. [2018](#); Majer, B. Liu, Woo, et al. [2019](#); Majer, B. Liu, Kreuk, et al. [2019](#); Tabeta et al. [2006](#)).

TLRs signal recognition of their respective ligands to downstream pathways in the cytosol via two adaptor proteins that bind to their cytosolic TIR domain: TIR-domain-containing adapter-inducing interferon- β (TRIF, also known as TIR domain containing adaptor molecule 1 (TICAM1)), for TLR3 and TLR4, and Myeloid differentiation primary response 88 (MyD88) for all other TLRs (Fitzgerald and Kagan [2020](#); O'Neill and Bowie [2007](#)). TLR4 can use both adaptors depending on its localization on the plasma membrane (MyD88) or the endosome (TRIF). Downstream of TRIF or MyD88, a network of signalling cascades amplifies the signal generated by TLR dimerisation,

1 Introduction

integrates inputs from various cellular sensors, and ultimately connects activation of TLRs to the activation of transcriptional programs. After the formation of a MyD88 assembly known as the myddosome and subsequent activation of Interleukin-1 receptor associated kinases (IRAKs) (Motshwene et al. [2009](#); S.-C. Lin et al. [2010](#)), the E3 ubiquitin ligase Tumor necrosis factor receptor (TNFR)-associated factor 6 (TRAF6) is recruited (Z. Cao et al. [1996](#)). TRAF6 facilitates recruitment of TAB1 and -2 to K63-linked polyubiquitin chains, which leads to activation of Transforming growth factor β -activated kinase 1 (TAK1) (C. Wang et al. [2001](#)), followed by Inhibitor of nuclear factor κ B kinase (IKK) α and IKK β , and ultimately to I κ B degradation and activation of the dimeric transcription factor Nuclear factor ' κ -light-chain-enhancer' of activated B-cells (NF- κ B), which initiates a pro-inflammatory transcriptional program (Israël [2010](#)). Depending on the cell type it is activated in, this program can include the production of paracrine mediators such as IL-6, cell surface proteins that signal to interacting cells, or lead to remodelling of the cytoskeleton for example to enable cell migration (Fitzgerald and Kagan [2020](#)). TAK1 also promotes mitogen-activated protein kinase (MAPK)-driven activation of the activator protein 1 (AP-1) transcription factor complex consisting of c-Fos and c-Jun, which in concert with NF- κ B facilitates the transcription of pro-inflammatory and chemotactic genes (Murphy et al. [2012](#)). TRAF6 additionally activates Tank binding kinase 1 (TBK1) and its homologue IKK ϵ . Via the kinase Akt they trigger rapid metabolic reprogramming towards an increase in glycolysis that is initially accompanied by an increase in tricarboxylic acid (TCA) cycle activity (O'Neill, Kishton, et al. [2016](#); Everts et al. [2014](#); Krawczyk et al. [2010](#)). At later stages promoted by the transcription factor hypoxia-inducible factor 1- α (Hif-1 α), immune cells can shift away from TCA cycle activity and instead generate ATP via aerobic glycolysis, a transition known as Warburg effect that was first discovered in highly proliferating cancer cells (Everts et al. [2014](#); Warburg et al. [1924](#)). The purpose of this metabolic switch in immune cells is unclear, but blocking the initial metabolic shift towards glycolysis in dendritic cells was shown to dampen inflammatory reactions (Everts et al. [2014](#); Krawczyk et al. [2010](#)). Current hypotheses state that the inefficient but rapid generation of ATP and the preservation of carbohydrates as building blocks for cellular materials are priorities for freshly activated immune cells that produce large quantities of effector molecules or proliferate quickly (O'Neill, Kishton, et al. [2016](#)).

The adaptor protein TRIF recruits TRAF3 to activate TBK1. TRIF harbours a pLxIS amino acid motif (S. Liu et al. [2015](#)) which, after phosphorylation by TBK1, can bind the transcription factors interferon regulatory factor 3 (IRF3) or IRF7. De-

pending on the cell type and activation circumstances the respective IRFs are then also phosphorylated by TBK1, homodimerize and translocate to the nucleus to initiate a type-I-interferon-driven antiviral transcriptional program (Fitzgerald and Kagan [2020](#)).

For the nucleic-acid sensing and therefore mostly antiviral endosomal TLRs 7-9 it has recently been shown that the pLxIS motif-containing adaptor protein TASL enables type-I interferon production downstream of MyD88 engagement (Heinz et al. [2020](#)). The kinase that phosphorylates this pLxIS motif has remained elusive.

RIG-I-like receptors

Retinoic acid-inducible gene I (RIG-I)-like receptors (RLRs) are cytosolic proteins with a helicase domain that detect the presence of non-self RNAs (Rehwinkel and Gack [2020](#)). As such, these proteins are important for the detection of many viral infections (Kato et al. [2006](#)). The RLR family consists of three members: RIG-I, melanoma differentiation-associated protein 5 (MDA5) and Laboratory of Genetics and Physiology 2 (LGP2) (Rehwinkel and Gack [2020](#)). Both RIG-I and MDA5 have an N-terminal CARD domain that mediates signalling to the mitochondrial outer membrane protein mitochondrial antiviral-signalling protein (MAVS, also known as IPS-1). MAVS, in turn, serves as an activation platform for the kinase TBK1, and ultimately, the transcription factors IRF3 and -7 as well as NF- κ B (S. Liu et al. [2015](#); Seth et al. [2005](#)). Since host RNA is abundant in the cytosol, RLRs have to sense particular pathogen-associated motifs on RNA to avoid aberrant activation. RIG-I senses a triphosphate moiety on an RNA's 5' end that on host messenger RNAs (mRNAs) is replaced by a 7-methylguanylate cap during splicing, but can be missing on unspliced virus-derived RNAs (Hornung, Ellegast, et al. [2006](#); Cui et al. [2008](#)). MDA5 senses long dsRNA in the cytosol, a hallmark of many viral infections that is produced either as a transcription intermediate or during replication of the viral genome (Berke and Modis [2012](#); B. Wu et al. [2013](#)). LGP2 is thought to play a regulatory role in RLR-mediated immune defense (Rodriguez et al. [2014](#); Rothenfusser et al. [2005](#)). Of note, the generation of double stranded host RNAs is actively prevented by enzymes called adenosine deaminase acting on RNA (ADAR) (Liddicoat et al. [2015](#); Rice et al. [2012](#)). These enzymes deaminate adenosine, generating inosine, thereby weakening the Watson-Crick base pairing between adenosine and uridine, destabilizing dsRNA.

Table 1.2 | Classification of human NLR proteins by their N-terminal domain.

NLR family	N-terminal domain homology	Examples
A	Acidic transactivator domain	CIITA
B	Baculovirus inhibitor repeats (BIR)	NAIP
C	Caspase activation and recruitment domain (CARD)	NOD1, NOD2, NLRC4
P	Pyrin domain (PYD)	NLRP1, NLRP3
X	None	NLRX1

NOD-like receptors

The Nucleotide-binding and oligomerization domain-like receptors with LRRs (Nod-like receptors, NLRs) are a group of cytosolic immune sensors named after their shared core nucleotide binding and oligomerization (NOD or NACHT) domain (Inohara and Nuñez [2003](#)). By their N-terminal domain, NLRs can be divided into five groups as shown in table [1.2](#).

NLRs are commonly activated by self-oligomerization upon ligand binding. Notable exceptions include CIITA (C2TA), a transcriptional transactivator controlling major histocompatibility complex (MHC) II gene expression (Harton et al. [1999](#); Steimle et al. [1993](#)) and NAIP, which does not have an LRR domain and after ligand engagement nucleates the oligomerization of NLRC4 (L. Zhang et al. [2015](#); Vance [2015](#); Roy et al. [1995](#)). NLRX1 localizes to mitochondria and was initially proposed to negatively regulate MAVS activation (C. B. Moore et al. [2008](#)). However, conflicting reports have since cast doubt on these conclusions and the function of NLRX1 remains unclear (Rebsamen et al. [2011](#); Wright et al. [2003](#); Diez et al. [2003](#)). Examples of sensor NLRs include NOD1 and NOD2 that sense peptidoglycans, the main component of gram-positive bacteria's cell walls (Caruso et al. [2014](#)). After oligomerization these receptors recruit the kinase Receptor-interacting serine/threonine-protein kinase 2 (RIPK2) via their CARD domains to activate NF- κ B. Several NLRs such as NLRP1, NLRP3 and NLRP10 as well as NLRC4 are known to form large protein complexes called inflammasomes that trigger lytic cell death in response to sensing MAMPs (Broz and V. M. Dixit [2016](#)).

cGAS-STING

Double-stranded DNA (dsDNA) occurring in the cytosol, a hallmark of several virus infections, is sensed by the cyclic GMP-AMP synthase (cGAS)-Stimulator of interferon genes (STING) pathway (Hopfner and Hornung [2020](#); Decout et al. [2021](#)). cGAS, upon binding dsDNA, synthesizes the second messenger cyclic Gp(2'-5')Ap(3'-5') (cGAMP), which in turn is sensed by the endoplasmic reticulum (ER)-resident protein stimulator of interferon genes (STING)(Gao et al. [2013](#); Sun et al. [2013](#); J. Wu et al. [2013](#); Ablasser et al. [2013](#)). Of note, STING can also sense other cyclic dinucleotides, for example of bacterial origin, where these molecules frequently act as second messengers (Burdette et al. [2011](#)). After activation, STING travels from the ER to the ER-Golgi-intermediate compartment (ERGIC) and the Golgi apparatus before its degradation in the lysosome, an acidic compartment for the degradation of extra- and intracellular material (de Duve et al. [1955](#)). At the ERGIC, STING interacts with TBK1 and via its pLxIS motif serves as a platform for the activation of IRF3, leading to a type-I-interferon response (S. Liu et al. [2015](#)). cGAS-like enzymes have also been discovered to synthesize cyclic di- and trinucleotides as second messengers in prokaryotes, and have recently been proposed as a new family of PRRs, the cGLRs (Slavik and Kranzusch [2023](#); Y. Li et al. [2023](#)). Given that DNA is not itself a MAMP, but is immunogenic only upon of its aberrant localization in the cytoplasm rather than the nucleus, its sensing need to be tightly regulated. Three prime repair exonuclease 1 (TREX1), a cytosolic DNA exonuclease, prevents accumulation of DNA in the cytosol (Stetson et al. [2008](#)). Its importance as a regulator is underscored by the fact that loss-of-function mutations in TREX1 can cause Aicardi-Goutières syndrome, a severe condition signified by constitutive type-I-interferon signalling caused by excessive activation of the innate immune system (Crow et al. [2006](#)). Similar findings have been made for other nucleases such as DNase II (Ahn et al. [2012](#)). In addition, cGAS binds to histones, structural DNA-binding proteins, with very high affinity, inhibiting its cGAMP synthesizing ability. This prevents cGAS from being engaged by the host's own DNA during cell division when the nuclear envelope breaks down (D. Cao et al. [2020](#); Kujirai et al. [2020](#); Pathare et al. [2020](#); B. Zhao et al. [2020](#); Uggenti et al. [2020](#); Michalski et al. [2020](#); Boyer et al. [2020](#)).

AIM2-like receptors

The absent in melanoma 2 (AIM2)-like receptors (ALRs), also called PYHIN proteins, are encoded in the diverse mammalian-specific ALR genetic locus (Lugrin and Martinon [2018](#)). The proteins encoded by this locus share a pyrin and a DNA-binding hematopoietic expression, interferon-inducible nature, and nuclear localization (HIN) domain, but only one orthologue, the ALR name giver AIM2, is present in multiple species. AIM2 is known for forming an inflammasome in response to DNA in mouse- and some human cells (Fernandes-Alnemri et al. [2009](#); Hornung, Ablasser, et al. [2009](#); Bürckstümmer et al. [2009](#)). Of note, a DNA inflammasome in human monocytes is formed by NLRP3 activation downstream of STING, independently of AIM2 (Gaidt, Ebert, Chauhan, Ramshorn, et al. [2017](#)). The human protein IFI16 and its mouse orthologue p204 have been proposed to form a nuclear inflammasome in response to several viruses, but evidence of caspase-1 activation by direct interaction has not been found (Doitsh et al. [2014](#); Monroe et al. [2014](#)).

1.1.2 Relaying signals and eliminating threats

After the engagement of its sensors, the immune system seeks to clear a threat or contain it until it can be cleared by other mechanisms. To this end, cells engage specific transcriptional programs that lead to the production of immune effectors, which can directly attack a pathogen or set off and sustain an immune reaction. For more serious cases, this often involves an immune reaction that is tailored to a given insult such as an inflammatory reaction or antiviral immunity. Inflammatory reactions are classically characterized by four symptoms: pain, redness, heat, and swelling of the affected region (Murphy et al. [2012](#)). Systemic reactions can involve fever. These symptoms are induced by specific mediators that are created or released upon activation of innate immunity. One class of such mediators are small soluble proteins that cause reactions in bystander cells, also known as cytokines. The cytokine tumour necrosis factor (TNF) was originally discovered to induce cell death in a cancer cell line (Carswell et al. [1975](#); W. P. Kolb and Granger [1968](#); Ruddle and Waksman [1968](#)). In addition to promoting cell death via the TNFR adaptor FAS-associated death domain protein (FADD) and formation of a cytosolic protein complex called “complex II”, TNF can potentiate inflammatory reactions by activating the transcription factor NF- κ B via interaction of the adaptor protein TNF receptor type 1-associated DEATH

domain protein (TRADD) with TRAF2, leading to the formation of the membrane-associated “complex I” (Micheau and Tschopp [2003](#); Hsu et al. [1996](#)). NF- κ B in turn leads to production of more TNF among other pro-inflammatory cytokines such as IL-6 and pro-IL-1 β . TNF also induces local redness, heat, and swelling by promoting vasodilation, increasing blood flow and causing fluid efflux from blood vessels into the surrounding tissue (Murphy et al. [2012](#)). This in turn leads to infiltration of immune cells into affected tissues, most abundantly a short-lived type of white blood cell (leukocyte) called neutrophil granulocyte. In addition to cytokines, lipid mediators generated by enzymes called cyclooxygenases (COX) can cause pain and other symptoms of inflammation (Baral et al. [2019](#)).

Type-I-interferon-driven immune reactions, named for their ability to interfere with viruses, in contrast to inflammatory reactions are primarily directed against viruses (McNab et al. [2015](#)). The major type-I-interferons (IFNs) α and β are soluble protein mediators that signal the presence of viral pathogens to neighbouring cells. On these bystander cells they engage the interferon- α/β receptor (IFNAR). Similar to other cytokine receptors, IFNAR dimerizes upon ligand binding and signals through Janus kinases (JAKs), which phosphorylate signal transducer and activator of transcription (STAT) proteins that dimerize and translocate to the nucleus to drive the expression of a large number of interferon stimulated genes (ISGs) (Platanias [2005](#); Schoggins et al. [2011](#)). In complex with the transcription factor IRF9, STAT1 and STAT2 form the IFN-stimulated gene (ISG) factor 3 (ISGF3) transcription factor complex that binds to a separate DNA motif termed IFN-stimulated response element (ISRE) and switches on a different set of ISGs. Notable ISGs include Viperin, an enzyme that produces an inhibitor of viral RNA polymerases (Gizzi et al. [2018](#)), and APOBEC3G, an ssDNA cytosine deaminase that is packaged into HIV-1 virions and restricts HIV-1 integration and replication (Sheehy et al. [2002](#)).

Specific effector mechanisms used by the innate immune system include the uptake (phagocytosis) and degradation of detected non-self structures in the lysosomal compartment of specialized cells called macrophages by their discoverer Elie Metchnikoff in 1882 (Gordon [2008](#)). These cells are also strong initiators of immune reactions upon non-self sensing (Takeuchi and Akira [2010](#)). Another potent mechanism that curbs the spread of pathogens is programmed cell death, in which cells compromise their own integrity to limit the replicative niche that is available to intracellular pathogens. The complement system, a protease and protein complex formation cascade that consists of proteins in the blood, becomes activated on non-self surfaces to induce inflammation, phagocytosis and membrane pores in its target (Ricklin et al. [2010](#)). Weakening

membrane integrity is also a frequent mechanism of action of antimicrobial peptides such as dermcidin or defensins (Ganz [2003](#)).

1.1.3 Emerging non-self sensing paradigms in innate immunity

In addition to pattern-triggered immunity (PTI), an alternative non-self sensing paradigm called effector-triggered immunity (ETI) has been proposed to underlie innate immunity (Remick et al. [2023](#)). Instead of sensing specific non-self structures such as MAMPs, effector-triggered immunity employs receptors that sense the action of a pathogen effector, often indirectly through the perturbation of a critical host process or structure. This so-called “guard immunity” describes the activation of immune pathways (the “guards”) upon the disruption of critical host processes (the “gardees”) (Vance [2010](#)). Originally discovered to be widespread in plants, examples of guard immunity have also been discovered in the human immune system (Dangl and Jones [2001](#); Remick et al. [2023](#)): The PRR Pyrin senses the perturbation of the GTPase RhoA (Xu et al. [2014](#)), and thereby the ability of host cells to remodel their cytoskeleton, by monitoring its downstream targets PKN1/2 (Park et al. [2016](#)). Upon loss of an inhibitory phosphorylation on Pyrin normally placed by these kinases, Pyrin is activated and initiates an immune response. The antiviral human protein MORC3, in addition to its direct antiviral activity, has recently been shown to act as a transcriptional repressor of the genetic IFNB1 locus that encodes the antiviral type-I interferon gene interferon- β (Gaidt, Morrow, et al. [2021](#)). When the HSV-1 effector ICP0 initiates MORC3 degradation by ubiquitination, it unleashes the derepression of an antiviral type-I-interferon response instead. By encoding two constitutively active functions with opposing roles, MORC3 guards its own antiviral effect, a paradigm named self-guarding (Remick et al. [2023](#)).

Another sensing paradigm that is more similar to PAMP or MAMP sensing is the sensing of danger-associated molecular patterns (DAMPs) and alarmins. In contrast to PAMPs and MAMPs, DAMPs and alarmins are host molecules that elicit an immune reaction upon detection by immune cells. While alarmins such as the IL-1 family members IL-1 α and IL-33 are direct activators of immune responses, DAMPs are host molecules with different functions that can also engage immune sensors, for example when they are mislocalized (Bertheloot and Latz [2017](#); Matzinger [1994](#)). Examples of DAMPs are ATP or uric acid crystals that activate NLRP3, or host DNA that can activate cGAS or AIM2.

1.1.4 Limitations of innate immune systems

Despite its ability to detect non-self structures and its power to clear out most pathogens before they establish an infection, our innate immune system has a few inadequacies that make it insufficient to defend our bodies from the breadth of pathogens we are exposed to on its own: First and foremost, the innate immune system can only deal with pathogens it has evolved to detect. While ETI expands the range of pathogens the innate immune system can respond to without the need for specific recognition, many pathogens have likewise evolved measures to avoid or delay detection or clearance, instigating an evolutionary arms race with their hosts (Tenthorey et al. [2022](#)). Second, innate immune systems have a limited capacity to remember and deal more effectively with future encounters of the same pathogen, especially across longer timescales (Netea et al. [2020](#)). These gaps are filled by the other branch of our immune system: the adaptive immune system.

1.2 The adaptive immune system

To effectively deal with pathogens that cannot be cleared by the passive and active mechanisms employed by our innate immune system, our adaptive immune system has evolved the ability to generate effector cells and -molecules that are specifically tailored to a given pathogen or non-self threat (Flajnik [2018](#)). In contrast to the innate immune system, the machinery behind adaptive immunity requires macroscopic tissue structures and organ systems and takes several days to mount an immune reaction. Underlying adaptive immunity is the ability of many cells to present fragments derived from degraded pathogen or non-self proteins on their surface, thereby signalling the presence of pathogens or non-self structures to neighbouring cells (Neefjes et al. [2011](#)). Depending on their source, antigens are presented on either of two proteins contained in the major histocompatibility complex (MHC) gene locus: MHC-I presents antigens from the cytosol, whereas MHC-II presents antigens from endo- and lysosomes that were taken up by cells through phagocytosis. The activation of adaptive immunity is triggered by non-self sensing of the innate immune system; paramount to this link is a cell type called “dendritic cell” (DC), named after its stellate morphology, that was originally discovered by visual inspection of mouse spleens under the microscope (Steinman and Cohn [1973](#); Cabeza-Cabrerizo et al. [2021](#)). In peripheral tissues, these cells take up extracellular content, surveilling it for the presence of MAMPs and other

non-self signatures. Upon activation of the extensive range of PRRs they express, DCs are triggered to migrate to the nearest lymphatic tissue to present antigens to T-lymphocytes circulating through lymphatic tissues (Cabeza-Cabrerizo et al. 2021). These T-lymphocytes originate from stem cells in the bone marrow and mature in the thymus – hence the name T-cell. Through semi-random recombination of their genetic material, a process known as V(D)J recombination named after the three variable genetic fragments that are combined into one gene, each T-cell expresses a unique surface receptor that can sense a peptide antigen presented on MHC-I or -II (Schatz and Ji 2011). During their maturation in the thymus, T-cells are selected to bind weakly to MHC-self antigen complexes, ensuring that a given T-cell receptor can both bind MHC (positive selection), but also isn't strongly self-reactive (negative selection) (Murphy et al. 2012). This procedure gives rise to a clonal repertoire of T-cells that is little self-reactive, preventing autoimmunity by a mechanism known as central tolerance, but at the same time functional and maximally diverse – the number of different T-cell receptors present in humans is estimated to be at least 100 million at a time (Qi et al. 2014). Two types of T-cells are distinguished based on their expression of the MHC-binding co-receptor proteins CD4, binding MHC-II, and CD8, binding MHC-I. When a T-cell encounters a PRR-activated dendritic cell presenting its matching “cognate” antigen in lymphatic tissues, the T-cell is licensed for an adaptive immune reaction and stimulated via autocrine interleukin-2 (IL-2) signalling to proliferate rapidly (Murphy et al. 2012). To activate MHC-I-binding CD8⁺ T-cells, DCs face a conundrum: If they are not infected by an intracellular pathogen themselves, they will only take up its components through endocytosis, which leads to antigen presentation on MHC-II, but not the CD8⁺-T-cell-activating MHC-I. To solve this problem, DCs can activate a mechanism called “cross-presentation” which leads to the presentation of antigens derived from endocytosed material on MHC-I either via MHC-I loading in the endosome or peptide release from the endosome into the cytosol (Joffre et al. 2012). Licensed effector T-cells can leave the lymphatic system and home in on sites of infection. There, CD8⁺ T-cells, also called cytotoxic T-cells (cytotoxic T-lymphocytes, CTLs), can induce cell death in infected cells that present the CTL's cognate antigen via MHC-I. In addition, fragments of altered self proteins presented by cancer cells can lead to these cells being targeted by CTLs (Murphy et al. 2012). To prevent pathogens or cancer cells from tampering with the expression of MHC molecules to escape detection by the adaptive immune system, a specialized cell type known as natural killer cell (NK cell) kills cells that do not express MHC molecules (Mujal et al. 2021). CD4⁺ T-cells, also known as helper T-cells, exert their effector function mainly by influencing other cells of both the innate and adaptive

immune system (Murphy et al. [2012](#)). For example they can activate macrophages that present their cognate antigen to clear an infection with endosomal pathogens by inducing the increased generation of reactive oxygen species (ROS). CD4⁺ T-cells are also strong producers of cytokines. Depending on the cytokine milieu in which they proliferate they can differentiate into several lineages signified by the activation of different master transcription factors. These lineages then in turn secrete different cytokine profiles, directing an immune reaction towards a more pro-inflammatory, anti-viral or anti-parasitic response. CD4⁺ T-cells also play a crucial role in the activation of another adaptive immune cell type: B-cells. Analogous to T-cells, B-cells are named for their maturation in the bone marrow (Murphy et al. [2012](#)). Also similar to T-cells, each B-cell expresses a unique antigen receptor that is generated by V(D)J recombination. However, B-cell receptors have two identical binding sites that recognize the binding of a soluble protein in its natural 3D structure instead of an MHC-bound peptide derived from the protein antigen as is the case for T-cells (Flajnik [2018](#)). Before licensing by DCs, antigens bound to the B-cell receptor are internalized and presented on MHC-II. After licensing by DCs, B-cells turn into effector cells called plasma cells. Alternative splicing turns their B-cell receptors into soluble proteins, the so-called antibodies. These antibodies bind to non-self antigens, neutralize them and mark them for phagocytosis. Affinity maturation in germinal centers, B-cell-rich structures in secondary lymphoid organs, can further enhance antibody specificity by selecting B-cell clones and modifying their antibodies on the genetic level through a process called somatic hypermutation. Here, B-cells semi-randomly modify part of the DNA that encodes the antigen-binding regions of their B-cell receptor during affinity maturation in germinal centers. The mechanisms that target this diversity-increasing mechanism to specific genomic regions have not been fully elucidated (Odegard and Schatz [2006](#)). Separate antibody isotypes that share antigen specificity but differ in their effector functions can irreversibly be generated from clones of the same B- or plasma cell by genome rearrangement in a process called class-switching. Both B- and T-cells can become memory cells that are “archived” in lymphatic tissues (Akkaya et al. [2020](#); Farber et al. [2014](#)). Upon re-encountering their cognate antigen, these memory cells can quickly be reactivated again without the help of a DC, forming the basis of adaptive immune memory. Immune memory, in turn, constitutes the biological basis of vaccination, also called active immunization, a pharmacological intervention aimed at targeting the immune system against a given threat (Pollard and Bijker [2021](#)). Indeed, in line with the role of DCs, vaccines typically contain an adjuvant, a substance that is known to trigger innate immunity in order to enhance activation of adaptive immunity.

1.3 Evolution of immune systems

It has become clear that many components of our innate immune defense pathways have been conserved through evolution (Wein and Sorek [2022](#)). Indeed, the origin of many human PRRs can be traced back to evolutionarily older organisms: Toll receptor, a homologue and the name giver of mammalian TLRs, was originally discovered to play a crucial role in *Drosophila* development in a genetic screen for anatomic defects in the 1980s (Nüsslein-Volhard and Wieschaus [1980](#)), but later discovered to also play a role in immunity (Lemaitre et al. [1996](#); Poltorak et al. [1998](#)). More recent research has revealed that immune signalling pathways are evolutionarily conserved at least functionally to an even larger extent, as various homologues and analogues of mammalian defense pathways have been found in prokaryotes (Wein and Sorek [2022](#)). Examples include cyclic oligonucleotide-based antiphage signalling system (CBASS), a bacterial immune mechanism that detects invading phages and executes cell death when engaged (Duncan-Lowey and Kranzusch [2022](#)). This system relies on cyclic di- or trinucleotides, produced by enzymes sharing homology with cGAS, as second messengers to activate the cell death-inducing effectors. NACHT domain-containing bacterial proteins that resemble NLRs and play a role in defense against phages have been identified as well (Kibby et al. [2023](#)). Bacterial Gasdermin homologues that are activated by proteolytic cleavage and removal of a C-terminal peptide to subsequently form membrane pores have also been described (Johnson et al. [2022](#)). The discovery of a new type of adaptive immune system illuminated how adaptive immune systems may have evolved from innate immune systems over time: Lamprey, a species of marine jawless vertebrates have an adaptive immune system with clonally different antigen receptor-expressing cell populations that resemble T- and B-cells (Boehm, McCurley, et al. [2012](#)). Their antigen receptors, called variable lymphocyte receptors (VLRs), are composed of LRR domains that are randomly arranged by a mechanism similar to gene conversion, in which DNA fragments from a different locus are sequentially integrated into the VLR locus (Boehm, McCurley, et al. [2012](#); Pancer et al. [2004](#)).

1.4 Cell death as the *ultima ratio* in host defense

A last resort in host defense is programmed cell death (PCD), a group of pathways leading to cells actively inducing their own death (J. P. Kolb et al. [2017](#); Bertheloot, Latz, and B. S. Franklin [2021](#)). This reaction is evolutionarily conserved in prokaryotes,

where it is termed abortive infection (ABI) (Lopatina et al. [2020](#)). PCD is thought to act by limiting the replicative or survival niche of pathogens, thereby restricting their proliferation and spread. In addition, many forms of cell death cause an immune reaction in neighbouring cells through the release of pro-inflammatory DAMPs and alarmins (Pinci et al. [2022](#)). While the main purpose of CTLs of the adaptive immune system is the induction of cell death in their target cells, PCD is frequently induced in close connection with non-self sensing as part of a rapid, early immune response and therefore mostly considered to be part of innate rather than adaptive immune defense. Although different PCD pathways often occur together and especially *in vivo* many pathways can contribute to defense against a given pathogen at the same time, the molecular players and downstream consequences of many cell death pathways are distinct and can be clearly defined. While a number of PCD pathways exist, three are particularly widespread and important for immunity: Apoptosis, Necroptosis and Pyroptosis.

1.4.1 Apoptosis

The first recognized PCD pathway was apoptosis, an evolutionarily conserved, immunologically silent type of cell death during which cells shred their DNA and decompose into small vesicular bodies without cytosolic content leaking to the extracellular space (Kerr et al. [1972](#)). *In vivo* these remnants are ultimately taken up and degraded by macrophages, a process known as efferocytosis (Doran et al. [2020](#)). Apoptosis requires the activity of enzymes named caspases (cystein-aspartic acid proteases) (Van Opdenbosch and Lamkanfi [2019](#); Ramirez and Salvesen [2018](#)). These enzymes are synthesized as inactive zymogens and become active after cleavage, often through proximity-induced trans-autoproteolysis. With the exception of caspase-8, all caspases are either involved in apoptosis (apoptotic caspases) or in inducing an inflammatory type of cell death (inflammatory caspases). Apoptosis can be initiated via two pathways, termed intrinsic or mitochondrial apoptosis and extrinsic apoptosis.

Intrinsic apoptosis is a homeostatic process. During embryonal development (Ke et al. [2018](#)), but also during adult life, cells constantly undergo apoptosis as a result of age, dysfunction or a lack of growth factors (Singh et al. [2019](#)). The master regulators of intrinsic apoptosis are the mitochondrial BCL-2 homology (BH) domain containing proteins BCL-2, BCL-XL and MCL1. To set off intrinsic apoptosis, cellular processes initiate the production or liberation of BH3-only proteins such as BIM, BID or PUMA.

These pro-apoptotic effectors bind and activate the mitochondrial pore-forming proteins BAX and BAK. However, they are themselves bound and kept in check by the pro-survival BCL-2 proteins. Intrinsic apoptosis is thus regulated by an equilibrium between pro-apoptotic and pro-survival effectors. Upon activation of BAX or BAK the mitochondrial outer membrane is permeabilized (MOMP), and proteins from the inter-membrane space spill into the cytosol. Cell death is inevitable at this point, even if the following downstream processes of apoptosis are inhibited. The mitochondrial protein cytochrome c, after leaking into the cytosol, binds apoptotic protease-activating factor 1 (APAF1) and together with the enzyme caspase-9 forms a protein complex called apoptosome (Pan et al. [1998](#); Tsujimoto [1998](#)). Formation of this complex leads to the activation of caspase-9. The initiator caspase 9 then activates the so-called effector caspases 3, 6 and 7. The effector caspases mediate the activation of nucleases such as CAD (X. Liu et al. [1997](#)), plasma membrane scramblases such as Xkr8 (J. Suzuki et al. [2013](#)) and proteases that induce the characteristic decomposed morphology of apoptotic cells. “Eat-me” signals such as PtdSer presented on the plasma membrane promote the engulfment of apoptotic remnants (J. Suzuki et al. [2013](#); Segawa et al. [2014](#)).

The extrinsic apoptosis pathway is initiated by the engagement of plasma membrane receptors such as Fas and TNFR1, among others by their respective ligands FasL and TNF (Ashkenazi and V. M. Dixit [1999](#)). Binding of these ligands leads to oligomerization of the receptor and ultimately to the recruitment of caspases 8 or 10 by homotypic DED and death domain interactions in protein complexes known as complex IIa (TNFR) or DISC (Fas). Active caspase-8 or -10 then induces the activation of the effector caspases, converging with intrinsic apoptosis.

Crosstalk between intrinsic and extrinsic apoptosis exists: Caspase-8 can cleave the molecule BID, which activates BAX and BAK, causing MOMP and activating intrinsic apoptosis via caspase-9 (Singh et al. [2019](#)). NF- κ B activation has pro-survival effects which are partially mediated by the transcription of the protein FLIP, which inhibits caspase-8, antagonizing the death induction by TNFR activation.

1.4.2 Necroptosis

In contrast to accidental necrosis, which refers to cell death by excessive membrane damage, for example through physical force, necroptosis is a programmed cell death pathway (Weinlich et al. [2017](#)). Unlike apoptotic cells, cells undergoing necroptosis

release their cytoplasmic content, making necroptosis an immunogenic form of cell death. Necroptosis is defined as programmed cell death executed by the pore-forming effector MLKL after its activation through the kinase RIPK3. While it is clear that MLKL is recruited to membranes and oligomerizes there, the exact mechanism of how MLKL weakens membrane integrity has not been determined.

The protein ZBP1, which binds cytosolic Z-form RNA or DNA, activates RIPK3 by homotypic interaction through its receptor-interacting protein (RIP) homotypic interaction motif (RHIM) domain. Z-form DNA is a hallmark of virus infections such as influenza virus, suggesting necroptosis to be part of a ZBP1-activated antiviral defense strategy (T. Zhang, Yin, Boyd, et al. [2020](#)). The aberrant activation of ZBP1 is prevented by the adenosine deaminase ADAR1 (Jiao et al. [2022](#); T. Zhang, Yin, Fedorov, et al. [2022](#); Reuver et al. [2022](#)).

Necroptosis can also be induced downstream of TNFR (Laster et al. [1988](#)) and TRIF-competent TLR signalling (Weinlich et al. [2017](#)). When downstream signalling via complex I is blocked, the cytosolic complex II can form with the adaptor FADD (Newton and Manning [2016](#)). Following inhibition of translation, complex IIa forms, leading to the activation of caspase-8 and apoptosis. Upon destabilization of complex I, for example by inhibition of TAK1 or IAPs, RIPK1 can leave complex I and form complex IIb, thereby initiating caspase-8 mediated apoptosis (Pasparakis and Vandenabeele [2015](#)). Necroptosis is then kept in check by the catalytic activity of caspase-8, which cleaves RIPK1 and RIPK3 to prevent necroptosis (Y. Lin et al. [1999](#); Feng et al. [2007](#)). This prevention of necroptosis is functional even in the absence of caspase-8 autoprocessing and homodimerization due to the formation of a catalytically active heterodimer of caspase-8 with the NF- κ B target protein FLIP. This heterodimer does not induce apoptosis, but instead inhibits necroptosis (Oberst et al. [2011](#)). Upon additional inhibition of caspase-8, necroptosis is induced through a RIPK1-RIPK3-MLKL axis. Of note, lytic cell death such as necroptosis can itself induce the release of membrane-bound TNF by activation of ADAM proteases (Pinci et al. [2022](#)).

1.4.3 Pyroptosis

Pyroptosis is morphologically characterised by cell swelling and eventual rupture of the plasma membrane, similar to necroptosis. However, the mediators of pyroptosis are a family of proteins known as “Gasdermins”, named after the gastrointestinal expression

1 Introduction

pattern of Gasdermin A in mice (Broz, Pelegrín, et al. [2020](#)). They were first identified as the ultimate mediators of pyroptosis by two landmark studies in 2015, both of which identified Gasdermin D (GSDMD) as the executioner of immune cell pyroptosis (Kayagaki, Stowe, et al. [2015](#); J. Shi, Y. Zhao, K. Wang, et al. [2015](#)). The Gasdermins all have two domains, a pore-forming and thereby death-inducing N-terminus that is held in check under steady-state conditions by the inhibitory C-terminus. Upon cleavage of Gasdermins in a linker region between their N- and C-terminus by proteases such as inflammatory caspases or neutrophil elastase the N-terminal fragment is released, translocates to the plasma membrane and induces pyroptosis (Xia et al. [2021](#); Devant and Kagan [2023](#)). Intriguingly, a membrane protein called NINJ1 has been shown to be required for cell rupture downstream of Gasdermin engagement despite the pore-forming ability of Gasdermins, with *NINJ1*^{-/-} cells swelling without rupturing (Kayagaki, Kornfeld, et al. [2021](#)). While recent studies shed light on the mechanism by which NINJ1 causes plasma membrane rupture (Degen et al. [2023](#); David et al. [2023](#)), the signalling events leading to its activation remain unclear. In addition to the leakage of cytosolic content, pyroptosis is a highly pro-inflammatory form of cell death due to its close connection with the activation of inflammatory caspases, which generate soluble pro-inflammatory mediators such as IL-1-family cytokines that are matured by proteolytic cleavage of their inactive zymogen precursors. These cytokines are released passively through Gasdermin pores, with their small size permitting release independently of membrane rupture (Xia et al. [2021](#)).

The inflammatory caspases -1 and -11 (in mice) and -1, -4 and -5 (in humans) are activated by the canonical and non-canonical inflammasomes (Jiménez Fernández and Lamkanfi [2015](#)). Importantly, the non-canonical inflammasome-forming caspases -4, -5 and -11 can cleave Gasdermin D, the predominant Gasdermin isoform in immune cells, but not pro-IL-1 β . However, release of these cytokines usually still accompanies pyroptosis initiated by activation of these caspases because Gasdermin D pore formation induces NLRP3 activation, and thereby results in caspase-1 activation. Other Gasdermins also initiate immunologically relevant pyroptosis: GSDME can be cleaved by caspase-3 and thereby convert apoptosis into pyroptosis in cells with high levels of GSDME (Y. Wang et al. [2017](#)). GSDMA has recently been shown to be cleaved directly by a protease of the skin pathogen *S. pyogenes*, inducing keratinocyte pyroptosis (Deng et al. [2022](#)). Gasdermin pore formation can be countered by the endosomal sorting complexes required for transport (ESCRT) membrane repair system, potentially creating a threshold of active Gasdermin molecules required for pyroptosis (Rühl et al. [2018](#)).

Table 1.3 | Human inflammasome sensors. NLRP1 and CARD8 can be activated by the destabilization of their respective N-termini, for example by protease-mediated degradation. The non-canonical inflammasome is formed in response to cytosolic LPS by caspase-4 or -5 in humans and caspase-11 in mice. IFI16 has not conclusively been proven to form an inflammasome. The molecular trigger for NLRP3 remains unclear.

Sensor	Trigger	Reference
NLRP1	DPP9 displacement	Okondo et al. 2017
		Hollingsworth et al. 2021
	Destabilized N-terminus	Sandstrom et al. 2019
		Chui et al. 2019
		Robinson et al. 2020
CARD8	dsRNA	Bauernfried et al. 2021
	DPP9 displacement	Rao et al. 2022
		Sharif et al. 2021
	Destabilized N-terminus	Q. Wang et al. 2021
NLRP3	TGN dispersal?	J. Chen and Z. J. Chen 2018
NAIP/NLRC4	T3SS Needle proteins	Kofoed and Vance 2011
		Y. Zhao et al. 2011
NLRP10	mitochondrial damage	Próchnicki et al. 2023
		Zheng et al. 2023
NLRP12	<i>Y. pestis</i>	Vladimer et al. 2012
AIM2	dsDNA	Rathinam et al. 2010
IFI16?	dsDNA	Unterholzner et al. 2010
Pyrin	RhoA inhibition	Xu et al. 2014
caspase 4, -5, -11	cytosolic LPS	Kayagaki, Warming, et al. 2011
		J. Shi, Y. Zhao, Y. Wang, et al. 2014
		Schmid-Burgk, Gaidt, et al. 2015

1.4.4 Inflammasomes

The term “inflammasome” was coined in Jürg Tschopp’s lab to describe the discovery of a large multiprotein complex that activates inflammatory caspases and hence leads to maturation of pro-IL-1 β (Martinon, Hofmann, et al. [2001](#); Martinon, Burns, et al. [2002](#)). It is now understood that inflammasomes are cytosolic multiprotein complexes that induce pyroptosis (Broz and V. M. Dixit [2016](#)). They follow a modular composition, where multiple sensors make use of the same protein complex architecture that leads to the activation of caspase-1. Inflammasome activation begins with circular oligomerization of an inflammasome sensor, often into 10- or 11-membered rings (L. Zhang et al. [2015](#)). A list of human inflammasome forming sensors and their activators is provided in table [1.3](#).

The inflammasomes that are activated by a PYD-containing sensor protein rely on the adaptor protein Apoptosis-associated speck-like protein containing a CARD (ASC) for caspase recruitment by homotypic PYD-PYD and CARD-CARD interactions. However, CARD-containing inflammasomes such as NAIP/NLRC4 and NLRP1 usually employ ASC despite their CARD domain to boost inflammasome activity: while ASC-deficient cells still undergo pyroptosis they release less IL-1 β (Franchi et al. [2006](#)). Upon nucleation by an active sensor, ASC forms a long filament from which caspase filaments are nucleated. This structure, known as the pyroptosome, is macroscopically visible as a single micrometer size “ASC speck” in the cytosol (Masumoto et al. [1999](#)).

The NLRP3 inflammasome

The NLRP3 inflammasome is formed by the sensor NLRP3, the adaptor ASC and caspase-1. NLRP3 has been intensively studied after its description as the target of cold-induced genetic disorders in 2001 owing to its substantial clinical relevance (Hoffman et al. [2001](#)): In addition to its involvement in infectious diseases it mediates the detrimental inflammatory component of sterile inflammatory conditions such as gout and atherosclerosis, and has been proposed to exacerbate Alzheimer’s disease (Halle et al. [2008](#); Hornung, Bauernfeind, et al. [2008](#); Martinon, Pétrilli, et al. [2006](#)). NLRP3 is strongly expressed in monocytes and macrophages.

The NLRP3 protein is composed of three domains: An N-terminal pyrin domain (PYD) that interacts with ASC as an adaptor for caspase-1, a central nucleotide-binding and oligomerization (NACHT) domain and a C-terminal array of LRRs (Lamkanfi and V. M. Dixit [2014](#)). The NACHT domain harbours walker A and B motifs which coordinate ATP for hydrolysis (Duncan et al. [2007](#)). ATP hydrolysis is required for inflammasome formation as shown by experiments with walker motif-defective mutants in which IL-1 β secretion was abolished. The activity of NLRP3 follows a complex, two-step regulation pattern (Swanson et al. [2019](#)): similar to pro-IL-1 β , the NLRP3 gene is not expressed in all NLRP3 inflammasome-competent cells under steady state conditions. Instead, its expression often has to be upregulated before it can be activated, a phenomenon known as transcriptional priming (McKee and Coll [2020](#)). While some cells express sufficient levels of NLRP3 under steady-state conditions, they can still benefit from modulation of the NLRP3 protein in other ways, a group of pathways collectively called non-transcriptional or post-translational priming. The necessity for this priming step is thought to be a unique feature of the NLRP3 inflammasome,

although emerging evidence suggests non-transcriptional modulation may play a role in NLRP1 activation as well (Jenster et al. [2023](#)). Processes that have been shown to modulate NLRP3 activity without activating it immediately include its phosphorylation (Song et al. [2017](#)), dephosphorylation (Stutz et al. [2017](#)), ubiquitination and deubiquitination (Py et al. [2013](#)), and subcellular relocation (Zhou et al. [2011](#); Schmacke, O’Duill, et al. [2022](#)) among others. These pathways can integrate various signals to represent an overall inflammatory status that is reflected in the priming state of NLRP3. However, many of them show high plasticity between species, cell types and conditions, with factors and pathways that are reported as essential in a given setting often being dispensable in another (Schmacke, O’Duill, et al. [2022](#); McKee and Coll [2020](#)). It is unclear why NLRP3 apparently depends on these different priming pathways so heavily, but one suggestion is that NLRP3 is activated through a host cell perturbation that is not specific to the presence of non-self. In this scenario, priming would act as a safety mechanism preventing aberrant NLRP3 activation, tying its activation to the activation of innate immunity.

A number of cellular perturbations can activate NLRP3: Ionophores (Perregaux and Gabel [1994](#); Gurcel et al. [2006](#)), crystals and particulate matter (Dostert et al. [2008](#); Hornung, Bauernfeind, et al. [2008](#)), extracellular ATP (Mariathasan et al. [2006](#)) and the small molecule imiquimod (Groß et al. [2016](#)) among others. Since it is unlikely that these diverse activators all interact with NLRP3 directly, even more so since some of them exert their effects from outside and some from inside cells, they are thought to converge on a common molecular event that causes NLRP3 activation. Different molecular triggers have been proposed to ultimately activate primed NLRP3 and lead to the assembly of the NLRP3 inflammasome. Early reports suggested reactive oxygen species (ROS) as the NLRP3 activator, but this idea is hard to prove conclusively owing to the volatile nature of ROS (Zhou et al. [2011](#); Dostert et al. [2008](#); Muñoz-Planillo et al. [2013](#)). A more recent theory is that efflux of K^+ from the cytosol activates NLRP3 (Muñoz-Planillo et al. [2013](#)). Indeed, many NLRP3 agonists converge on the induction of K^+ -efflux. However, experiments with the TLR7 and TLR8 agonist imiquimod and the activation of NLRP3 in response to LPS alone have shown that K^+ -efflux-independent NLRP3 activation is possible (Groß et al. [2016](#); Gaidt, Ebert, Chauhan, Schmidt, et al. [2016](#)). A recent groundbreaking study has proposed trans-Golgi network (TGN) dispersal as a unifying trigger for NLRP3 activation (J. Chen and Z. J. Chen [2018](#)). In this model K^+ -efflux serves to bring NLRP3 to the TGN through increased charge-charge interaction of a poly-lysine patch within NLRP3 with the lipid PtdIns4P on the TGN, but is not sufficient to activate NLRP3

for inflammasome formation. However, dispersal of the TGN is a visible correlate of a complex and reversible biological process that is not always associated with inflammasome activation (Sáenz et al. [2009](#)). Even though there appears to be a strong correlation between these two processes, a specific trigger for NLRP3 still has not been found.

Curiously, priming and activation signals can be provided through the same PRR: Studies in human monocytes have shown that TLR4 activation by LPS can lead to inflammasome activation by activating both NF- κ B signalling and caspase-8 (Zewinger et al. [2020](#); Gaidt, Ebert, Chauhan, Schmidt, et al. [2016](#)). Another puzzling finding regarding NLRP3 is the requirement for its protein cofactor Never in mitosis gene A (NIMA)-related kinase 7 (NEK7). Originally described to facilitate the proper assembly of mitotic spindles using its kinase function, it has recently been shown that NEK7 is essential for NLRP3 activation in mice (Schmid-Burgk, Chauhan, et al. [2016](#); H. Shi et al. [2016](#); He et al. [2016](#)). Rescue experiments with a kinase-dead mutant have shown that the kinase activity of NEK7 is not required for its role in NLRP3 activation. Despite NEK7 being a direct interactor of NLRP3 (Xiao et al. [2023](#)), the molecular mechanism by which it affects NLRP3 remains elusive. Findings like the involvement of NEK7 have demonstrated that the two-step model for NLRP3 inflammasome formation is likely an oversimplification that does not live up to the biological reality. In fact, the ultimate contributions to NLRP3 inflammasome formation of pathways classically ascribed to either priming or activation have often blurred rather than sharpened the line between the two. Recent structural studies have described non-functional cage-like NLRP3 assemblies that reflect an inactive state of NLRP3 (Andreeva et al. [2021](#); Hochheiser et al. [2022](#)). It has been hypothesized that priming may work to dissolve this cage, enabling oligomerization of NLRP3 in response to its activating stimuli, but it has so far not been clarified at which step of the NLRP3 inflammasome formation cascade these cages emerge, leaving their physiological relevance unclear.

1.5 Molecular genetics

The entirety of an organism's genetic material, called the genome, contains the instructions for building all its structures and implementing its behaviours (Alberts et al. [2008](#)). Reproduction of all known biological entities entails the duplication of their genome, and the growth of a descendant based on the instructions contained in the

genome. With the exception of some viruses, whose genome is made from single- or double stranded RNA, all known genomes take the form of one or several long, usually double-stranded molecules of DNA (R. E. Franklin and Gosling [1953]; Watson and Crick [1953]; Avery et al. [1944]). Part of an organism's genome consists of instructions for transcription of DNA into messenger RNAs that serve as templates for the assembly of proteins, highly diverse chains of amino acids with varying length that fold into complex three dimensional assemblies. Their diversity allows proteins to efficiently fulfil various roles from enzymes catalyzing chemical reactions to structural components building intra- and extracellular skeletons and transport pathways. The genetic code that determines how DNA is translated into proteins – a triplet of three nucleobases codes for one amino acid – is universal across all currently known forms of life (Nirenberg and Matthaei [1961]). This finding provided the basis for genetic engineering, powering research disciplines such as synthetic biology and nowadays making rapid progress towards interpreting and modulating protein function directly from DNA sequence (Jumper et al. [2021]; Baek et al. [2021]). Other parts of the genome contain instructions for non-protein-coding RNAs that can have catalytic or regulatory functions including ribosomal (rRNA) and transfer RNAs (tRNA) in addition to species such as long non-coding RNAs (lncRNAs) (Alberts et al. [2008]; Statello et al. [2021]). Finally, a large part especially of the more complex genomes of eukaryotic organisms is not transcribed into RNAs at all, but instead serves a regulatory function for example by modulating 3D genome architecture or serving as a binding site for proteins regulating RNA transcription (Rowley and Corces [2018]).

Progress in genetic engineering has enabled the most specific targeted perturbation of biological processes to date (J. Y. Wang and Doudna [2023]): The ability to alter a genome in a defined manner allows targeted disruption of individual genes (“knock-outs”) and the insertion of short fragments or entire genes into random or defined genetic loci (“knock-ins”). Perturbing a specific genetic locus enables the investigation of causal relations between genome and function instead of the correlational analyses provided by observational studies.

1.5.1 The CRISPR era of genome editing

A recent leap in genome editing technologies has come from harnessing a prokaryotic immune system termed clustered regularly interspaced short palindromic repeats

1 Introduction

(CRISPR) for genome editing in mammalian cells (Gasiunas et al. [2012](#); Jinek, Chylinski, et al. [2012](#); Mali et al. [2013](#); Cong et al. [2013](#); Jinek, Chylinski, et al. [2012](#)): CRISPR systems were originally discovered in bacteria as defense systems against bacteria-targeting viruses called bacteriophages or phages (Hille et al. [2018](#)). After detecting an invading phage, a prokaryote can actively integrate parts of the phage's genome into a specific region of its own genome (Wiedenheft et al. [2012](#)). This region contains so-called protospacer fragments of different invading phages separated by homogenous sequences, coining the term CRISPR. These fragments are transcribed into CRISPR RNAs (crRNAs) that are complimentary to the original phage's genome. Upon reinfection with a phage, CRISPR associated (Cas) proteins with nuclease activity are targeted to the phage genome by the crRNAs and then cleave its genome, disabling the phage. The presence of a conserved sequence motif called protospacer adjacent motif (PAM) in the phage's but not the prokaryote's genome prevents this system from targeting its host's genome in an autoimmune manner (Wiedenheft et al. [2012](#)). CRISPR systems mark a simple case of adaptive immunity with a memory in evolutionarily old organisms.

Expressing the components of these CRISPR systems, specifically Cas9 and a modified crRNA that already contains the tracrRNA, called single guide RNA (sgRNA), in mammalian cells, enables mammalian genome editing with unprecedented efficiency and precision (J. Y. Wang and Doudna [2023](#)). By exchanging the 18-20bp protospacer region in the sgRNA it is possible to program Cas9 to target specific DNA regions. The Cas9 enzyme contains two nuclease domains, HNH and RuvC, that are required for cleaving the complementary and non-complementary DNA strand, respectively (Jinek, Jiang, et al. [2014](#)). These DNA double strand breaks are then repaired via either of two major pathways: non-homologous end joining (NHEJ) or Homology directed repair (HDR) (J. K. Moore and Haber [1996](#); Scully et al. [2019](#)). NHEJ works by recognizing free DNA ends with the heterodimer Ku70-Ku80 that is also essential for V(D)J recombination of variable adaptive immune system genes – in fact, loss of function mutations in NHEJ genes are often associated with severe combined immunodeficiency (SCID), a disease marked by the complete loss of T- and B-lymphocytes (Murphy et al. [2012](#)). In case of the blunt ends that are most frequently introduced by Cas9, the Ku70-Ku80 dimers on both DNA ends form a complex with the proteins X-ray repair cross-complementing protein 4 (XRCC4) and DNA ligase IV, leading to rejoining of the DNA strands (Scully et al. [2019](#)). However, in cases where DNA repair works to perfectly restore the original sequence, it remains complementary to the sgRNA, so that Cas9 can cut again. This process is repeated until one of the

nucleases and polymerases that usually make incompatible DNA double strand break ends compatible is recruited and introduces a mutation (Chang et al. 2017). If this mutation causes an insertion or deletion (indel) of a number of nucleotides that is not a multiple of three it breaks the reading frame of the genetic code, a so-called frameshift mutation. This leads to nonsensical translation, and, given that three of 64 possible nucleobase triplets encode a translation stop instead of the addition of another amino acid, to the premature termination of the polypeptide. The resulting defective ribosomal peptide (DRiP) is then degraded in the proteasome. mRNAs with such premature termination codons (PTCs) are degraded by nonsense-mediated decay (NMD), which upon recognition of a PTC based on its distance from the polyA tail or the existence of an exon-junction complex after the PTC activates its central regulator UPF1 to recruit endo- and exonucleases that dismantle and degrade RNA (Lykke-Andersen and Jensen 2015). This leads to a targeted functional genetic knockout. In contrast to NHEJ, HDR uses a homologous DNA strand to facilitate double strand break repair (Jasin and Rothstein 2013). HDR is slower and engaged less frequently for CRISPR-induced double strand breaks than NHEJ, but can be exploited to introduce a specific mutation at the site of a DNA cut by providing a donor oligonucleotide, thereby allowing the “writing” of genetic information into genomes (Schmid-Burgk, Höning, et al. 2016; K. Suzuki et al. 2016; Anzalone et al. 2019).

A number of other CRISPR systems originating from different bacteria targeting both DNA and RNA have been described since the discovery of Cas9 (Zetsche et al. 2015; Abudayyeh et al. 2016; J. Y. Wang and Doudna 2023). CRISPR systems have dramatically accelerated the generation of genetic knockouts in mice and mammalian cells. By providing access to model systems lacking specific genes, CRISPR systems have simplified the investigation of a wide range of biological questions with perturbational rather than purely observational approaches. Only a decade after the discovery of their potential for genome editing, CRISPR-based therapies are now being evaluated in the clinic as a potential cure for several diseases (Katti et al. 2022).

1.5.2 Genetic screening

The genetic basis of a biological process can be investigated in an unbiased manner by conducting so-called “forward genetic screens”. In these experiments, a library of genetic variants is generated by introducing random genetic perturbations into many individuals of a biological model system. Mutants with interesting phenotypes are

1 Introduction

then isolated from the library and their perturbation is determined, for example by genome sequencing. Thereby, genotypes are mapped to phenotypes. Forward genetic screens conducted in model organism such as *D. melanogaster*, *C. elegans* or mice led to a number of groundbreaking biological discoveries in the past (Brenner [1974]; Nüsslein-Volhard and Wieschaus [1980]; Kayagaki, Stowe, et al. [2015]).

With the advent of modern genome-editing technologies, forward genetic screens have been miniaturized to the level of individual cells (Shalem et al. [2015]). In these cell-based screens a library of cells, each of which carries a different genetic perturbation, is searched for phenotypes of interest. Interesting cells are then isolated from the library and their perturbations analyzed by sequencing. In addition to CRISPR-mediated genome editing, such screens can be conducted using random genomic integration in haploid cell lines, a technique known as haploid genetic screening (Carette et al. [2009]; Fessler et al. [2020]).

The two approaches have different strengths: CRISPR can target multiple copies of the same gene in a vast range of cell types and organisms. However, since perturbations introduced by CRISPR are not entirely random, but determined by sgRNAs, CRISPR screens rely on complex libraries containing many thousands of sgRNAs. These screens are therefore limited in their targeting space, with genome-wide screens usually only targeting protein-coding genes (Shalem et al. [2015]). Haploid genetic screening in contrast is based on the truly random integration of gene trap-containing DNA pieces – translation stop-inducing genetic sequences – into the genome, and therefore by design also targets non-coding RNAs and regulatory regions (Carette et al. [2009]). However, since haploid screens depend on cells with a haploid genome, they can only be conducted in specialized cells that are limited in the range of biological phenomena they can model. Since they cover a wider range of genomic mutations, the cell libraries generated by haploid genetic screens can be more than an order of magnitude larger than those used in CRISPR screens, requiring cell isolation methods with an appropriate throughput.

From a screening cell library with a single mutation in each cell either generated via insertional mutagenesis including gene traps or CRISPR, cells with interesting phenotypes have to be isolated. In most screens conducted so far, this has been achieved by either of three methods:

1. Faster proliferation of target cells that eventually outgrow other cells enable screens for proliferation speed (S. Chen et al. [2015]).

2. Protection from cell death as a phenotype allows for the expansion and analysis of surviving cells (Kayagaki, Stowe, et al. [2015](#)).
3. Fluorescence-activated cell sorting (FACS) as the most versatile method can isolate cells based on changes in the intensity of fluorescently labelled markers (Parnas et al. [2015](#)).

The versatility of FACS notwithstanding, these technologies limit the phenotypes that are amenable to cell-based forward genetic screening at genome scale (Bock et al. [2022](#)). Several approaches have therefore tried to extend genetic screening to other modalities: Perturb-seq and CROP-seq use single cell RNA sequencing to determine cellular phenotypes, but do not contain an enrichment step, requiring enormous sequencing throughput, making genome-scale screens costly (Replogle et al. [2022](#); A. Dixit et al. [2016](#); Datlinger et al. [2017](#)). Technologies for screens based on microscopy images have been developed as well: *In situ* sequencing uses sequencing by synthesis, the method behind large scale short read sequencing directly in cells to sequence sgRNA-associated barcodes (Feldman et al. [2019](#)). Image-based cell sorters separate dissociated cells with protein distribution phenotypes assessed by low-resolution, microsecond exposure flow imaging at unprecedented throughput (Schraivogel et al. [2022](#)). Originally developed to isolate specific cells from their tissue context for further analysis, marking individual cells by converting photoswitchable or photoactivatable fluorophores with a FRAP laser at single cell resolution promises to connect the throughput and ease of sorting cells via FACS to information rich high-resolution images obtained by state-of-the-art microscopy (Victoria et al. [2010](#); Yan et al. [2021](#); Kanfer et al. [2021](#); J. Lee et al. [2020](#)). Still, a technology that does not impose limits on screening library size to ensure representation of rare phenotypes, allows for the unbiased identification of phenotypes using the latest computer vision methods, and permits reanalysis of past screens as new analysis methods become available while being compatible with both state-of-the-art and widespread microscopy techniques had not been available until now (Schmacke, Mädler, et al. [2023](#)).

2 Summary

2.1 NLRP3 priming by translocation

Working on the role of NEK7 in NLRP3 activation, we had discovered that, in contrast to the role of NEK7 in mouse cells, human cells activate NLRP3 independently of NEK7. “Transplanting” mouse NLRP3 into a model of human monocytes rescued the activity of mouse NLRP3 in the absence of NEK7. From this result we concluded that rather than a difference between the two NLRP3 orthologues, a difference between cellular signalling must be responsible for the differential requirement of NEK7 for NLRP3 activation. Coupled with the finding that TLR4 stimulation via LPS can bypass the requirement for NEK7 in mouse cells, we concluded that a pathway activated downstream of TLR4 can bypass NEK7 by priming NLRP3. Tracing the signalling cascade of TLR4 by genetically knocking out its components, we arrived at the kinase IKK β . Indeed, experiments with knockouts of IKK β in mouse and human cells explained both phenotypes: LPS could no longer bypass NEK7 in mouse cells and NLRP3 signalling in human cells was blunted. Why human cells are incapable of using NEK7 to prime NLRP3 in the absence of IKK β remains unclear. Using human induced pluripotent stem cell-derived macrophages that we could genetically engineer to lack NEK7 as a model system, we confirmed that human cells in contrast to mouse cells do not require NEK7, but instead fully rely on IKK β to prime NLRP3. Elucidating the mechanism by which IKK β primes NLRP3 for NEK7-independent inflammasome activation, we found that IKK β activity recruits a fluorescently tagged NLRP3 variant to the trans-Golgi network, a finding we corroborated by mass spectrometry analysis of subcellular fractions. Our results define recruitment of NLRP3 to a specific organelle as a new priming modality of the NLRP3 inflammasome.

2.2 CRISPR screening for subcellular spatial phenotypes at genome scale

The development of charge coupled device (CCD) chips has enabled the acquisition of digital images at high resolution (Boyle and Smith [1970](#)). In combination with modern microscopes the latest development of such chips has enabled the collection of large digital datasets representing the spatial composition of cells. A technology that can profile this composition and connect it to the genetic identity of individual cells at scale could generate insights into complex cellular biology. Here we developed a new genetic screening technology for image-based phenotypes. We first generated a library of 40 million human U2OS cells with one genetic knockout in each cell using CRISPR/Cas9. The cells in this library had been genetically engineered to express the fluorescently labelled autophagosome marker LC3 (mCherry-LC3). We stimulated these cells with the mTOR inhibitor Torin-1 to induce autophagy, during which LC3 gets redistributed onto autophagosomes. We then acquired microscopy images of this library and segmented these images into single cells using a nuclear stain to identify individual cells and a membrane stain to associate a the cytosol of a cell with its nucleus. This resulted in a dataset of single cell images across three channels: Nucleus and membrane that were used for segmentation and an image corresponding to the distribution of LC3 in each cell. Given that each cell in this library harboured a different genetic knockout, we expected some cells to have been unable to redistribute LC3 onto autophagosomes following Torin-1 stimulation owing to the lack of a gene that is essential for this process. We then sought to identify these cells based on their LC3 images. Since these data are inherently large and complex, we made use of the recent breakthrough in image analysis by machine learning models (LeCun et al. [2015](#)). Using a knockout of *ATG5*, an essential autophagy gene, as a positive control, we trained a binary classifier based on a convolutional neural network to differentiate between images of cell undergoing autophagy and images of cells that had a blunted response to Torin-1 or were left unstimulated, and therefore not undergoing autophagy. With this classifier we were able to identify individual cells in our library that were incapable of forming autophagosomes in response to Torin-1. We then used fully automated laser microdissection to isolate the nuclei of these cells and subsequently sequenced their genetic perturbations. Here we found almost all genes known to be essential for autophagy to be defective in this pool of selected cells. This experiment demonstrates that our technology is capable of associating image-based phenotypes with the genotype of individual cells at genome scale.

3 Publications

3.1 IKK β primes inflammasome formation by recruiting NLRP3 to the trans-Golgi network

The following research article was originally published here:

Schmacke, N. A., O’Duill, F., et al. (Dec. 2022). “IKK β primes inflammasome formation by recruiting NLRP3 to the trans-Golgi network.” eng. In: *Immunity* 55.12, pp. 2271–2284. ISSN: 1097-4180 (Electronic); 1074-7613 (Print); 1074-7613 (Linking). DOI: [10.1016/j.immuni.2022.10.021](https://doi.org/10.1016/j.immuni.2022.10.021)

Europe PMC Funders Group

Author Manuscript

Immunity. Author manuscript; available in PMC 2023 June 13.

Published in final edited form as:

Immunity. 2022 December 13; 55(12): 2271–2284.e7. doi:10.1016/j.immuni.2022.10.021.

IKK β primes inflammasome formation by recruiting NLRP3 to the trans-Golgi network

Niklas A. Schmacke¹, Fionan O’Duill¹, Moritz M. Gaidt^{1,7}, Inga Szymanska¹, Julia M. Kamper¹, Jonathan L. Schmid-Burgk^{1,8}, Sophia C. Mädler², Timur Mackens-Kiani¹, Tatsuya Kozaki³, Dhruv Chauhan¹, Dennis Nagl¹, Che A. Stafford¹, Hartmann Harz⁴, Adrian L. Fröhlich¹, Francesca Pinci¹, Florent Ginhoux^{3,5,6}, Roland Beckmann¹, Matthias Mann², Heinrich Leonhardt⁴, Veit Hornung^{1,9,*}

¹Gene Center and Department of Biochemistry, Ludwig-Maximilians-Universität München, 81377 Munich, Germany

²Department of Proteomics and Signal Transduction, Max Planck Institute of Biochemistry, 82152 Martinsried, Germany

³Singapore Immunology Network (SIgN), Agency for Science, Technology & Research (A*STAR), 8A Biomedical Grove, Immunos Building #3-4, Biopolis, Singapore 138648, Singapore

⁴Faculty of Biology, Human Biology and Biomedicine, Ludwig-Maximilians-Universität München, Planegg-Martinsried, Germany

⁵Shanghai Institute of Immunology, Shanghai JiaoTong University School of Medicine, 280 South Chongqing Road, Shanghai 200025, China

⁶Translational Immunology Institute, SingHealth Duke-NUS Academic Medical Centre, Singapore 169856, Singapore

Summary

The NLRP3 inflammasome plays a central role in antimicrobial defense as well as in the context of sterile inflammatory conditions. NLRP3 activity is governed by two independent signals: the first signal primes NLRP3, rendering it responsive to the second signal, which then triggers inflammasome formation. Our understanding of how NLRP3 priming contributes to inflammasome activation remains limited. Here, we show that IKK β , a kinase activated during priming, induces recruitment of NLRP3 to phosphatidylinositol-4-phosphate (PI4P), a phospholipid enriched on the trans-Golgi network. NEK7, a mitotic spindle kinase that

*Correspondence: hornung@genzentrum.lmu.de.

⁷Present address: Research Institute of Molecular Pathology (IMP), Vienna BioCenter (VBC) Campus-Vienna-Biocenter 1, 1030 Vienna, Austria

⁸Present address: Institute of Clinical Chemistry and Clinical Pharmacology, University of Bonn and University Hospital Bonn, Bonn, Germany

⁹Lead contact

Author Contributions

Conceptualization: N.A.S., M.M.G., J.L.S.-B., and V.H.; formal analysis, software: N.A.S. and S.C.M.; investigation: N.A.S., F.O., M.M.G., I.S., J.M.K., J.L.S.-B., S.C.M., T.M.-K., D.C., D.N., C.A.S., H.H., A.L.F., and F.P.; resources: F.G., R.B., M.M., H.L., and V.H.; writing: N.A.S., M.M.G., and V.H. with input from all authors; funding acquisition: V.H.; supervision: V.H.

Declaration of interests

The authors declare no competing interests.

had previously been thought to be indispensable for NLRP3 activation, was redundant for inflammasome formation when IKK β recruited NLRP3 to PI4P. Studying iPSC-derived human macrophages revealed that the IKK β -mediated NEK7-independent pathway constitutes the predominant NLRP3 priming mechanism in human myeloid cells. Our results suggest that PI4P binding represents a primed state into which NLRP3 is brought by IKK β activity.

Introduction

Cells of the innate immune system employ a repertoire of so-called pattern recognition receptors (PRRs) to discriminate self from non-self. Engagement of these PRRs triggers a broad array of effector functions geared toward eliminating a microbial threat. The inflammasome pathway constitutes a special class of this PRR system that is signified by the activation of the cysteine protease caspase-1 in a large supramolecular protein complex.¹ Activation of caspase-1 causes maturation of pro-inflammatory cytokines, most prominently IL-1 β ,² as well as the induction of a special type of cell death, known as pyroptosis.³ Among inflammasome sensors, NLRP3 plays a pivotal role in antimicrobial defense as well as sterile inflammatory diseases.⁴ This is owed to the fact that NLRP3 is a highly sensitive, yet non-specific PRR. In this regard, NLRP3 has been shown to respond to the perturbation of cellular homeostasis by a broad array of diverse stimuli, rather than being activated by a specific microbe-derived molecule.⁵ K⁺ efflux from the cytosol has been identified as a common denominator of many NLRP3 triggers.⁶ In this function, several types of lytic cell death have been shown to result in secondary engagement of the NLRP3 inflammasome pathway.⁷ However, K⁺ efflux-independent NLRP3 stimuli have also been described,^{8,9} and a recent report has identified dispersal of the *trans*-Golgi network (TGN) as a common denominator of both K⁺ efflux-dependent and -independent NLRP3 triggers.¹⁰

Unlike other inflammasome sensors, NLRP3 critically depends on the engagement of a priming step.¹¹ This priming signal can be provided by different types of receptors, typically PRRs that trigger NF- κ B activation. Lipopolysaccharide (LPS) activating TLR4 is commonly used to provide a priming signal preceding the actual NLRP3 activation step. Initially, the necessity of priming had been ascribed to the fact that NLRP3 is expressed at limiting amounts in murine macrophages. In this respect, it has been shown that in a process now also called “transcriptional priming,” NF- κ B activating stimuli drive the expression of *Nlrp3*, thereby facilitating its activation.^{12,13} In line with these findings, inhibition of transcription blocks this mode of NLRP3 priming, whereas transgenic expression of NLRP3 bypasses the requirement of transcriptional priming.^{12,13} Extending this concept, NLRP3 can also be primed non-transcriptionally, e.g., by a short pulse of LPS treatment.^{14–16} These modes of priming have been ascribed to a variety of post-translational modifications of NLRP3, including phosphorylation, de-phosphorylation, de-ubiquitination, and de-sumoylation.^{17,18} Although being mechanistically unrelated, these events are commonly referred to as post-translational or non-transcriptional priming. The fact that many cells already express NLRP3 at sufficient amounts under steady-state conditions underscores the importance of non-transcriptional priming.¹⁹

Despite considerable insight into pathways that result in NLRP3 priming, the activation step of the NLRP3 inflammasome and its interconnection with priming have remained enigmatic. In this regard, we and others have identified the mitotic spindle kinase NEK7 (NIMA-related kinase 7) as a critical cofactor in NLRP3 activation in murine cells.^{20–22} Notably, this role of NEK7 is distinct from its function in the cell cycle, as its kinase activity is not required for NLRP3 activation.^{21,22} NEK7 has been suggested to interact with NLRP3 in a K⁺ efflux-dependent manner, and deletion of NEK7 does not affect transcriptional NLRP3 priming.^{21,22} This, in combination with a study modeling a NEK7-containing NLRP3 pyroptosome based on a cryo-EM structure of the NLRP3/NEK7 complex,²³ has led to the conclusion that NEK7 is involved in NLRP3 activation downstream of K⁺ efflux.²⁴ Of note, studies identifying NEK7 as an indispensable factor for NLRP3 activation have mainly been conducted in murine models. Here, we report that reductionist genetic dissection of NLRP3 signaling in human cells revealed an additional pathway of NLRP3 priming that enables NLRP3 inflammasome activation independently of NEK7.

Results

Human iPSC-derived macrophages and human myeloid cell lines activate NLRP3 independently of NEK7

We and others have previously described NEK7 to be essential for the activation of the NLRP3 inflammasome in the murine system.^{20–22} To study the role of NEK7 in the human system, we adopted a recently described iPSC-derived macrophage model, in which human iPSC cells are differentiated into macrophages *in vitro* (hiPS-Macs).²⁵ hiPS-Macs are fully capable of inflammasome activation: after priming with LPS, activation of the NLRP3 inflammasome with the ionophore Nigericin or the NAIP-NLRC4 inflammasome with Needle Tox resulted in pyroptosis (LDH release) accompanied by the release of IL-1 β and IL-18 (Figures S1A and S1B). Both cytokine and LDH release in response to Nigericin, but not Needle Tox, were sensitive to the NLRP3 inhibitor MCC950 (Figures S1A and S1B). To investigate the role of NEK7 in NLRP3 inflammasome activation in hiPS-Macs, we generated *NEK7*^{-/-} iPSC cell clones via CRISPR-Cas9 genome editing. NEK7 deficiency neither affected macrophage differentiation nor did it lead to altered NLRP3 expression levels (Figure S1C). Contrasting previous reports from mouse cells,^{20–22} NEK7-deficient hiPS-Macs showed no major impairment of their NLRP3 inflammasome response (Figures 1A and S1D). Cytokine and LDH release following Nigericin stimulation remained sensitive to MCC950 in *NEK7*^{-/-} hiPS-Macs, confirming that Nigericin-induced pyroptosis was still mediated by NLRP3 in these cells (Figure 1A). As expected, NAIP-NLRC4 activation and IL-6 release also proceeded unperturbed in *NEK7*^{-/-} hiPS-Macs (Figures 1A and S1D).

We then sought to further characterize NEK7-independent NLRP3 activation in human cells. To this end, we used the BLaER1 transdifferentiation system that we have previously adopted to study innate immune sensing.^{26,27} Mirroring hiPS-Macs, NEK7-deficiency showed no impact on NLRP3 inflammasome activation as assessed by release of LDH and IL-1 β (Figures 1B and S1E). To address whether the role of NEK7 for NLRP3 activation in human cells was overshadowed by a functional redundancy with its close homolog NEK6, we generated cells deficient for both NEK6 and NEK7. Analogous to NEK7-deficient

cells, *NEK6*^{-/-} × *NEK7*^{-/-} BLaER1 cells displayed unimpaired activation of the NLRP3 inflammasome (Figures 1B and S1E). As expected, *NLRP3*^{-/-} BLaER1 cells showed no response to Nigericin stimulation, whereas they remained responsive to NAIP-NLRC4 inflammasome activation (Figures 1B and S1E). In line with these observations, caspase-1 maturation upon Nigericin treatment also proceeded independently of NEK7 (Figure 1C). Pretreatment with the NLRP3-specific inhibitor MCC950²⁸ or prevention of K⁺ efflux by increased extracellular K⁺ concentration⁶ blunted NLRP3 activation in wild type, *NEK7*^{-/-} and *NEK6*^{-/-} × *NEK7*^{-/-} cells stimulated with Nigericin, whereas it left the NAIP-NLRC4 inflammasome intact (Figures S1F and S2A–S2D), indicating that Nigericin still relied on inducing K⁺ efflux to trigger NLRP3 inflammasome activation in absence of NEK7. In line with the results obtained in BLaER1 cells, THP-1 cells deficient in NEK7 showed no attenuation of Nigericin-triggered inflammasome activation, whereas *NLRP3*^{-/-} THP-1 cells were completely defective (Figures 1D, 1E, and S2E).

NEK7-independent NLRP3 activation in human cells contrasts with NEK7-dependent NLRP3 activation in mouse cells published by us and others.^{20–22} To investigate if this difference is caused by species-specific features of the human and mouse orthologs of NLRP3, we reconstituted *NLRP3*^{-/-} BLaER1 cells with different NLRP3 orthologs. Phenocopying the human ortholog, NEK7-deficient BLaER1 cells expressing mouse NLRP3 (*mmNlrp3*) mounted an unperturbed response to Nigericin (NLRP3) and Needle Tox (NAIP-NLRC4) (Figures 1F, 1G, and S2F). Taken together, these results demonstrate that unlike mouse cells, human cells are intrinsically capable of activating NLRP3 in a NEK6- and NEK7-independent manner.

Priming activates IKKβ to enable NEK7-independent NLRP3 inflammasome formation

Having established that human cells activate NLRP3 in absence of NEK7, we wondered whether the NEK7-independent pathway could be triggered in mouse cells where NLRP3 activation has been shown to depend on NEK7.²¹ Here, we used an immortalized mouse macrophage cell line constitutively expressing *mmNlrp3* (*mmMacs*) in which we had initially discovered the requirement of NEK7 for NLRP3 activation through a forward genetic screen.²⁰ These cells do not require transcriptional priming of NLRP3 for inflammasome activation, and stimulation with Nigericin alone already activated NLRP3 in a fully NEK7-dependent manner (Figures 2A and 2B). When testing different priming modalities, we found that simultaneous treatment with LPS and Nigericin led to NLRP3 activation independently of NEK7, as determined by LDH release and caspase-1 maturation 4 h after stimulation (Figures 2A and 2B). Concurrent stimulation with Pam3CSK4 or R848 instead of LPS (Figures S3A–S3D) and with ATP instead of Nigericin (Figure 2C) similarly resulted in a NEK7-independent response. Of note, this NEK7 bypass triggered by concurrent priming and stimulation was only uncovered when studying the inflammasome response several hours after treatment (Figure S3E). Indeed, the NLRP3 inflammasome response 1 h following concurrent LPS + Nigericin treatment was still NEK7-dependent (Figure S3F). However, concomitant LPS treatment enhanced this early NEK7-dependent NLRP3 inflammasome response compared with Nigericin treatment alone. This is consistent with previous reports on rapid, non-transcriptional NLRP3 priming enabling accelerated inflammasome formation.^{14,15,29} Taken together, these results suggest that NEK7-mediated

priming and the LPS-induced NEK7 bypass pathway are not only functionally redundant but may also act synergistically to accelerate NLRP3 activation.

LPS sensing initiates diverse transcriptional programs. However, NEK7-independent priming remained functional in the presence of translation-blocking concentrations of cycloheximide (CHX), indicating that it does not require *de novo* protein synthesis (Figures 2D and S3G). To elucidate the signaling cascade of NEK7-independent post-translational priming, we genetically perturbed TLR4 and its downstream signaling adaptors TRIF (*Ticam1*) and MyD88 in either unmodified or *Nek7*^{-/-} mmMac cells. NLRP3 activation in response to Nigericin treatment remained intact in *Ticam1*^{-/-} or *Myd88*^{-/-} cells (Figure 2E, right panel; Table S1), whereas these cells displayed a selective lack of antiviral (IP-10) or pro-inflammatory (TNF) gene expression, respectively (Figure 2E, left and middle panels). TLR4 deficiency abrogated LPS-dependent cytokine production altogether (Figure 2E, left and middle panels). Accordingly, unlike their TLR4-sufficient counterparts, *Nek7*^{-/-} × *Tlr4*^{-/-} cells were fully defective in NLRP3 activation (Figure 2E). In contrast, *Nek7*^{-/-} cells additionally deficient in either MyD88 or TRIF were still able to mount an NLRP3 inflammasome response after LPS + Nigericin treatment, albeit less effectively (Figure 2E). As expected, *Myd88*^{-/-} × *Ticam1*^{-/-} cells deficient in NEK7 were fully defective in NEK7-independent NLRP3 activation (Figure 2E). Altogether, these results indicate that the NEK7 bypass can be induced downstream of both Myd88 and TRIF signaling. To identify the common factor mediating the NEK7 bypass, we turned our attention to the TAK and IKK complexes that constitute the apical kinase complexes governing pro-inflammatory signal transduction downstream of both MyD88 and TRIF. When we used the small molecule Takinib to block the activity of TAK1, the key kinase of the TAK complex, we found that the NEK7 bypass was largely inhibited, whereas NLRP3 activation in response to Nigericin remained intact (Figure S4A). We obtained analogous results when we blocked IKK β , a kinase in the IKK complex, using TPCA-1 (Figure S4B). Of note, for both inhibitors, the NEK7 bypass was not fully abrogated; however, it was attenuated to the same extent as the production of the NF- κ B-dependent cytokine TNF (Figures S4A and S4B). The NEK7 bypass was blocked when we deleted *Ikkb*, the gene coding for IKK β , but remained unperturbed when we deleted *Chuk*, the gene coding for IKK α (Figures 2F–2H). *Nek7*^{-/-} × *Ikkb*^{-/-} mmMac cells were almost completely defective in NLRP3 inflammasome activation, whereas AIM2 inflammasome activation in response to dsDNA transfection remained intact (Figures 2F–2H). Priming with R848 or NLRP3 activation with ATP similarly resulted in IKK β -dependent NLRP3 inflammasome formation independently of NEK7 (Figures S4C and S4D). In conclusion, since IKK β is activated downstream of the TAK1 complex, these findings suggest that IKK β constitutes the critical kinase mediating NEK7-independent NLRP3 inflammasome formation.

RIPK1 and caspase-8 have been implicated in non-transcriptional NLRP3 priming.³⁰ Although the NEK7 bypass continued to function in *Nek7*^{-/-} × *Ripk1*^{-/-} mmMac cells (Figure S4E), *Nek7*^{-/-} × *Casp8*^{-/-} mmMacs were fully defective in activating the NLRP3 inflammasome despite *Casp8*^{-/-} cells displaying unperturbed NLRP3 activation (Figure S4F). ASC specking was also abrogated in *Nek7*^{-/-} × *Casp8*^{-/-} mmMacs in response to LPS + Nigericin (Figure S4G), showing that caspase-8 deficiency affects NEK7-independent NLRP3 priming upstream of inflammasome formation. Since we found IKK β to be crucial

for the NEK7 bypass, we checked whether caspase-8 deficiency had an effect on IKK β activity.³¹ Indeed, we observed reduced IKK β phosphorylation after LPS stimulation of *Casp8*^{-/-} mmMacs (Figure S4H), suggesting that reduced IKK β activity, rather than a specific role of caspase-8, explains the inability of *Nek7*^{-/-} \times *Casp8*^{-/-} mmMacs to activate NLRP3 in response to LPS + Nigericin.

In contrast to ATP and Nigericin, which depend on K⁺ efflux to engage NLRP3, the TLR7 agonist Imiquimod (R837) has been shown to induce NEK7-dependent NLRP3 inflammasome formation independently of K⁺ efflux.⁹ In mmMac cells, Imiquimod strongly depended on NEK7 for NLRP3 activation even in combination with LPS (Figure 3A). Given that all K⁺ efflux-dependent stimuli tested here can engage the NEK7 bypass with concurrent IKK β activation, we investigated whether K⁺ efflux might boost Imiquimod-driven NLRP3 activation in *Nek7*^{-/-} mmMacs. Indeed, under low extracellular K⁺ conditions that facilitate K⁺ efflux,¹⁰ Imiquimod stimulation together with LPS led to a NEK7-independent response that was significantly increased over LPS stimulation alone and not detectable with a physiological extracellular K⁺ concentration of 5 mM (Figures 3B and 3C). Although the relative contributions of LPS- or Imiquimod- induced IKK β activity and K⁺ efflux- or Imiquimod-induced NLRP3 activation remain unclear, these data indicate that K⁺ efflux enhances the NEK7-bypassing effect of IKK β activation.

Human myeloid cells use IKK β instead of NEK7 to prime NLRP3 by default

Moving back into the human system, we wondered whether NLRP3 priming through IKK β was also responsible for the NEK7-independence of NLRP3 activation in human cells. Using the hiPS-Mac model, we found that *IKBKB*^{-/-} cells showed a strong defect in NLRP3 inflammasome activation, whereas NAIP-NLRC4 activation proceeded normally, with IL-18 release being partially compromised (Figures S5A and S5B). However, we also observed a reduction in IL-6 amounts in IKK β -deficient hiPS-Macs following LPS stimulation (Figure S5C). IKK β , by governing NF- κ B-dependent NLRP3 expression and also mediating the non-transcriptional NEK7 bypass, fulfills a dual role in NLRP3 priming. Hence, any effects on NLRP3 priming in *IKBKB*^{-/-} hiPS-Macs cannot unequivocally be ascribed to either transcriptional or non-transcriptional NLRP3 priming based on these experiments. Although these results establish that IKK β is critical for NLRP3 priming in human cells, the relative contributions of transcriptional and non-transcriptional priming remain unclear in the hiPS-Mac model.

To clarify whether transcriptional or non-transcriptional NLRP3 priming is the predominant priming modality in the human system, we employed the BLaER1 model system. Given that hiPS-Macs express NLRP3 under steady-state conditions without transcriptional priming, we first sought to clarify if transcriptional priming was required for NLRP3 activation in BLaER1 cells. Although BLaER1 cells deficient in TAK1 (*MAP3K7*), in which NF- κ B-mediated transcription after LPS sensing is completely abrogated, did indeed not produce pro-IL-1 β upon LPS treatment anymore, they still expressed NLRP3 (Figure S5D). Congruently, blocking protein translation with CHX did not affect NLRP3 activation in these cells (Figure S5E). These data show that in BLaER1 cells, transcriptional priming is not required for NLRP3 inflammasome activation. Still, again mirroring hiPS-Macs,

stimulation with Nigericin alone was not sufficient to activate NLRP3, but additional treatment with LPS was required to enable NLRP3 inflammasome formation in BLaER1 cells (Figure S5F). The NAIP-NLRC4 inflammasome formed in response to Needle Tox irrespectively of LPS priming as expected (Figure S5F). These data demonstrate that BLaER1 cells require non-transcriptional priming of NLRP3 for inflammasome activation. In line with these findings, a short pulse of concomitant LPS + Nigericin treatment led to robust NLRP3 activation in BLaER1 cells (Figure S5G). RIPK1, RIPK3, and caspase-8 were dispensable for NLRP3 activation in response to Nigericin and NLRC4 activation, but in *GSDMD*^{-/-} BLaER1 cells, LDH release for both inflammasomes was blunted (Figure S5H).

Given that non-transcriptional priming was still dependent on TAK1 in BLaER1 cells and that TAK1 activates IKK β , we then assessed NLRP3 activation in BLaER1 cells deficient for IKK β . Corroborating our findings from hiPS-Macs and the murine system, LDH release and caspase-1 maturation following NLRP3 activation were blunted in *IKBKB*^{-/-} BLaER1 cells (Figures 4A, 4B, and S5I). In contrast, cells deficient in IKK α (*CHUK*), a close homolog of IKK β , did not display a defect in inflammasome formation (Figure 4A). Cells deficient in both IKK α and IKK β (*CHUK*^{-/-} \times *IKBKB*^{-/-}) phenocopied *IKBKB*^{-/-} cells (Figures 4A and 4B). As expected, given the steady-state expression of NLRP3 in BLaER1 cells, *RELA*^{-/-} \times *RELB*^{-/-} cells displayed unperturbed NLRP3 activation (Figures 4A and S5I) despite strongly reduced pro-inflammatory cytokine transcription (Figure S5J). Reconstitution of *IKBKB*^{-/-} BLaER1 cells with wildtype IKK β , but not IKK β -K44M, a kinase-dead mutant of IKK β ,³² rescued NLRP3 activation, showing that the kinase activity of IKK β was required for non-transcriptional NLRP3 priming (Figures 4C and 4D).

To investigate the kinetics of IKK β -mediated non-transcriptional NLRP3 priming, we added the IKK β inhibitor TPCA-1 to BLaER1 cells at different time points pre and post NLRP3 priming. Expectedly, adding TPCA-1 concurrently with LPS blocked all priming and abrogated NLRP3 activity (Figure 4E). However, adding TPCA-1 concurrently with or 30 min after Nigericin also blocked or strongly reduced NLRP3 activity, respectively (Figure 4E). Experiments with primary human monocytes corroborated these findings (Figure S5K). In summary, these data show that rapid, non-transcriptional priming by IKK β is required for NLRP3 activation, further suggesting that human cells are NLRP3 inflammasome competent in the absence of NEK7 because they engage IKK β by default.

Synergistically with IKK β , NEK7 can accelerate NLRP3 activation human cells

Having demonstrated that IKK β activation constitutes the predominant priming pathway in the human system, we wondered whether NEK7-mediated priming could be used by human cells at all. A hallmark of NEK7-mediated NLRP3 priming is the direct interaction of NEK7 and NLRP3.²¹ NLRP3 co-immunoprecipitated with NEK7 from THP-1 cells, indicating that the human NEK7 protein (hsNEK7) could in principle function to prime NLRP3 (Figures 5A and S6A). Of note, this interaction was independent of K⁺ efflux. We then reconstituted NLRP3 inflammasome signaling in HEK-293T cells, which normally do not express NLRP3 or ASC, the core signaling components of the NLRP3 inflammasome (Figures S6B and S6C). Notably, in this reconstitution system, inflammasome activation is

driven by overexpression of NLRP3 and proceeds without stimulation by Nigericin. Hence, we consider inflammasome formation in this HEK-293T inflammasome assay to directly report the priming status of NLRP3. Here, we found that the mouse and human orthologs of NEK7 enhanced the activation of both NLRP3 orthologs, showing that hsNEK7 is capable of priming NLRP3 (Figures 5B and S6D). To investigate if NEK7 has a physiological role in NLRP3 priming, we went back to our hiPS-Mac system. Since we had found NLRP3 activation to require both NEK7 and LPS priming after concomitant LPS + Nigericin stimulation at early time points in mouse cells (Figure S3F), we tested the same condition in hiPS-Macs. Indeed, concomitant stimulation with LPS + Nigericin for 1 h resulted in NEK7-dependent release of LDH, whereas 4 h of LPS + Nigericin stimulation rendered NLRP3 activation NEK7-independent (Figures 5C and 5D).

From these data, we conclude that IKK β , which is required to activate NLRP3 in all human cell lines tested here, operates in synergy with NEK7 to drive NLRP3 priming. NEK7 can accelerate NLRP3 priming at early time points, when IKK β is not yet fully active. At later time points, IKK β becomes redundant with NEK7.

Recruitment of NLRP3 to PtdIns4P induces NEK7-independent inflammasome activation. Finally, we investigated how IKK β activation enables NEK7-independent NLRP3 activation. As it has recently been reported that interaction of NLRP3 with phosphatidylinositol-4-phosphate (PI4P) on the TGN is an essential requirement for inflammasome formation,¹⁰ we investigated the subcellular localization of NLRP3 during priming. To this end we generated *Pycard*^{-/-} J774 mouse macrophages expressing a fusion protein of the PI4P-binding pleckstrin homology (PH)-domain of oxysterol-binding protein (OSBP) and mCherry (OSBP[PH]-mCherry). In these cells, we found LPS treatment to result in the accumulation of NLRP3 at PI4P-rich sites (Figures 6A and 6B). Of note, this translocation cannot be caused by NLRP3-mediated pyroptosis, since *Pycard*^{-/-} cells are incapable of NLRP3 inflammasome formation. The recruitment of NLRP3 to PI4P was markedly reduced by the IKK β inhibitor TPCA-1 (Figures 6A and 6B). In line with our findings on LPS-dependent non-transcriptional priming in human and mouse cells, NLRP3 recruitment to PI4P occurred rapidly, generally within 30 min after LPS stimulation (Figure S6E). We did not observe NLRP3 translocation to mitochondria — in fact, PI4P-rich sites appeared mostly distinct from mitochondria (Figure S6F). To identify the cellular compartment that NLRP3 is recruited to, we fractionated lysates of *Pycard*^{-/-} J774 cells. Post-nuclear lysates were centrifuged at 5,000 $\times g$ to obtain a pellet (P5) and supernatant (S5) fraction. The S5 fraction was further subjected to centrifugation at 100,000 $\times g$ to yield a pellet (P100) and supernatant (S100) fraction. We found NLRP3 in all fractions irrespectively of LPS priming or concomitant IKK β inhibition (Figure 6C). However, when we further fractionated P100 across a linear sucrose gradient, we found NLRP3 to become enriched in the top fractions upon LPS stimulation, where we also found the PI4P-binding OSBP(PH)-mCherry fusion protein (Figure 6D). This enrichment of NLRP3 was blocked in the presence of TPCA-1, and, in line with our imaging data, unstimulated cells showed some NLRP3 enrichment on both ends of the gradient. Of note, the mitochondrial membrane protein TOMM40 was also present in the P100 fraction, but at the opposite end of where the OSBP(PH)-mCherry construct was found. We then analyzed the organelles present in fractions #2 and #11 via mass spectrometry (Table S2). The TGN, but not the *cis*-Golgi network, was highly enriched

in fraction #2 along with weakly PI4P⁺ organelles such as endosomes³³ (Figures 6E and S6G). Taken together, upon priming, NLRP3 translocates to PI4P-rich sites mostly on the TGN.

Based on these data, we hypothesized that the accumulation of NLRP3 on PI4P-rich sites induces NEK7-independent NLRP3 activation. To confirm this hypothesis, we directly tethered NLRP3 to PI4P by fusing it to the PH-domain of OSBP as reported before.¹⁰ Although a previously described K127A, K128A, K129A, and K130A quadruple mutant of mmNlrp3 (Nlrp3(4KA)) was incapable of localizing to the TGN in J774 cells, Nlrp3(4KA-OSBP(PH)) constitutively localized to the TGN as expected (Figure S6H). When we expressed wild-type Nlrp3, Nlrp3(4KA), and Nlrp3(4KA-OSBP(PH)) in *Nlrp3*^{-/-} J774 mouse macrophages, we found wild-type Nlrp3 to facilitate caspase-1 maturation in a NEK7-dependent manner and Nlrp3(4KA-OSBP(PH)) to activate caspase-1 independently of NEK7 (Figure 6F). Nlrp3(4KA) expectedly did not lead to any detectable caspase-1 processing (Figure 6F). Of note, these cells did not require priming with LPS, as they expressed Nlrp3 under the control of a doxycycline-inducible promoter, mirroring above results (Figure 2).

Together, these results demonstrate that IKK β induces NEK7-independent NLRP3 priming by increasing the recruitment of NLRP3 to PI4P and establish PI4P-recruitment of NLRP3 as a priming modality of the inflammasome (Figure S6I).

Discussion

Since its first description in 2001,³⁴ NLRP3 has attracted much attention as a key driver of antimicrobial and sterile inflammation.⁷ Nonetheless, despite being in the focus for almost two decades, the molecular mechanism of NLRP3 activation has remained obscure. The two-step model of inflammasome priming and activation predates the discovery of NLRP3 and inflammasomes altogether, originating from the notion that both a pro-inflammatory and a cell-death inducing signal are required to release mature IL-1 β from murine bone marrow-derived macrophages.³⁵ In retrospect, these early studies had assessed NLRP3 inflammasome activation employing a K⁺ efflux-inducing trigger. Subsequent studies have revealed that the pro-inflammatory signal indeed serves two independent functions in the context of NLRP3 inflammasome activation. Although this signal is critically required to induce pro-IL-1 β expression, it is also necessary to render NLRP3 activatable in the first place. This became apparent when studying the maturation of caspase-1, the expression of which is independent of a pro-inflammatory signal, as a proxy of NLRP3 inflammasome activation. Here, it has been revealed that unprimed macrophages do not mature caspase-1 upon K⁺ efflux-inducing stimuli^{13,36} but that additional priming by a pro-inflammatory signal was required to facilitate this step. Of note, this unique requirement of NLRP3 priming by a pro-inflammatory signal (referred to as signal 1 or priming in this manuscript) must not be confused with the signal that induces pro-IL-1 β expression. Indeed, although both signals can be provided through the same PRR, they can also be separated, and the pro-IL-1 β inducing stimulus is not necessary for NLRP3 inflammasome activation.

Although the two-step activation model constitutes an important conceptual framework for NLRP3 activation, it has proven to be an enormous conundrum because it is not trivial to allocate signaling events upstream of NLRP3 to either priming or activation. The fact that several pathways toward NLRP3 priming have been described³⁷ is likely attributable to stimulus-, cell type-, and species-dependent aspects as well as temporal dynamics playing an important role in this context. We conceptualize that priming serves the function to increase the cellular pool of NLRP3 molecules that are able to respond to an activating stimulus, either by upregulating production of the NLRP3 protein or by lowering the activation threshold of individual NLRP3 molecules. In this regard, we would interpret the existence of multiple redundant NLRP3 priming pathways as the possibility to integrate diverse pro-inflammatory inputs to achieve this activatable state. In fact, we consider this pleiotropy to be a key trait of NLRP3 priming, but not activation pathways. The mitotic spindle kinase NEK7 has been shown to be an essential cofactor of NLRP3 activation,^{20–22} and it has been suggested that NEK7 facilitates inflammasome formation by mediating recognition of the second signal.^{21,23} Studying the role of NEK7 in iPSC-cell-derived human macrophages, we made the unexpected discovery that NLRP3 activation can be fully operational in the absence of NEK7. By genetically dissecting NLRP3 inflammasome signaling, we uncovered that these cells employ a NEK7-independent signaling cascade instead that drives IKK β -dependent, post-translational priming of NLRP3. Although this IKK β -dependent priming signal is the default pathway by which human cells engage the NLRP3 inflammasome, murine macrophages predominantly rely on NEK7 for NLRP3 priming. However, they can bypass NEK7 and switch to IKK β -dependent priming under pro-inflammatory conditions signified by, for example, TLR activation. The NEK7-independence in human myeloid cells could not be attributed to species-specific constitutions of the NEK7 or NLRP3 molecules themselves: immunoprecipitation and reconstitution experiments showed that human NEK7 interacted with human NLRP3 and that NEK7 was able to facilitate NLRP3 activity. In line with this notion, iPSC-derived human macrophages also employ NEK7 to activate the NLRP3 inflammasome; however, this requires LPS priming and indicates a synergy between NEK7 and IKK β only observed at an early time point, when the IKK β post-translational priming mechanism is not yet fully operational. Indeed, in these cells, NEK7 becomes obsolete after prolonged LPS-priming when the IKK β priming cascade is active. Mechanistically, IKK β activity recruited NLRP3 to PI4P, a phospholipid enriched on the TGN. Tethering NLRP3 to PI4P led to inflammasome activation independently of NEK7, confirming that increased PI4P interaction serves to prime NLRP3 for inflammasome formation. Based on the redundancy between IKK β and NEK7 in facilitating NLRP3 inflammasome formation, we conclude that NEK7 serves as a priming factor of the NLRP3 inflammasome.

NEK7 holds a unique position among NLRP3 priming pathways in that it is constitutively expressed and apparently uncoupled from upstream signals in its pro-inflammatory capacity. It has been suggested that NEK7 is employed for NLRP3 activation to avoid inflammasome formation during mitosis, when NEK7 is not available.²² Furthermore, it has been speculated that the cellular perturbation triggering NLRP3 commonly occurs during mitosis, and thus, the dependency on NEK7 prevents inadvertent inflammasome activation during cell division.²³ However, the here-uncovered redundancy of NEK7 priming with other cell

cycle-independent priming pathways (e.g., IKK β) advocates against a specific de-coupling of NLRP3 inflammasome activation and proliferation. This is also in line with the fact that many NLRP3 inflammasome-competent cells of the innate immune system are postmitotic. As such, despite detailed mechanistic insight into how NEK7 can accelerate NLRP3 inflammasome activation, the physiological role of NEK7 remains to be determined. The redundancy of NEK7 with a priming factor that acts by enhancing the interaction of NLRP3 and PI4P suggests that NEK7 itself might be involved in recruiting NLRP3 to PI4P at the TGN.

The role of K⁺ efflux is currently debated in the field: although it was recently shown that K⁺ efflux alone is not sufficient to drive inflammasome activation in primed BMDMs and consequently argued that K⁺ efflux only promotes recruitment of NLRP3 to the TGN,¹⁰ an older report demonstrated that K⁺ efflux does indeed suffice: inflammasome activation did occur in response to K⁺ efflux in primed BMDMs.⁶ Our study shows that recruitment of NLRP3 to PI4P can be induced by IKK β activation independently of K⁺ efflux. In line with the latter report, K⁺ efflux was still required for inflammasome formation following IKK β -mediated PI4P recruitment of NLRP3, hinting at a role of K⁺ efflux beyond recruiting NLRP3 to PI4P. Whether K⁺ efflux or dispersal of the TGN serves as the ultimate trigger of NLRP3 inflammasome formation remains to be investigated. From the fact that both IKK β - and NEK7-mediated NLRP3 priming still require K⁺ efflux for inflammasome formation but that IKK β -mediated priming can bypass NEK7, we conclude that NEK7 itself acts as a priming factor upstream of K⁺ efflux. Of note, K⁺ efflux-independent NLRP3 activators have also been described.^{8,9} For one such agonist, Imiquimod, the NEK7 bypass was only activated in the presence of K⁺ efflux, suggesting that K⁺ efflux boosts NEK7-independent NLRP3 activation synergistically with IKK β .

Another study recently implicated IKK β in the recruitment of NLRP3 to the TGN.³⁸ In contrast with our findings, in their setting, Nigericin stimulation was still required for TGN recruitment of NLRP3, as reported previously.¹⁰ The authors concluded that IKK β enhances Nigericin-dependent TGN dispersal, which they suggested to be the cause of increased NLRP3 activity.³⁸ However, whether increased TGN dispersal is a cause or an effect of increased cell death cannot be concluded from their work. In our study, we observed that IKK β activation recruited NLRP3 to PI4P on an undispersed TGN independently of Nigericin stimulation or TGN dispersal in pyroptosis-deficient *Pycard*^{-/-} cells. We showed that recruiting NLRP3 to an intact TGN was sufficient for subsequent inflammasome formation independently of an additional priming stimulus. Hence, it is unlikely that the increased TGN dispersal observed by Nanda and colleagues would explain the priming effect of IKK β that we describe here. Rather, given that we observe K⁺ efflux to act synergistically with IKK β and NEK7, increased recruitment of NLRP3 to the TGN might explain the previously reported effects.³⁸

This study establishes NEK7 as a priming rather than an activation signal for NLRP3. Moreover, in its capacity as a priming factor NEK7 does not constitute an absolute requirement for NLRP3 inflammasome activation. Instead, a priming signal emanating from IKK β can fully compensate for NEK7 by enhancing the interaction of NLRP3 and

PI4P. This signal supersedes the NEK7 requirement in human myeloid cell lines and also represents the dominant priming entity in iPSC-derived human macrophages.

Limitations of the study

We have shown that NEK7-independent priming of NLRP3 depends on the kinase activity of IKK β but does not require *de novo* translation. However, the target that is phosphorylated by IKK β remains to be determined in future studies. To confirm that recruitment of NLRP3 to PI4P is sufficient for NEK7-independent inflammasome activation, we overexpressed an engineered fusion protein of NLRP3(4KA) and the PI4P-interacting PH domain of the protein OSBP that constitutively interacts with PI4P, as reported previously.¹⁰ Although we controlled for unspecific NLRP3 activation by expressing NLRP3 fused to a non-PI4P-binding point- mutated version of the same PH domain, we cannot exclude that engineering NLRP3 influenced its dependency on NEK7. Finally, owing to the fact that *Nek7*^{-/-} mice are not viable,³⁹ this study does not include an experiment showing that IKK β activation bypasses NEK7 *in vivo*.

Methods

Key Resources Table

REAGENT or RESOURCE	SOURCE	IDENTIFIER
Antibodies		
anti-Caspase-1 (p20) (human), mAb (Bally-1)	AdipoGen, San Diego, CA	Cat# AG-20B-0048-C100
anti-Caspase-1 (p20) (mouse), mAb (Casper-1)	AdipoGen	Cat# AG-20B-0042-C100
anti-NEK7	Abcam, Cambridge, UK	Cat# ab133514
anti-NLRP3/NALP3, mAb (Cryo-2)	AdipoGen	Cat# AG-20B-0014-C100
anti-Human IL-1 beta /IL-1F2	R&D Systems Inc, Minneapolis, MN	Cat# AF-201-NA
Chemicals, peptides, and recombinant proteins		
1-Thioglycerol (MTG)	Sigma-Aldrich, St. Louis, MO	Cat# M6145
Accutase	Stemcell Technologies, Vancouver, Canada	Cat# 07920
Adenosine 5'-triphosphate disodium salt hydrate	Sigma-Aldrich	Cat# A6419
Ascorbic Acid	Sigma-Aldrich	Cat# A4544-100G
B-27 supplement	Thermo Fisher Scientific, Waltham, MA	Cat# 17504-001
Blasticidin S HCl (10 mg/ml)	Thermo Fisher Scientific	Cat# A1113903
BSA	GE Healthcare, Chicago, IL	Cat# SH30574.01
CHIR99021	Miltenyi Biotec, Bergisch Gladbach, Germany	Cat# 130-103-926
Cycloheximide	Carl Roth, Karlsruhe, Germany	Cat# 8682.1
Doxycycline hyclate	Sigma-Aldrich	Cat# D9891-1G

Immunity. Author manuscript; available in PMC 2023 June 13.

3.1 IKK β primes inflammasome formation by recruiting NLRP3 to the trans-Golgi network

REAGENT or RESOURCE	SOURCE	IDENTIFIER
Geltrex	Thermo Fisher Scientific	Cat# A1413302
GeneJuice	Merck, Darmstadt, Germany	Cat# 70967-3
Ham's F12 nutrient mix	Thermo Fisher Scientific	Cat# 21765029
Herring Testis(HT)-DNA sodium salt	Sigma Aldrich	Cat# D6898
Hoechst-33342	Sigma-Aldrich	Cat# B2261-25MG
Human CSF-1 (M-CSF) (iPSC differentiation)	R&D Systems	Cat# 216-MC-005
Human Transferrin	Roche, Basel, Switzerland	Cat# 10-652-202-001
IMDM with GlutaMAX	Thermo Fisher Scientific	Cat# 31980022
Imiquimod (R837)	Invivogen	Cat# tlr1-imq
L-Glutamine	Thermo Fisher Scientific	Cat# 25030024
LFn-YscF	Rauch et al. ⁴⁰	N/A
Lipofectamine 2000 Transfection Reagent	Thermo Fisher Scientific	Cat# 11668019
LPS-EB Ultrapure	Invivogen, San Diego, CA	Cat# tlr1-3pelps
LysC	Wako	Cat# 12902541
MCC950	Sigma-Aldrich	Cat# PZ0280
MitoTracker DeepRed	Thermo Fisher Scientific	Cat# M22426
mTeSR1	Stemcell Technologies	Cat# 85850
N-2 Supplement	Thermo Fisher Scientific	Cat# 17502048
Nigericin sodium salt	Sigma-Aldrich	Cat# N7143
Pam3CSK4	Invivogen	Cat# tlr1-pms
Phorbol 12-myristate 13-acetate	ENZO Life Sciences, Farmingdale, NY	Cat# BML-PE160-0005
Protective antigen (pA)	Biotrend, Cologne, Germany	Cat# LL-171E
Puromycin Dihydrochloride	Carl Roth	Cat# 0240.4
R848	Invivogen	Cat# tlr1-r848-5
Recombinant Human BMP-4	R&D Systems	Cat# 314-BP-010
Recombinant Human CSF-1 (M-CSF) (BlaER1 differentiation)	Recombinantly produced	N/A
Recombinant Human DKK-1	R&D Systems	Cat# 5439-DK-010
Recombinant Human FGF2	R&D Systems	Cat# 233-FB-025
Recombinant Human IL-3	R&D Systems	Cat# 203-IL-010
Recombinant Human IL-3 (BLaER1 differentiation)	Recombinantly produced	N/A
Recombinant Human IL-6	R&D Systems	Cat# 206-IL-010
Recombinant Human SCF	R&D Systems	Cat# 255-SC-010
Recombinant Human VEGF	R&D Systems	Cat# 293-VE-010
ROCK Inhibitor Y-27632	Stemcell Technologies	Cat# 72302
Stempro-34 SFM	Thermo Fisher Scientific	Cat# 10639-011
Takinib	Selleck Chemicals, Houston, TX	Cat# S8663
TPCA-1	R&D Systems	Cat# 2559/10

Immunity. Author manuscript; available in PMC 2023 June 13.

REAGENT or RESOURCE	SOURCE	IDENTIFIER
Trypsin	Sigma-Aldrich	Cat# T6567
b-Estradiol	Sigma-Aldrich	Cat# E8875
Critical commercial assays		
Human IL-1 β ELISA Set II	BD Biosciences, San José, CA	Cat# 557953
Human Total IL-18 DuoSet ELISA	R&D Systems	Cat# DY318-05
MiSeq Reagent Kit v2, 300 Cycles	Illumina, San Diego, CA	Cat# MS-102-2002
Mouse CXCL10/IP-10/CRG-2 DuoSet ELISA	R&D Systems	Cat# DY466
Mouse TNF (Mono/Mono) ELISA Set II	BD Biosciences	Cat# 558534
OptEIA Human IL-6 ELISA Set	BD Biosciences	Cat# 555220
OptEIA Mouse IL-1 β Elisa Set	BD Biosciences	Cat# 559603
Pierce LDH Cytotoxicity Assay Kit	Thermo Fisher Scientific	Cat# 88954
Deposited data		
Mass spectrometry data of Figure 6E	This study	PRIDE: PXD035302
Immunoblot source data and raw numerical data used to plot the figures	This study	Mendeley data: https://doi.org/10.17632/h7vc8hnb7j.1
Experimental models: Cell lines		
BLaER1	Rapino et al. ²⁶	N/A
HEK-293T	Cavlar et al. ⁴¹	N/A
iPSC	Camargo Ortega et al. ⁴²	N/A
Mouse Macrophages, <i>Nlrp3</i> , <i>Asc-CFP</i> , <i>Cas9</i> -expressing	Franklin et al. ⁴³	N/A
THP-1	ATCC, Manassas, VA	Cat# TIB-202
Target sites of sgRNAs used in this study		
hsMAP3K7	GTAACACCAACTCATTGCGTGG	
hsNEK6	GTCTTTTCGCTGCTCGCTGGCGG	
hsNEK7	ATTACAGAAGGCTTACGACCGG	
hsNLRP3	GCTAATGATCGACTTCAATGGGG	
hsIKKB	ATGAAGGTATCTAAGCGCAGAGG	
mmMyd88	GGTCAAGAACAGCGATAGGCGG	
mmNek7	GTCTCTTGGATGGAGTGCCGG	
mmNlrp3	CCTCTCTGCTCATAACGACGAGG	
mmTicam1	GTACAGGCGAGCCACCGTCCAGG	
mmTlr4	GATCTACTCGAGTCAGAATGAGG	
mmPycard	GTGCAACTGCGAGAAGGCTATGG	
Recombinant DNA		
LentiCas9-Blast	Sanjana et al. ⁴⁴	N/A
LentiGuide-Puro	Sanjana et al. ⁴⁴	N/A
pBabe-U6-sgRNA-Cas9	Schmidt et al. ⁴⁵	N/A

Immunity. Author manuscript; available in PMC 2023 June 13.

REAGENT or RESOURCE	SOURCE	IDENTIFIER
pBlast-hsNEK7	This study	N/A
pBlast-mCherry-OSBP(PH)	This study	N/A
pBlast-mmNek7	This study	N/A
pLIX-hsNLRP3	This study	N/A
pLIX-mmNlrp3	This study	N/A
pLIX-mVenus-mmNlrp3	This study	N/A
pLIX-mVenus-mmNlrp3(4KA)	This study	N/A
pLIX-mVenus-mmNlrp3(4KA-OSBP(PH))	This study	N/A
pLK0.1-sgRNA-CMV-GFP	Schmid-Burgk et al. ⁴⁶	N/A
pRP-Asc-RFP	This study	N/A
prZ-CMV-Cas9	Schmid-Burgk et al. ⁴⁵	N/A
Software and algorithms		
CellProfiler 3.1.5	Carpenter et al. ⁴⁷	https://cellprofiler.org
CHOPCHOP	Labu et al. ⁴⁸	https://chopchop.cbu.uib.no
MaxQuant 2.0.3	Cox and Mann ⁴⁹	https://maxquant.org
Outknocker	Schmid-Burgk et al. ⁴⁶	http://www.outknocker.org
Perseus	Tyanova et al. ⁵⁰	https://maxquant.org/perseus/
Prism 9.0	GraphPad, San Diego, CA	https://www.graphpad.com/scientific-software/prism/

Experimental Model and Subject Details

BLaER1 cells—BLaER1 cells (female) were cultivated in RPMI supplemented with 10 % FCS, 1 mM pyruvate, 100 U/ml penicillin and 100 mg/ml streptomycin at 37 °C and 5 % CO₂. BLaER1 cells were differentiated in medium containing 10 ng/ml hrIL-3, 10 ng/ml hrCSF-1 (MCSF) and 100 nM b-estradiol for 5-6 days. In the course of these studies, we serendipitously identified that BLaER1 cells express transcripts of SMRV (squirrel monkey retrovirus) and subsequent experiments confirmed that BLaER1 cells harbor the SMRV proviral genome. Testing early passages of BLaER1 cells by Dr. Thomas Graf (personal communication) confirmed that the parental BLaER1 cell line²⁶ is positive for SMRV. Of note, extensive characterization of BLaER1 monocytes in comparison to other human myeloid cells has not provided any indication that SMRV positivity would impact on the functionality of these cells as myeloid cells. Samples of other cell lines used in this work were confirmed to be free of SMRV by PCR. All BLaER1 cell experiments were conducted on a *CASP4*^{-/-} background (herein referred to as control).

THP-1 cells—THP-1 cells (male) were obtained from ATCC and cultivated in RPMI supplemented with 10 % FCS, 1 mM pyruvate, 100 U/ml penicillin and 100 mg/ml streptomycin at 37 °C and 5 % CO₂. THP-1 cells were differentiated by adding 100 ng/ml PMA to the medium for 18 hours, rinsed off with ice-cold PBS and replated for experiments.

mmMacs and J774 mouse macrophages—Mouse macrophages were cultivated in DMEM supplemented with 10 % FCS, 1 mM pyruvate 100 U/ml penicillin and 100 mg/ml streptomycin at 37 °C and 5 % CO₂. mmMacs were detached for passaging with 0.05 % Trypsin at 37 °C for 15 minutes after one PBS wash and then rinsed off with DMEM. J774 cells were passaged by scraping in 5 ml fresh DMEM and transferred to new flasks.

hiPSC, hiPS-Macs cell culture—Human induced pluripotent stem cells (hiPSCs) used to make NEK7^{-/-} hiPSCs were kindly provided by Adam O’Neill and Magdalena Götz.⁴² hiPSCs for IKKB^{-/-} were purchased from XCell Science. hiPSCs were cultivated on Geltrex-coated plates in complete mTeSR1 Medium at 37 °C and 5 % CO₂ and detached for passaging using 1.5 ml Accutase for 5 minutes at 37 °C after a PBS wash. After passaging, cells were cultivated in the presence of 5 mM ROCK-Inhibitor overnight.

Differentiation of hiPSCs into hiPS-Macs—Differentiation into iPS-Macs was achieved as described previously.²⁵ Briefly, 150,000 hiPSC were plated into a one well of a Geltrex- coated 6-well plate and differentiated in StemPro base medium with StemPro Supplement, 200 mg/ml human transferrin, 2 mM glutamine, 0.45 mM MTG and 0.5 mM ascorbic acid (= StemPro medium, ascorbic acid was added just before use) by stimulation with 50 ng/ml VEGF, 5 ng/ml BMP-4 and 2 mM CHIR99021 at 5 % oxygen for two days, followed by two days of stimulation with 50 ng/ml VEGF, 5 ng/ml BMP-4 and 20 ng/ml FGF2. From day four, StemPro medium was supplemented with 15 ng/ml VEGF and 5 ng/ml FGF2. Starting at day six, 10 ng/ml VEGF, 10 ng/ml FGF2, 50 ng/ml SCF, 30 ng/ml DKK-1, 10 ng/ml IL-6 and 20 ng/ml IL-3 were added to StemPro medium until day ten. From day eight, cells were cultivated under normoxic conditions. From day twelve, 10 ng/ml FGF2, 50 ng/ml SCF, 10 ng/ml IL-6 and 20 ng/ml IL-3 were added to StemPro medium. Starting at day sixteen, cells were cultivated in 75 % IMDM with 25 % F12 supplement, N2 supplement, B-27 supplement, 0.05 % BSA and 100 U/ml penicillin and 100 mg/ml streptomycin (= SF-Diff medium) supplemented with 50 ng/ml rhCSF-1 (M-CSF) at least until day 28. Culture medium was exchanged as necessary, but at least every two days. After differentiation, hiPS-Macs were carefully harvested from the supernatant, spun down and replated in RPMI with 10 % FCS, 1 mM Pyruvate, 100 U/ml Penicillin and 100 mg/ml Streptomycin for experiments.

HEK-293T cells—HEK-293T cells were cultivated in DMEM with 10 % FCS, 1 mM pyruvate, 100 U/ml penicillin and 100 mg/ml streptomycin at 37 °C and 5 % CO₂. For passaging, cells were washed with PBS once and then incubated with 0.05 % Trypsin at 37° for 5 minutes. Cells were then rinsed off with DMEM.

Trans-Golgi network imaging—J774 macrophages expressing mVenus-mmNlrp3 and the PH-domain of hsOSBP (OSBP-PH) fused to mCherry were plated in ibidi 8-well slides (100,000 per well in 200 ml of DMEM) and imaged on a Nikon Eclipse Ti spinning disk confocal microscope with 100× magnification on the following day. Results were manually quantified from at least 10 randomly selected areas per condition per replicate using FIJI.⁵¹ For nuclear staining, Hoechst-33342 was diluted to a final concentration of 10 mg/ml.

ASC speck imaging—ASC specks in transiently transfected HEK-293T cells were imaged 24 hours after transfection on a Leica Hi8 epifluorescence microscope using 10 \times magnification. Specks were quantified with CellProfiler.⁴⁷

Immunoblotting—Cells were lysed at approximately 5 Mio/ml in 1 \times Lämmli Buffer and boiled for 5 minutes at 95 °C. For precipitation of total protein from supernatants, stimulations were done in medium containing 3% FCS. Precipitation of total protein from supernatants was achieved by combining 700 μ l of supernatant with 700 μ l MeOH and 150 μ l of CHCl₃. Samples were spun down at 20.000 g for 20 minutes, and the upper phase was discarded. Again, 700 μ l MeOH were added and samples were centrifuged at 20.000 g for 20 minutes. The pellet was then dried and resuspended in 100 μ l 1 \times Lämmli buffer and boiled at 95 °C for 5 minutes. Samples were run on 12% SDS-PAGE gels at 150 V for 85 minutes and were subsequently transferred onto a nitrocellulose membrane at 100 V for 75 minutes at 4 °C. Membranes were then blocked in 5 % milk for 1 hour at room temperature. Primary and secondary antibodies were diluted in 1-5 % milk.

ELISA and LDH assay—LDH assays were done on supernatants immediately after experiments. Results are presented relative to a lysis control from the same experiment with the values of unstimulated controls subtracted as background. ELISAs were done according to manufacturer's instructions on supernatants stored at -20 °C.

Stimulation of immune signaling—NLRP3 was primed as indicated with 1 mg/ml Pam₃CSK₄ or 200 ng/ml LPS. NLRP3 was activated with 5 mM ATP or Nigericin at

6.5 mM (BLaER1 cells) or 10 mM (all other cells) as indicated. To activate the AIM2 inflammasome 400 ng HT-DNA were transfected into a 96-well with 0.5 ml Lipofectamine in 50 μ l OptiMEM by incubating OptiMEM and Lipofectamine for 5 minutes followed by 20 minutes of incubation of the Lipofectamine-DNA mix in OptiMEM and dropwise addition of the mix to the cells. For immunoblots, transfections were done in a 12-well format. The amount of Lipofectamine and HT-DNA was scaled accordingly by well area. The NAIP- NLRC4 inflammasome was activated with an anthrax toxin lethal factor fused to the *Burkholderia* T3SS needle protein (LFn-YscF, 0.025 mg/ml), which was delivered into cells with protective antigen (pA, 0.25 mg/ml).⁴⁰ If not otherwise indicated, cells were stimulated with this construct (herein referred to as Needle Tox) for 2 hours.

Inhibition of translation—For mmMacs, cycloheximide (CHX) was added to the medium 30 minutes before stimulation to a final concentration of 10 mg/ml. For BLaER1 cells, CHX was added to the medium simultaneously with LPS at the indicated concentrations in the range of 1-10 mg/ml.

Doxycyclin-inducible gene expression—In BLaER1 cells and J774 *Pycard*^{-/-} cells transduced with pLIX-Puro derived vectors, gene expression was induced by adding medium to a final concentration of 1 mg/ml doxycycline for the last 24 hours of differentiation. J774 cells transduced with Nlrp3 variants for analysis of caspase-1 processing were stimulated with 1 mg/ml doxycycline for 18 hours before stimulation for inflammasome activation.

Inhibition of TAK1, IKK β and NLRP3—Takinib was added to a final concentration of 50 mM as indicated. TPCA-1 was used at 5 mM final concentration as indicated. MCC950 was added as indicated to a final concentration of 10 mM.

Inhibition and induction of K⁺ efflux—To block K⁺ efflux, Potassium chloride (KCl) was added to medium together with the priming stimulus to the indicated final concentrations. The osmolarity of the medium was kept constant over all conditions. To induce K⁺ efflux, cells were stimulated in sterile Hank's balanced salt solution with (140 mM NaCl, 5 mM KCl, 1.3 mM CaCl₂, 1.0 mM MgSO₄, 10 mM HEPES (pH 7.5), 5.5 mM glucose) or without potassium (145 mM NaCl, 1.3 mM CaCl₂, 1.0 mM MgSO₄, 10 mM HEPES (pH 7.5), 5.5 mM glucose) with 10% FCS as described before.¹⁰

Sucrose gradient fractionation—For the fractionation experiment, *Nlrp3*^{-/-} × *Pycard*^{+/-} J774 cells stably transduced with pLI-mVenus-mmNLRP3, pBlast-AUG- OSBP(PH)-mCherry were used.

Two days prior to stimulation, 1310⁷ cells were plated per 15 cm dish, using 2 dishes per condition (unstimulated, LPS, TPCA-1 > LPS). 18-20 hours prior to stimulation, doxycycline was added to a final concentration of 1 mg/ml to induce expression of mVenus-mmNLRP3. As indicated, cells were pre-treated with 5 mM TPCA-1 for 30 minutes. Subsequently, cells were stimulated with 200 ng/ml LPS for 30 minutes. Cells were washed once with PBS and scraped using 500 mL of ice-cold isotonic buffer (0.25 M sucrose, 10 mM Tris-HCl (pH 7.5), 10 mM KCl, 1.5 mM MgCl₂, 1 mM DTT) supplemented with protease inhibitor. Then, cells were homogenized by performing 30 strokes with a 29G needle (VWR, BDAM324891). Lysates were centrifuged at 10003g for 5 minutes at 4°C to remove nuclei and any remaining cells. The resulting supernatant was centrifuged at 50003g for 10 minutes at 4°C to obtain the heavy membrane fraction (pellet, P5). The resulting supernatant was centrifuged at 100,000g for 20 minutes at 4°C in a TLA 120.2 rotor (Beckman Coulter) to obtain the light membrane fraction (pellet, P100) and the cytosolic fraction (supernatant, S100). The fractions P5 and P100 were washed once with isotonic buffer, pelleted repeating the centrifugation step at 50003g and 100,000g, respectively, and resuspended in 500 mL isotonic buffer.

The fraction P100 was then loaded onto a 20%-60% continuous sucrose density gradient (10 mM Tris-HCl (pH 7.5), 100 mM KCl, 1.5 mM MgCl₂, 1 mM DTT, and protease inhibitor cocktail). The gradients were centrifuged in an SW40Ti rotor (Beckman Coulter) at 170,085g for two hours at 4°C and 13 fractions of 0.93 ml each were collected using a BioComp Gradient Station. 30 mL of each fraction were used for SDS-PAGE followed by immunoblotting.

Furthermore, to analyze the distribution of various organelle markers, the fractions P5, P100 and S100 were subjected to SDS- PAGE followed by immunoblotting. Protein concentrations were determined by BCA assay and adjusted between samples (unstimulated, LPS, TPCA-1 > LPS) for each of the fractions separately.

Mass spectrometry sample preparation—Sucrose gradient fractions #2 and #11 were lysed in 1% SDC with 100mM Tris-HCl. Protein amounts from each sample were adjusted to 30 mg with a BCA protein assay kit. Samples were reduced with 10mM tris(2-carboxy(ethyl)phosphine) (TCEP), alkylated with 40mM 2-chloroacetamide (CAA), and digested with trypsin and lysC (1:50, enzyme/protein, w/w) overnight. Digested peptides were desalted using SDB-RPS-stage tips. Desalted peptides were resolubilized in 5ml 2% ACN and 0.3% TFA and about 200 ng of peptides were injected into the mass spectrometer.

Samples were loaded onto 50-cm columns packed in-house with C18 1.9mM ReproSil particles (Dr. Maisch GmbH), with an EASY- nLC 1200 system (Thermo Fisher Scientific) coupled to the MS (Orbitrap Exploris 480, Thermo Fisher Scientific). A homemade column oven maintained the column temperature at 60°C. Peptides were introduced onto the column with buffer A (0.1% formic acid) and were eluted with a 120-min gradient starting at 5% buffer B (80% ACN, 0.1% formic acid) followed by a stepwise increase to 30% in 95 min, 65% in 5 min, 95% in 235 min and 5% in 235 min at a flow rate of 300 nL/min. Samples were measured in data-dependent acquisition with a TopN MS method in which one full scan (300–1650 m/z, R=60,000 at 200m/z) at an Automatic Gain Control (AGC) target of 3310e6 ions was first performed, followed by 15 data-dependent MS/MS scans with higher-energy collisional dissociation (AGC target 1×10e5 ions, maximum injection time at 25ms, isolation window 1.4 m/z, normalized collision energy 30%, and R=15,000 at 200 m/z). Dynamic exclusion of 30 s was enabled.

Analysis of MS samples—The MS raw files were processed in MaxQuant version 2.0.3.0⁴⁹ and fragment lists were queried against the mouse UniProt FASTA database (25,320 entries, 10/2020) with cysteine carbamidomethylation as a fixed modification and N-terminal acetylation and methionine oxidations as variable modifications. Enzyme specificity was set as C-terminal to arginine and lysine as expected using trypsin and lysC as proteases and a maximum of two missed cleavages.

Bioinformatics analysis of the MS data was performed using the Perseus software suite (version 1.6.7.0).⁵⁰ After filtering to remove potential contaminants, reverse hits, and proteins only identified by modification sites, the remaining summed intensities were log₂-transformed. Quantified proteins were filtered for at least 2 valid values in one fraction across three biological replicates. Missing values were imputed by sampling from a normal distribution (width 0.3, downshift 1.8) and significantly up- or downregulated proteins were determined by two-sided Student's t-test (FDR < 0.05, S0 R 1.5). To determine the systematic enrichment or de-enrichment of a select list of GOCC annotated organelles in each fraction a Fisher's exact test was performed on the significantly differentially regulated proteins between the two fractions.

Transient Transfection of HEK-293T cells—HEK-293T cells were transiently transfected with 400 ng plasmid DNA in 50 ml OptiMEM with 1 ml GeneJuice by incubating GeneJuice with OptiMEM for 5 minutes followed by 15 minutes of incubation of the DNA-GeneJuice mix in OptiMEM. DNA concentrations were kept constant across all conditions using pBluescript as stuffer DNA.

Plasmid DNA purification—Plasmid DNA was purified from *E.Coli* DH5a using a Thermo HiPure Maxiprep Kit according to manufacturer's instructions.

Preparation of lentiviral particles—Lentiviral particles were prepared according to.⁵² Briefly, HEK-293T cells were transfected with 20 mg transfer plasmid, 15 mg pCMVD8.91 packaging plasmid and 6 mg pMD2.G VSV-G pseudotyping plasmid dish by diluting the plasmids in 1 ml 1× HBS, adding 50 ml 2.5 M Calcium chloride and gently pipetting the mix onto a 10-cm dish with approximately 6 Mio. HEK-293T cells in fresh medium. Alternatively, pMDLg/pRRE and pRSV-REV were used as packaging plasmids.⁵³ After 8 hours the medium was exchanged. Supernatants were harvested 48 hours later, spun down and filtered before being used to transduce target cells. Successfully transduced cells were selected with 2.5 - 5 mg/ml puromycin or 10 mg/ml blasticidin S for 48 hours, or FACSsorted for fluorescence markers.

Genome editing and overexpression—sgRNA oligos were designed using CHOPCHOP⁴⁸ and cloned into expression plasmids as described previously.^{44,46} BLaER1 cells were electroporated in OptiMEM with 5 mg of plasmids driving expression of Cas9 and an sgRNA on a BioRad GenePulser XCell as described previously.⁴⁵ THP-1 cells and murine macrophages were transduced with lentiviral particles driving expression of Cas9 (Lenti-Cas9-Blast⁴⁴) or an sgRNA (LentiGuide-Puro⁴⁴). HEK-293T cells were transiently transfected with plasmids driving expression of Cas9 or an sgRNA.

hiPS cells conditioned to grow as single clones were electroporated with Cas9-crRNA-trRNA complexes (RNPs) targeting *NEK7* on a 4D-Nucleofector (Lonza Bioscience). Grown single clones were duplicated, lysed and out-of-frame editing in *NEK7* was analyzed via deep sequencing as described previously.⁴⁶ Several *NEK7*^{-/-} and *NEK7*^{+/+} clones were expanded and used for experiments. To generate *IKBKB*^{-/-} hiPSCs, XCL1 hiPS cells were electroporated with 0.5 mg of plasmids driving expression of Cas9 and an sgRNA targeting *IKBKB* with a 4D-Nucleofector (Lonza Bioscience). Grown single clones were picked and the sequence of the targeted *IKBKB* region was confirmed by Sanger sequencing.

Plasmids—Cloning of genes of interest into pLIX, pRP and pFUGW backbones was performed by conventional restriction enzyme cloning. pMDLg/pRRE was a gift from Didier Trono (Addgene plasmid #12251; <http://n2t.net/addgene:12251>; RRID:Addgene_12251), pRSV-Rev was a gift from Didier Trono (Addgene plasmid #12253; <http://n2t.net/addgene:12253>; RRID:Addgene_12253), pLIX_403 (herein referred to as pLIX) was a gift from David Root (Addgene plasmid #41395; <http://n2t.net/addgene:41395>; RRID:Addgene_41395). LentiGuide-Puro (Addgene plasmid #52963; <http://n2t.net/addgene:52963>; RRID:Addgene_52963) and lentiCas9-Blast (Addgene plasmid #52962; <http://n2t.net/addgene:52962>; RRID:Addgene_52962) were a gift from Feng Zhang. pTY-zeo-NLRP3(127-128-129-130 4KA)-GFP and pTY-zeo-Flag-NLRP3(DKDKK OSBPPH) were a gift from Zhijian J. Chen.¹⁰

Quantification And Statistical Analysis

Numbers of independent replicates (n) are reported in the respective figure legends. p-values were calculated based on two-way ANOVAs followed by Šidák's multiple comparisons test for groups containing two elements, or Tukey's test for larger groups. Dunnett's test was used wherever comparing all experimental conditions to one control instead of all other conditions was appropriate as indicated in the respective figure legends. All statistical analyses were done using GraphPad Prism 9. *p < 0.05, **p < 0.01, ***p < 0.001, ns p \geq 0.05.

Supplementary Material

Refer to Web version on PubMed Central for supplementary material.

Acknowledgements

We kindly thank Larissa Hansbauer, Jochen Rech, Claudia Ludwig, and Andreas Wegerer (Gene Center, LMU) for great technical support; the BioSysM FACS Core Facility (Gene Center, LMU) for cell sorting; the BioSysM Liquid Handling Unit (Gene Center, LMU) for lab automation; the Center for Advanced Light Microscopy (CALM) for support with confocal microscopy; Adam O'Neill and Magdalena Götz (Department of Physiological Genomics, LMU) for providing us with the hiPSCs and helping us set up experiments with these cells; Russell Vance (UC Berkeley, USA) for providing us with the Needle Tox expression plasmid; and Manuela Moldt and Karl-Peter Hopfner (Gene Center, LMU) for help in producing the Needle Tox protein. This work was funded by the European Research Council grant ERC-2020-ADG ENGINES (101018672), the Deutsche Forschungsgemeinschaft (DFG, German Research Foundation) CRC 1403 (project number 414786233), and the Fondation Bettencourt Schueller to V.H.

Data and code availability

Mass spectrometry data have been deposited to the ProteomeXchange Consortium via the PRIDE partner repository (PRIDE: PXD035302) and are publicly available as of the date of publication.

Immunoblot source data and raw numerical data used to plot the figures were deposited on Mendeley Data: <https://doi.org/10.17632/h7vc8hnb7j.1>

Any additional information required to reanalyze the data reported in this paper is available from the lead contact upon request. This paper does not report original code.

References

1. Broz P, Dixit VM. Inflammasomes: mechanism of assembly, regulation and signalling. *Nat Rev Immunol.* 2016; 16: 407–420. DOI: 10.1038/nri.2016.58 [PubMed: 27291964]
2. Dinarello CA. Overview of the IL-1 family in innate inflammation and acquired immunity. *Immunol Rev.* 2018; 281: 8–27. DOI: 10.1111/imr.12621 [PubMed: 29247995]
3. Vande Walle L, Lamkanfi M. Pyroptosis. *Curr Biol.* 2016; 26: R568–R572. DOI: 10.1016/j.cub.2016.02.019 [PubMed: 27404251]
4. Patel MN, Carroll RG, Galván-Peña S, Mills EL, Olden R, Triantafilou M, Wolf AI, Bryant CE, Triantafilou K, Masters SL. Inflammasome priming in sterile inflammatory disease. *Trends Mol Med.* 2017; 23: 165–180. DOI: 10.1016/j.molmed.2016.12.007 [PubMed: 28109721]
5. Swanson KV, Deng M, Ting JP-Y. The NLRP3 inflammasome: molecular activation and regulation to therapeutics. *Nat Rev Immunol.* 2019; 19: 477–489. DOI: 10.1038/s41577-019-0165-0 [PubMed: 31036962]

6. Muñoz-Planillo R, Kuffa P, Martínez-Colón G, Smith BL, Rajendiran TM, Nuñez G. K⁺ efflux is the common trigger of NLRP3 inflammasome activation by bacterial toxins and particulate matter. *Immunity*. 2013; 38: 1142–1153. DOI: 10.1016/j.immuni.2013.05.016 [PubMed: 23809161]
7. Gaidt MM, Hornung V. The NLRP3 inflammasome renders cell death pro-inflammatory. *J Mol Biol*. 2018; 430: 133–141. DOI: 10.1016/j.jmb.2017.11.013 [PubMed: 29203171]
8. Gaidt MM, Ebert TS, Chauhan D, Schmidt T, Schmid-Burgk JL, Rapino F, Robertson AAB, Cooper MA, Graf T, Hornung V. Human monocytes engage an alternative inflammasome pathway. *Immunity*. 2016; 44: 833–846. [PubMed: 27037191]
9. Groß CJ, Mishra R, Schneider KS, Médard G, Wettmarshausen J, Dittlein DC, Shi H, Gorka O, Koenig PA, Fromm S, et al. K⁽⁺⁾ efflux-independent NLRP3 inflammasome activation by small molecules targeting mitochondria. *Immunity*. 2016; 45: 761–773. DOI: 10.1016/j.immuni.2016.08.010 [PubMed: 27692612]
10. Chen J, Chen ZJ. PtdIns4P on dispersed trans-Golgi network mediates NLRP3 inflammasome activation. *Nature*. 2018; 564: 71–76. DOI: 10.1038/s41586-018-0761-3 [PubMed: 30487600]
11. Hornung V, Latz E. Critical functions of priming and lysosomal damage for NLRP3 activation. *Eur J Immunol*. 2010; 40: 620–623. DOI: 10.1002/eji.200940185 [PubMed: 20201015]
12. Bauernfeind FG, Horvath G, Stutz A, Alnemri ES, MacDonald K, Speert D, Fernandes-Alnemri T, Wu J, Monks BG, Fitzgerald KA, et al. Cutting edge: NF- κ B activating pattern recognition and cytokine receptors license NLRP3 inflammasome activation by regulating NLRP3 expression. *J Immunol*. 2009; 183: 787–791. DOI: 10.4049/jimmunol.0901363 [PubMed: 19570822]
13. Kahlenberg JM, Lundberg KC, Kertesz SB, Qu Y, Dubyak GR. Potentiation of caspase-1 activation by the P2X7 receptor is dependent on TLR signals and requires NF- κ B-driven protein synthesis. *J Immunol*. 2005; 175: 7611–7622. DOI: 10.4049/jimmunol.175.11.7611 [PubMed: 16301671]
14. Juliana C, Fernandes-Alnemri T, Kang S, Farias A, Qin F, Alnemri ES. Non-transcriptional priming and deubiquitination regulate NLRP3 inflammasome activation. *J Biol Chem*. 2012; 287: 36617–36622. DOI: 10.1074/jbc.M112.407130 [PubMed: 22948162]
15. Lin K-M, Hu W, Troutman TD, Jennings M, Brewer T, Li X, Nanda S, Cohen P, Thomas JA, Pasare C. IRAK-1 bypasses priming and directly links TLRs to rapid NLRP3 inflammasome activation. *Proc Natl Acad Sci USA*. 2014; 111: 775–780. [PubMed: 24379360]
16. Bauernfeind F, Niepmann S, Knolle PA, Hornung V. Aging-associated TNF production primes inflammasome activation and NLRP3-related metabolic disturbances. *J Immunol*. 2016; 197: 2900–2908. DOI: 10.4049/jimmunol.1501336 [PubMed: 27566828]
17. Shim D-W, Lee K-H. Posttranslational regulation of the NLR family pyrin domain-containing 3 inflammasome. *Front Immunol*. 2018; 9: 1054. doi: 10.3389/fimmu.2018.01054 [PubMed: 29868015]
18. Barry R, John SW, Liccardi G, Tenev T, Jaco I, Chen CH, Choi J, Kasperkiewicz P, Fernandes-Alnemri T, Alnemri E, et al. SUMO-mediated regulation of NLRP3 modulates inflammasome activity. *Nat Commun*. 2018; 9: 3001 doi: 10.1038/s41467-018-05321-2 [PubMed: 30069026]
19. McKee CM, Coll RC. NLRP3 inflammasome priming: a riddle wrapped in a mystery inside an enigma. *J Leukoc Biol*. 2020; 108: 937–952. DOI: 10.1002/JLB.3MR0720-513R [PubMed: 32745339]
20. Schmid-Burgk JL, Chauhan D, Schmidt T, Ebert TS, Reinhardt J, Endl E, Hornung V. A genome-wide CRISPR screen identifies NEK7 as an essential component of NLRP3 inflammasome activation. *J Biol Chem*. 2015; 291: 103–109. DOI: 10.1074/jbc.C115.700492 [PubMed: 26553871]
21. He Y, Zeng MY, Yang D, Motro B, Nuñez G. NEK7 is an essential mediator of NLRP3 activation downstream of potassium efflux. *Nature*. 2016; 530: 354–357. DOI: 10.1038/nature16959 [PubMed: 26814970]
22. Shi H, Wang Y, Li X, Zhan X, Tang M, Fina M, Su L, Pratt D, Bu CH, Hildebrand S, et al. NLRP3 activation and mitosis are mutually exclusive events coordinated by NEK7, a new inflammasome component. *Nat Immunol*. 2016; 17: 250–258. DOI: 10.1038/ni.3333 [PubMed: 26642356]
23. Sharif H, Wang L, Wang WL, Magupalli VG, Andreeva L, Qiao Q, Hauenstein AV, Wu Z, Nuñez G, Mao Y, Wu H. Structural mechanism for NEK7-licensed activation of NLRP3 inflammasome. *Nature*. 2019; 570: 338–343. DOI: 10.1038/s41586-019-1295-z [PubMed: 31189953]

24. He Y, Hara H, Nuñez G. Mechanism and regulation of NLRP3 inflammasome activation. *Trends Biochem Sci.* 2016; 41: 1012–1021. DOI: 10.1016/j.tibs.2016.09.002 [PubMed: 27669650]
25. Takata K, Kozaki T, Lee CZW, Thion MS, Otsuka M, Lim S, Utami KH, Fidan K, Park DS, Malleret B, et al. Induced-pluripotent-stem-cell-derived primitive macrophages provide a platform for modeling tissue-resident macrophage differentiation and function. *Immunity.* 2017; 47: 183–198. e6 doi: 10.1016/j.immuni.2017.06.017 [PubMed: 28723550]
26. Rapino F, Robles EF, Richter-Larrea JA, Kallin EM, Martinez-Climent JA, Graf T. C/EBP α induces highly efficient macrophage transdifferentiation of B lymphoma and leukemia cell lines and impairs their tumorigenicity. *Cell Rep.* 2013; 3: 1153–1163. DOI: 10.1016/j.celrep.2013.03.003 [PubMed: 23545498]
27. Gaidt MM, Ebert TS, Chauhan D, Ramshorn K, Pinci F, Zuber S, O’Duill F, Schmid-Burgk JL, Hoss F, Buhmann R, et al. The DNA inflammasome in human myeloid cells is initiated by a STING-cell death program upstream of NLRP3. *Cell.* 2017; 171: 1110–1124. e18 doi: 10.1016/j.cell.2017.09.039 [PubMed: 29033128]
28. Coll RC, Robertson AAB, Chae JJ, Higgins SC, Muñoz-Planillo R, Inserra MC, Vetter I, Dungan LS, Monks BG, Stutz A, et al. A small-molecule inhibitor of the NLRP3 inflammasome for the treatment of inflammatory diseases. *Nat Med.* 2015; 21: 248–255. [PubMed: 25686105]
29. Fernandes-Alnemri T, Kang S, Anderson C, Sagara J, Fitzgerald KA, Alnemri ES. Cutting edge: TLR signaling licenses IRAK1 for rapid activation of the NLRP3 inflammasome. *J Immunol.* 2013; 191: 3995–3999. DOI: 10.4049/jimmunol.1301681 [PubMed: 24043892]
30. Kang S, Fernandes-Alnemri T, Rogers C, Mayes L, Wang Y, Dillon C, Roback L, Kaiser W, Oberst A, Sagara J, et al. Caspase-8 scaffolding function and MLKL regulate NLRP3 inflammasome activation downstream of TLR3. *Nat Commun.* 2015; 6 7515 doi: 10.1038/ncomms8515 [PubMed: 26104484]
31. DeLaney AA, Berry CT, Christian DA, Hart A, Bjanes E, Wynosky-Dolfi MA, Li X, Tummers B, Udalova IA, Chen YH, et al. Caspase-8 promotes c-Rel-dependent inflammatory cytokine expression and resistance against *Toxoplasma gondii*. *Proc Natl Acad Sci USA.* 2019; 116: 11926–11935. DOI: 10.1073/pnas.1820529116 [PubMed: 31147458]
32. Mercurio F, Zhu H, Murray BW, Shevchenko A, Bennett BL, Li J, Young DB, Barbosa M, Mann M, Manning A, Rao A. IKK-1 and IKK-2: cytokine-activated I κ B kinases essential for NF- κ B activation. *Science.* 1997; 278: 860–866. DOI: 10.1126/science.278.5339.860 [PubMed: 9346484]
33. Posor Y, Jang W, Haucke V. Phosphoinositides as membrane organizers. *Nat Rev Mol Cell Biol.* 2022; doi: 10.1038/s41580-022-00490-x
34. Hoffman HM, Mueller JL, Broide DH, Wanderer AA, Kolodner RD. Mutation of a new gene encoding a putative pyrin-like protein causes familial cold autoinflammatory syndrome and Muckle-Wells syndrome. *Nat Genet.* 2001; 29: 301–305. DOI: 10.1038/ng756 [PubMed: 11687797]
35. Hogquist KA, Nett MA, Unanue ER, Chaplin DD. Interleukin 1 is processed and released during apoptosis. *Proc Natl Acad Sci USA.* 1991; 88: 8485–8489. DOI: 10.1073/pnas.88.19.8485 [PubMed: 1924307]
36. Mariathasan S, Newton K, Monack DM, Vucic D, French DM, Lee WP, Roose-Girma M, Erickson S, Dixit VM. Differential activation of the inflammasome by caspase-1 adaptors ASC and Ipaf. *Nature.* 2004; 430: 213–218. DOI: 10.1038/nature02664 [PubMed: 15190255]
37. Gros Lambert M, Py BF. Spotlight on the NLRP3 inflammasome pathway. *J Inflamm Res.* 2018; 11: 359–374. DOI: 10.2147/JIR.S141220 [PubMed: 30288079]
38. Nanda SK, Prescott AR, Figueras-Vadillo C, Cohen P. IKK β is required for the formation of the NLRP3 inflammasome. *EMBO Rep.* 2021; 22 e50743 doi: 10.15252/embr.202050743 [PubMed: 34403206]
39. Salem H, Rachmin I, Yissachar N, Cohen S, Amiel A, Haffner R, Lavi L, Motro B. Nek7 kinase targeting leads to early mortality, cytokinesis disturbance and polyploidy. *Oncogene.* 2010; 29: 4046–4057. DOI: 10.1038/onc.2010.162 [PubMed: 20473324]

40. Rauch I, Tenthorey JL, Nichols RD, Al Moussawi K, Kang JJ, Kang C, Kazmierczak BI, Vance RE. NAIP proteins are required for cytosolic detection of specific bacterial ligands in vivo. *J Exp Med.* 2016; 213: 657–665. DOI: 10.1084/jem.20151809 [PubMed: 27045008]
41. Cavlar T, Deimling T, Ablasser A, Hopfner K-P, Hornung V. Species-specific detection of the antiviral small-molecule compound CMA by STING. *EMBO J.* 2013; 32: 1440–1450. DOI: 10.1038/emboj.2013.86 [PubMed: 23604073]
42. Camargo Ortega G, Falk S, Johansson PA, Peyre E, Broix L, Sahu SK, Hirst W, Schlichthaerle T, De Juan Romero C, Draganova K, et al. The centrosome protein AKNA regulates neurogenesis via microtubule organization. *Nature.* 2019; 567: 113–117. DOI: 10.1038/s41586-019-0962-4 [PubMed: 30787442]
43. Franklin BS, Bossaller L, De Nardo D, Ratter JM, Stutz A, Engels G, Brenker C, Nordhoff M, Mirandola SR, Al-Amoudi A, et al. The adaptor ASC has extracellular and ‘prionoid’ activities that propagate inflammation. *Nat Immunol.* 2014; 15: 727–737. [PubMed: 24952505]
44. Sanjana NE, Shalem O, Zhang F. Improved vectors and genome-wide libraries for CRISPR screening. *Nat Methods.* 2014; 11: 783–784. DOI: 10.1038/nmeth.3047 [PubMed: 25075903]
45. Schmidt T, Schmid-Burgk JL, Hornung V. Synthesis of an arrayed sgRNA library targeting the human genome. *Sci Rep.* 2015; 5: 14987 doi: 10.1038/srep14987 [PubMed: 26446710]
46. Schmid-Burgk JL, Schmidt T, Gaidt MM, Pelka K, Latz E, Ebert TS, Hornung V. OutKnocker: a web tool for rapid and simple genotyping of designer nuclease edited cell lines. *Genome Res.* 2014; 24: 1719–1723. DOI: 10.1101/gr.176701.114 [PubMed: 25186908]
47. Carpenter AE, Jones TR, Lamprecht MR, Clarke C, Kang IH, Friman O, Guertin DA, Chang JH, Lindquist RA, Moffat J, et al. CellProfiler: image analysis software for identifying and quantifying cell phenotypes. *Genome Biol.* 2006; 7: R100. doi: 10.1186/gb-2006-7-10-r100 [PubMed: 17076895]
48. Labun K, Montague TG, Krause M, Torres Cleuren YN, Tjeldnes H, Valen E. CHOPCHOP v3: expanding the CRISPR web toolbox beyond genome editing. *Nucleic Acids Res.* 2019; 47: W171–W174. DOI: 10.1093/nar/gkz365 [PubMed: 31106371]
49. Cox J, Mann M. MaxQuant enables high peptide identification rates, individualized p.p.b.-range mass accuracies and proteome-wide protein quantification. *Nat Biotechnol.* 2008; 26: 1367–1372. DOI: 10.1038/nbt.1511 [PubMed: 19029910]
50. Tyanova S, Temu T, Sinitcyn P, Carlson A, Hein MY, Geiger T, Mann M, Cox J. The Perseus computational platform for comprehensive analysis of (prote)omics data. *Nat Methods.* 2016; 13: 731–740. DOI: 10.1038/nmeth.3901 [PubMed: 27348712]
51. Schindelin J, Arganda-Carreras I, Frise E, Kaynig V, Longair M, Pietzsch T, Preibisch S, Rueden C, Saalfeld S, Schmid B, et al. Fiji: an open-source platform for biological-image analysis. *Nat Methods.* 2012; 9: 676–682. DOI: 10.1038/nmeth.2019 [PubMed: 22743772]
52. Kutner RH, Zhang X-Y, Reiser J. Production, concentration and titration of pseudotyped HIV-1-based lentiviral vectors. *Nat Protoc.* 2009; 4: 495–505. DOI: 10.1038/nprot.2009.22 [PubMed: 19300443]
53. Dull T, Zufferey R, Kelly M, Mandel RJ, Nguyen M, Trono D, Naldini L. A third-generation lentivirus vector with a conditional packaging system. *J Virol.* 1998; 72: 8463–8471. DOI: 10.1128/JVI.72.11.8463-8471.1998 [PubMed: 9765382]

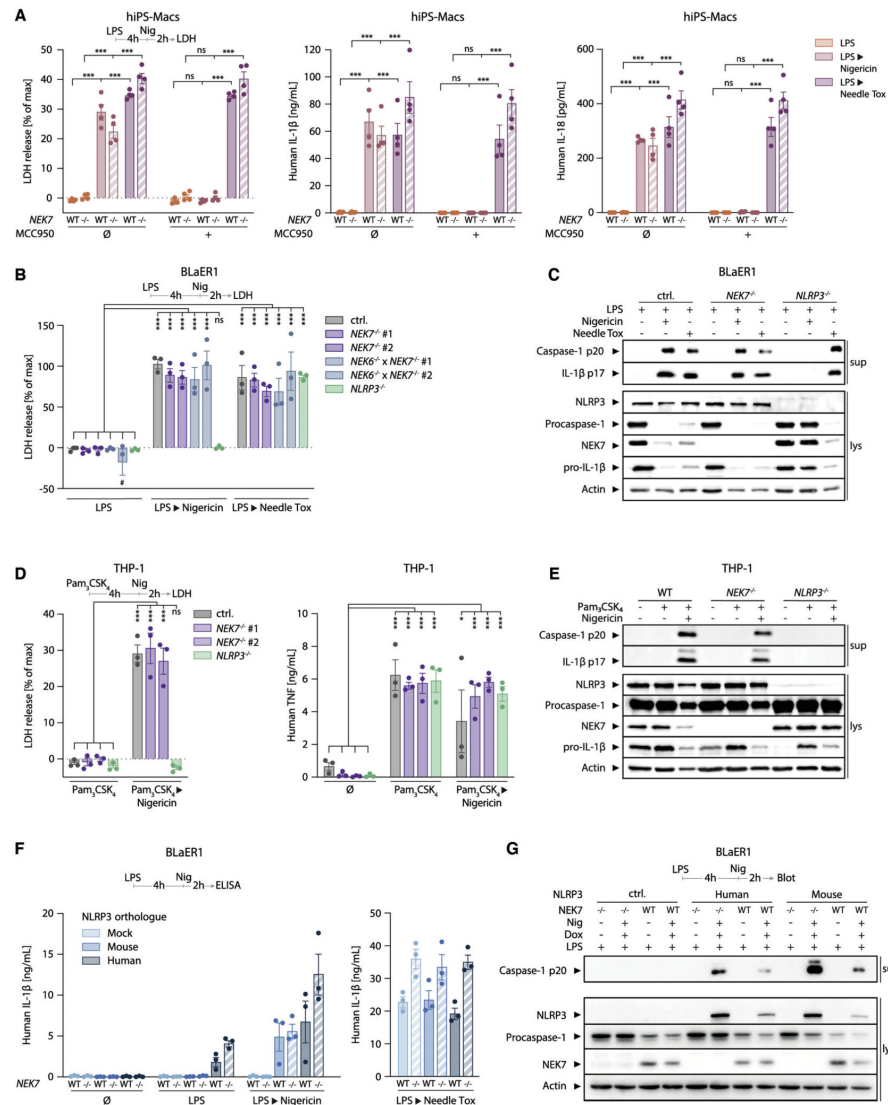


Figure 1. Human iPSC-derived macrophages and human myeloid cell lines activate the NLRP3 inflammasome independently of NEK7

(A) Four clones per indicated genotype of human iPSCs were differentiated into macrophages (hiPS-Macs), primed with LPS for 4 h and then treated with the inflammasome activators Nigercin (NLRP3) or Needle Tox (NAIP-NLRC4) in the presence of the NLRP3 inhibitor MCC950 as indicated before release of LDH (left), IL-1 β (middle), and IL-18 (right) was measured. Dots represent separately differentiated iPS cell clones of the indicated genotypes.

(B and C) BLaER1 monocytes of the indicated genotypes were primed with LPS for 4 h and subsequently stimulated with Nigericin or Needle Tox. LDH release (B) of one or two clones per genotype is depicted. (C) One representative immunoblot of three independent experiments is shown.

(D) Three clones of THP-1 cells of the indicated genotypes were primed with Pam3CSK4 for 4 h and subsequently stimulated with Nigericin for 2 h before release of LDH (left) and TNF (right) were measured. Two different sgRNAs against *NEK7* were used (#1 and #2). Dots represent individual clones.

(E) THP-1 cells of the indicated genotypes were primed with Pam3CSK4 for 4 h and subsequently stimulated with Nigericin for 2 h before immunoblotting. One representative immunoblot of three independent experiments is shown.

(F) *NLRP3*^{-/-} BLaER1 cells expressing the indicated NLRP3 orthologs under the control of a doxycycline-inducible promoter were treated with doxycycline for the last 24 h of differentiation, primed with LPS for 4 h and subsequently stimulated with Nigericin (left) or Needle Tox (right) for 2 h. The same vector expressing mCherry instead of NLRP3 was used as a mock control.

(G) Western blot of cells treated as in (F), one representative of three independent experiments is shown.

Data are represented as mean \pm SEM with dots representing biological replicates conducted on separate days unless indicated otherwise (one outlier in B is not depicted #). *** $p < 0.001$, ** $p < 0.01$, * $p < 0.05$, ns $p \geq 0.05$ calculated by two-way ANOVA followed by Tukey's test (A, B, and D: TNF) or Šidák's test (D: LDH).

See also Figures S1 and S2.

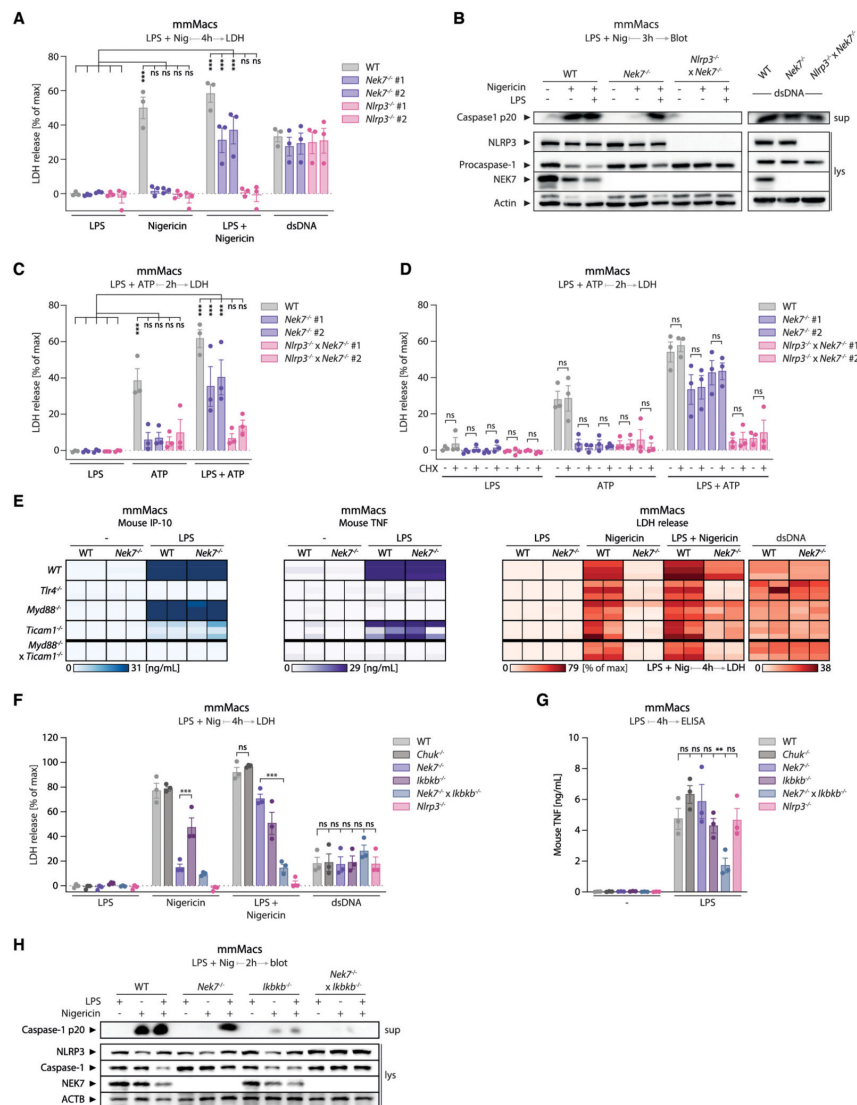


Figure 2. Priming activates IKK β to bypass NEK7 via a translation-independent mechanism in mouse cells

(A–C) Mouse macrophages constitutively expressing mmNlrp3 (mmMac) of the indicated genotypes were stimulated with LPS + Nigericin simultaneously for 4 h, with DNA for 28 h or with LPS + ATP for 2 h. (B) One immunoblot representative of two clones from two independent experiments is shown.

(D) mmMac were pretreated with cycloheximide (CHX) for 30 min and stimulated as in (C).

(E) Two mMacs clones per genotype were stimulated as indicated. Release of IP-10 (left), TNF (middle), and LDH (right) of two clones (sub-columns) from three independent experiments (sub-rows) are depicted as heatmaps.

(F and G) mMacs of the indicated genotypes were stimulated as in (A) before the release of LDH (F) and TNF (G) was measured.

(H) mMacs of the indicated genotypes were stimulated as in (A) for 2 h. One representative of three independent biological replicates is shown.

Data are represented as mean \pm SEM with dots representing biological replicates conducted on separate days. *** $p < 0.001$, ** $p < 0.01$, * $p < 0.05$, ns $p \geq 0.05$ calculated by two-way ANOVA followed by Tukey's test (A, C, and F), Šidák's test (D), or Dunnett's test (G). See also Figures S3 and S4 and Table S1.

Data are represented as mean \pm SEM with dots representing biological replicates conducted on separate days unless indicated otherwise. *** $p < 0.001$, ** $p < 0.01$, * $p < 0.05$, ns $p \geq 0.05$ calculated by two-way ANOVA followed by Tukey's test.

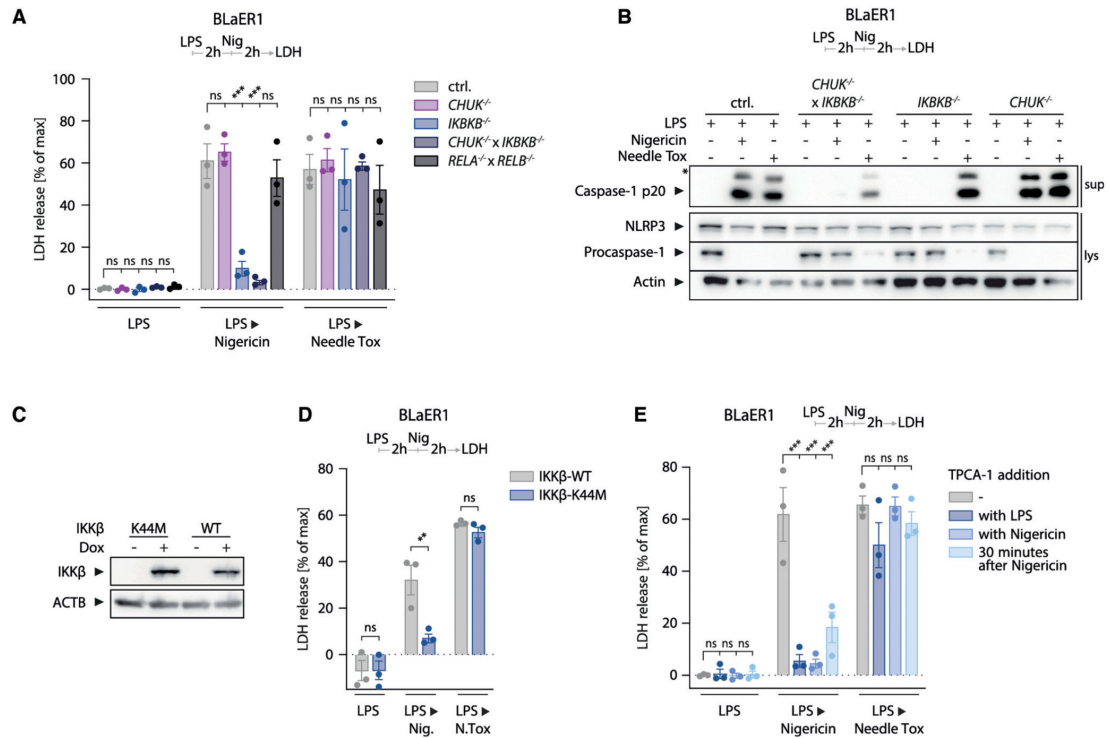


Figure 4. NLRP3 priming through *IKK β* is required for inflammasome activation in human myeloid cell lines

(A) LDH release from BLaER1 clones of the indicated genotypes primed with LPS for 2 h and subsequently treated with Nigericin or Needle Tox for 2 h.

(B) One representative of three immunoblots from cells treated as in (A). The asterisk denotes an unspecific band.

(C) Immunoblot of *IKKB β* ^{-/-} BLaER1 cells expressing wild-type *IKK β* or kinase-dead *IKK β* -K44M under the control of a doxycycline-inducible promoter treated with doxycycline during the last 8 h of differentiation.

(D) LDH release from BLaER1 cells as in (C) primed with LPS for 2 h and subsequently treated with Nigericin or Needle Tox as indicated.

(E) LDH release from BLaER1 monocytes primed with LPS for 2 h before stimulation with Nigericin or Needle Tox. TPCA-1 was added at different time points as indicated.

Data are represented as mean \pm SEM with dots representing biological replicates conducted on separate days. ****p* < 0.001, ***p* < 0.01, **p* < 0.05, ns *p* \geq 0.05 calculated by two-way ANOVA followed by Dunnett's test (A and E) or Šidák's test (D).

See also Figure S5.

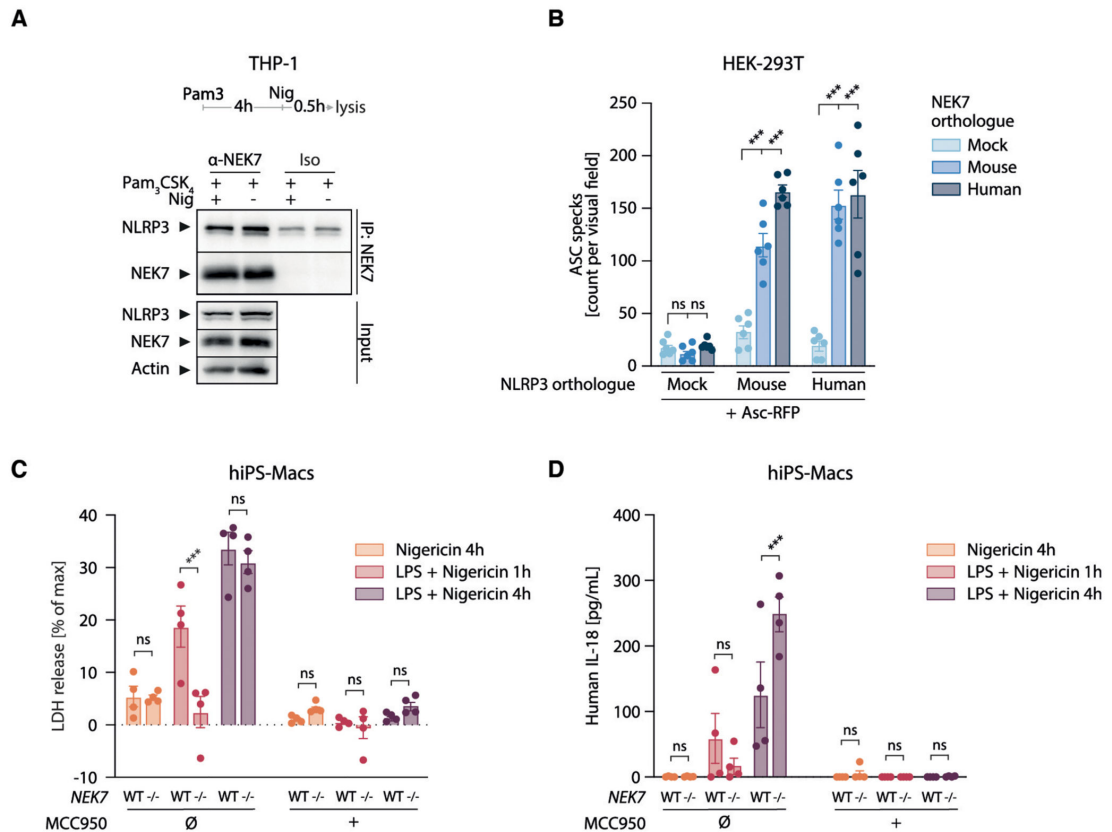


Figure 5. NEK7 accelerates NLRP3 activation at early priming time points in iPS-derived human macrophages

(A) THP-1 cells were primed with Pam₃CSK₄ for 4 h and then stimulated with Nigericin for 30 min before lysates were immunoprecipitated with anti-NEK7 antibody or isotype control. One representative immunoblot of three independent experiments is shown.

(B) *NEK7*^{-/-} HEK293T cells were transiently transfected with plasmids driving expression of an ASC-RFP fusion protein and mouse or human orthologues of NLRP3 and NEK7 as indicated. ASC-RFP specks were imaged 24 h after transfection. Dots represent technical replicates from one representative of three independent experiments.

(C and D) Four clones per genotype of *NEK7*^{-/-} or wild-type human iPS cells were differentiated into hiPS-Macs and treated with Nigericin or LPS + Nigericin for 4 h or LPS + Nigericin for 1 h in the presence of the NLRP3 inhibitor MCC950 as indicated. Dots represent individual clones.

****p* < 0.001, ***p* < 0.01, **p* < 0.05, ns *p* ≥ 0.05 calculated by two-way ANOVA followed by Dunnett's test (B) or Šidák's test (C and D).

See also Figure S6.

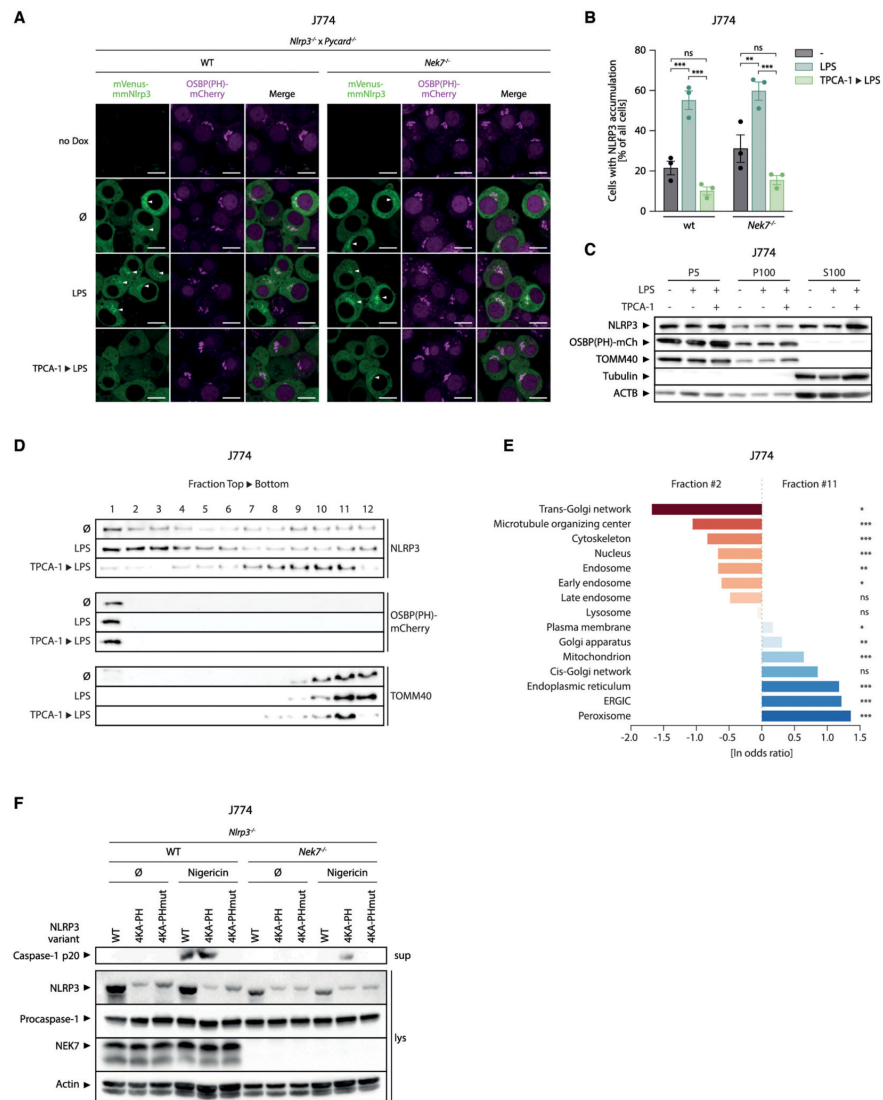


Figure 6. IKK β -mediated recruitment of NLRP3 to PI4P enables NEK7-independent inflammasome formation

(A) *Nlrp3^{-/-} × Pycard⁺* J774 cells of the indicated *Nek7* genotypes expressing mCherry tethered to phosphatidylinositol-4-phosphate (PI4P) via the PH domain of OSBP (OSBP(PH)-mCherry) and doxycycline-inducible mVenus-mmNlrp3 were treated with doxycycline for 24 h and TPCA-1 for 1 h before stimulation with LPS for 30 min. Scale bars represent 10 μ m.

(B) Quantification of at least 10 randomly chosen fields of view per experimental condition from three independent experiments described in (A). Data are represented as mean \pm SEM with dots representing biological replicates conducted on separate days.

(C) Lysates of J774 cells pretreated with TPCA-1 for 1 h and then stimulated with LPS for 30 min were depleted of nuclei (5 min $1,000 \times g$), and the supernatant was then centrifuged at $5,000 \times g$ for 10 min (pellet P5) followed by $100,000 \times g$ for 20 min (pellet P100, supernatant S100) before immunoblotting. One representative of three independent experiments is shown.

(D) P100 fractions from (C) were further fractionated across a linear sucrose gradient (20%–60%) into 12 fractions which were then immunoblotted. One representative of three independent biological replicates is shown.

(E) Enrichment of organelle-specific protein sets identified via mass spectrometry analysis of the protein content of fractions #2 and #11. p-values for set enrichment were calculated based on proteins differing between the two fractions (FC R 1.5, FDR < 0.05) using Fisher's exact test with Benjamini-Hochberg correction.

(F) *Nlrp3*^{-/-} J774 cells of the indicated *Nek7* genotypes expressing doxycycline-inducible variants of Nlrp3 as indicated were treated with doxycycline for 18 h followed by 2 h of Nigericin before immunoblotting.

***p < 0.001, **p < 0.01, *p < 0.05, ns \geq 0.05 calculated by two-way ANOVA followed by Tukey's test unless indicated otherwise.

See also Figure S6 and Table S2.

3.2 SPARCS, a platform for genome-scale CRISPR screening for spatial cellular phenotypes

The following research article was originally published here:

Schmacke, N. A., Mädler, S. C., et al. (2023). “SPARCS, a platform for genome-scale CRISPR screening for spatial cellular phenotypes”. In: *bioRxiv*. DOI: [10.1101/2023.06.01.542416](https://doi.org/10.1101/2023.06.01.542416)

bioRxiv preprint doi: <https://doi.org/10.1101/2023.06.01.542416>; this version posted June 1, 2023. The copyright holder for this preprint (which was not certified by peer review) is the author/funder, who has granted bioRxiv a license to display the preprint in perpetuity. It is made available under a [CC-BY-NC-ND 4.0 International license](#).

SPARCS, a platform for genome-scale CRISPR screening for spatial cellular phenotypes

Niklas A. Schmacke¹†, Sophia C. Mädler²‡, Georg Wallmann^{1,2}, Andreas Metousis², Marleen Bérouti¹, Hartmann Harz³, Heinrich Leonhardt³, Matthias Mann^{2*}†‡, Veit Hornung^{1*}†‡

¹Gene Center and Department of Biochemistry, Ludwig-Maximilians-Universität München, 81377 Munich, Germany.

²Department of Proteomics and Signal Transduction, Max Planck Institute of Biochemistry, 82152 Martinsried, Germany.

³Faculty of Biology, Human Biology and BioImaging, Ludwig-Maximilians-Universität München, Planegg-Martinsried, Germany.

†, ‡ These authors contributed equally to this work

*Corresponding authors. Email: mmann@biochem.mpg.de, hornung@genzentrum.lmu.de

Abstract

Forward genetic screening associates phenotypes with genotypes by randomly inducing mutations and then identifying those that result in phenotypic changes of interest. Here we present spatially resolved CRISPR screening (SPARCS), a platform for microscopy-based genetic screening for spatial cellular phenotypes. SPARCS uses automated high-speed laser microdissection to physically isolate phenotypic variants *in situ* from virtually unlimited library sizes. We demonstrate the potential of SPARCS in a genome-wide CRISPR-KO screen on autophagosome formation in 40 million cells. Coupled to deep learning image analysis, SPARCS recovered almost all known macroautophagy genes in a single experiment and discovered a role for the ER-resident protein EI24 in autophagosome biogenesis. Harnessing the full power of advanced imaging technologies, SPARCS enables genome-wide forward genetic screening for diverse spatial phenotypes *in situ*.

bioRxiv preprint doi: <https://doi.org/10.1101/2023.06.01.542416>; this version posted June 1, 2023. The copyright holder for this preprint (which was not certified by peer review) is the author/funder, who has granted bioRxiv a license to display the preprint in perpetuity. It is made available under a [CC-BY-NC-ND 4.0 International license](#).

Introduction

Genetic screens offer a powerful approach to dissecting the complexity inherent in biological systems. Within this space, forward genetic screening is an unbiased way to map phenotypic changes to changes in the genome: From a library of genetic variants generated by random mutagenesis, mutants with interesting phenotypes are selected and their genotypes determined. This approach has led to groundbreaking discoveries in a variety of model organisms (1-3). Now, with the ability to specifically target mutagenesis to exonic regions of interest and disrupt both alleles of a given genetic locus, CRISPR-based genome editing technologies (4) have enabled the generation of large mutant libraries in which a single gene is knocked out in each cell (5). Individual genetically perturbed cells can now be profiled for their transcriptome (6-10), protein expression (11), spatial composition (12) and chromatin landscape (13). However, genome-wide screening libraries typically contain tens of millions of cells, a scale with which most of these techniques are currently incompatible. To overcome this limitation, only those cells with an interesting phenotype are typically isolated from the library and subsequently genotyped. This paradigm has largely limited cell-based genome-wide screens to three types of easily selectable phenotypes: a difference in proliferation rate, an inhibition of cell death, or a change in fluorescence intensity compatible with fluorescence-activated cell sorting (FACS) (14-17).

Increasingly powerful microscopic imaging provides information-rich data on diverse cellular phenotypes (18) and would therefore be an ideal technology to read out biological phenotypes of interest, particularly if combined with recent advances in deep learning. However, its application in genome-wide forward genetic screening has been hampered by a lack of scalability and other limitations: ‘in situ sequencing by synthesis’, a technology originally developed to profile the cellular transcriptome in tissue samples, has been adapted to sequencing short perturbation-encoding barcodes on the DNA level (19, 20). This method separates genotyping and image collection, resulting in complete image datasets for unbiased identification of new phenotypes. However, by design it does not include an enrichment step for selected phenotypes, requiring all cells in a mutant library to be sequenced irrespectively of whether they show a phenotype. In addition, the genotype can only be determined for a fraction of cells due to low sequencing fidelity even in low-complexity libraries (20), which in combination with the technology’s high costs has limited its applicability for screening genome-wide libraries at sufficient coverage (21). Image-based flow cytometers with sorting capabilities have recently enabled the investigation of spatial phenotypes at high throughput (22, 23). These devices rely on low-resolution flow-based microscopy of detached cells, preventing the identification of complex phenotypes. In addition, this technology makes sorting decisions in real time, restricting it to the identification of predefined phenotypes and preventing reanalysis of past screens. A method originally proposed for the transcriptomic characterization of B-cell populations (24) photoactivates fluorophores to mark cells for subsequent isolation by FACS (25-27). This approach can only separate few different phenotypes by fluorophore brightness (28). It also requires a real time

bioRxiv preprint doi: <https://doi.org/10.1101/2023.06.01.542416>; this version posted June 1, 2023. The copyright holder for this preprint (which was not certified by peer review) is the author/funder, who has granted bioRxiv a license to display the preprint in perpetuity. It is made available under a [CC-BY-NC-ND 4.0 International license](#).

decision on which cells to isolate, preventing whole-dataset analysis to discover unexpected new phenotypes and has not been demonstrated to be compatible with cell fixation, which is necessary for antibody-based staining of intracellular targets.

To enable robust genome-wide high-throughput screening for spatial cellular phenotypes, we set out to develop a technology that meets four key requirements: First, it should work on cells *in situ* and utilize state-of-the-art microscopy techniques. Second, it should accommodate large screening libraries to ensure adequate representation of rare phenotypes. Third, it should be compatible with the unbiased identification of previously unknown phenotypes from entire complex image datasets rather than single images in real time. Fourth, it should allow for reanalysis and reselection of cells for genotyping from previous archived screens. Importantly, the latter feature would allow the application of novel image analysis methods to previously performed screens as they become available.

Results

Spatial genotyping by laser microdissection

To analyze the spatial composition of tissues and clinical samples by mass spectrometry, we have been advancing workflows based on laser microdissection (LMD), a technique that uses a focused UV laser to cut out and collect arbitrary shapes from tissue sections (29, 30). In a most recent development, deep visual proteomics (DVP), we use LMD to excise defined tissue regions for subsequent proteomic characterization of individual cell types or extracellular zones by mass spectrometry (31, 32). We reasoned that the isolation of single phenotypically interesting cells from a pooled library by LMD would provide an ideal basis for a forward genetic screening technology for spatial phenotypes.

LMD requires samples to be present on a membrane that can be cut by a UV laser, so we first tested whether cells could be grown and imaged directly on such polymer membranes. Indeed, on polyphenylene sulfide (PPS) membranes, spinning disk confocal microscopy produced high-quality images that showed normal cellular morphology (fig. 1A). By segmenting these images into individual cells, we generated multi-channel perturbation image datasets from which we aimed to identify cells with phenotypes of interest for genotyping (fig. 1B). We then developed a rapid cutting protocol for LMD that is compatible with subsequent genotyping by minimizing autofocus time and optimizing the trade-off between laser speed and accuracy. Compressing the cutting path and leveraging the fact that it is sufficient to isolate nuclei to determine a cell's CRISPR perturbation by sequencing, we ultimately reached a speed of 1,000 nuclei per hour.

Counting of excised membrane regions collected in a microwell plate using this protocol showed a yield of approximately 80 % (fig. 1C). We then tested the genotyping of excised nuclei by generating a pool of U2OS cells each expressing one of 77,441 unique sgRNAs in the Brunello CRISPR library (33),

3.2 SPARCS, a platform for genome-scale CRISPR screening for spatial cellular phenotypes

bioRxiv preprint doi: <https://doi.org/10.1101/2023.06.01.542416>; this version posted June 1, 2023. The copyright holder for this preprint (which was not certified by peer review) is the author/funder, who has granted bioRxiv a license to display the preprint in perpetuity. It is made available under a [CC-BY-NC-ND 4.0 International license](#).

plated these cells onto PPS membranes and imaged them. To register membrane slides between imaging microscopes and the LMD microscope, we marked the membrane with calibration crosses as landmarks that define a coordinate system across each slide, allowing us to find the positions of cells to excise. We stitched individual field of view images of a slide into one whole slide image (WSI), segmented nuclei based on a DNA stain, generated a cutting map using our newly developed open-source python library `py-lmd` (fig. S1) and then excised and lysed 1,000 nuclei. Sequencing identified 549 unique sgRNAs on average in these lysates, demonstrating that isolating individual nuclei for subsequent CRISPR genotyping is feasible with LMD (fig. 1D). Comparing the number of unique sgRNAs in the LMD lysate with a lysate of cells from the same library isolated by FACS revealed that both techniques recovered an sgRNA from approximately 50 % of cells (fig. 1D). From these data we concluded that potential DNA damage induced by laser microdissection does not hamper sgRNA recovery. In summary, our results show that it is possible to employ LMD to recover genetic information from imaged cells at a throughput compatible with genetic screening (fig. 1E). We call this approach spatially resolved CRISPR screening (SPARCS).

Validating SPARCS for genetic screening

To further develop SPARCS we applied it to screen for regulators of starvation-induced macroautophagy (hereafter referred to as autophagy), a fundamental process for cellular energy management (34, 35). The signature of autophagy is the formation of vesicles called autophagosomes. These are covalently decorated with proteins from the ATG8 family, including the well-studied human protein LC3B. During a key event in autophagosome biogenesis LC3B is conjugated to the head group of the lipid phosphatidylethanolamine (PE) through a series of ubiquitin ligation-like reactions. A critical component of this cascade is the protein ATG5 that forms an E3-like complex with ATG12 to mediate the covalent attachment of LC3B to PE. To follow the formation of autophagosomes during starvation we stably expressed LC3B tagged with mCherry in U2OS cells, because – unlike GFP – mCherry remains fluorescent upon fusion with the lysosome. We then treated these cells with the mTOR inhibitor Torin-1 to mimic starvation, which induces autophagy. Cells treated this way began to accumulate mCherry-LC3-positive puncta over the course of 14 hours (fig. 2A).

In a screen, those cells containing sgRNAs against essential regulators of autophagy are unable to form these puncta. To identify these cells we trained a deep learning-based image classifier to differentiate between cells with or without autophagosomes (fig. 2B, fig. S2A). The training dataset was composed of segmented single cell images of mCherry-LC3 expressing U2OS cells that were treated with Torin-1 (autophagy-on class) or left untreated (autophagy-off class). As an additional group we introduced cells treated with Torin-1, yet deficient in ATG5 (autophagy-off class). We used images from several biological replicates to avoid overfitting of our classifier to batch-specific characteristics such as staining intensity or cell density (table S1). To evaluate the performance of this classifier 1.0, we

bioRxiv preprint doi: <https://doi.org/10.1101/2023.06.01.542416>; this version posted June 1, 2023. The copyright holder for this preprint (which was not certified by peer review) is the author/funder, who has granted bioRxiv a license to display the preprint in perpetuity. It is made available under a [CC-BY-NC-ND 4.0 International license](#).

generated a new test dataset of images from unstimulated and Torin-1 stimulated wildtype and *ATG5*^{-/-} mCherry-LC3-expressing U2OS cells that had not been part of the training set and as such had never been seen by the classifier before. Classifier 1.0 achieved a false discovery rate (FDR) of < 1% (fig. S2B) at the chosen threshold, meaning that less than 1% of cells classified as potential hits with an autophagy-off phenotype were instead false positives that actually came from the autophagy-on class.

We then validated SPARCS by performing a small pilot screen on autophagosome formation in 1.2 million Torin-1-stimulated mCherry-LC3 U2OS cells transduced with the Brunello CRISPR knockout (KO) library (fig. 2C). From this library we isolated the top 0.1 % of cells classified as autophagy-off by classifier 1.0 with a score > 0.94, corresponding to a test set FDR of 0.38 %. Compared to the entire library, we found sgRNAs targeting *ATG5* to be highly enriched among isolated cells (median 200-fold) (fig. 2D). sgRNAs targeting other autophagy-related genes had a median of 60-fold enrichment with the most strongly enriched sgRNAs even exceeding 700-fold (fig. 2D). Control sgRNAs not targeting any human genes ('non targeting controls' (NTCs)) were rare among isolated cells with a median enrichment of 10-fold (fig. 2D). These results confirm that the SPARCS protocol stitches and registers WSI with sufficient accuracy for the isolation of the nuclei of interest. They also demonstrate that assessing autophagosome formation based on images is feasible with a deep learning classifier, and that in SPARCS, this classifier can be used to screen for autophagosome formation.

Accurate detection of autophagy defects in single cell images

A classifier's Receiver Operating Characteristic (ROC) curve visualizes the tradeoff between true positive rate (the fraction of all autophagy-off cells that are correctly identified) and false positive rate (the fraction of autophagy-on cells incorrectly predicted as autophagy-off). The ROC curve of our classifier 1.0 confirmed its overall accuracy with an area under the curve (AUC) of > 0.92 (fig. S2C). However, at the precision (the fraction of predicted autophagy-off cells that are actually autophagy-off, 1-FDR) corresponding to 1 % FDR, the recall (= true positive rate) of classifier 1.0 was below 26% (fig. S2D). Closer analysis of the different categories of cells in the test dataset revealed that the classifier excelled at identifying autophagy-on cells, but performed poorly at recognizing autophagy-off cells (fig. S2E, F).

To improve classification of autophagy-off cells we refined our staining and imaging protocol and then trained a new version of our classifier. For this version 2.0 we decided to use a more streamlined multilayer perceptron (MLP) head with fewer trainable parameters, add another linear layer and increase the number of cells and biological replicates in the training dataset to capture as much biological variance as possible (fig. 3A, B, table S1). We also prefiltered the unstimulated and Torin-1 stimulated images for autophagy-off and -on cells to minimize the number of mislabeled training examples (table S1). To evaluate classifier 2.0, we first used parametric UMAP (36) to investigate if layers of the CNN had learned to differentiate between images of autophagy-on and autophagy-off cells.

3.2 SPARCS, a platform for genome-scale CRISPR screening for spatial cellular phenotypes

bioRxiv preprint doi: <https://doi.org/10.1101/2023.06.01.542416>; this version posted June 1, 2023. The copyright holder for this preprint (which was not certified by peer review) is the author/funder, who has granted bioRxiv a license to display the preprint in perpetuity. It is made available under aCC-BY-NC-ND 4.0 International license.

This revealed that wildtype cells stimulated with Torin-1, unstimulated wildtype cells and *ATG5*^{-/-} cells clustered separately in representations of lower layers, most prominently in the 8th of 9 convolutional layers (fig. 3C). These results suggested that our CNN had now learned to featurize images of LC3 distribution in a way that enables accurate classification of cells undergoing autophagy. Of note, the network of classifier 2.0 was capable of discriminating between *ATG5*^{-/-} and unstimulated wildtype cells despite those cells being in the same training class (fig. 3C), a clear improvement over classifier 1.0 (fig. S2G). Its ROC curve was also drastically improved with an AUC of > 0.999 (fig. 3D). Remarkably, in the binary classification output almost all cells were correctly classified according to their autophagy status even with a simple classification score threshold of 0.5 (fig. 3E, F). With classifier 2.0, classification thresholds > 0.98 produced FDRs of < 1 %, with higher thresholds reducing the FDR further without yet diminishing the excellent recall of nearly 100 % (fig. 3G, fig. S2H). Thus, for a complex biological process such as autophagy, training a CNN-based classifier on images from comparatively few biological replicates achieves excellent performance.

Genome-wide autophagy screen with SPARCS

Encouraged by these results we used SPARCS to conduct a genome-wide screen on autophagosome formation. We screened a library of 40 million mCherry-LC3 expressing U2OS cells at a median coverage of 1,818 cells per gene in the human genome in batches of 5 and 35 million cells (fig. S3). Classifying autophagy based on the distribution of LC3 within the first batch showed that 0.56% of cells had a score > 0.98. We regarded these cells as potential autophagy-defective hits and, upon examining the 8th CNN layer featurization of their LC3 distribution using parametric UMAP, found them to cluster separately from autophagy-on cells in the library with a classification score < 0.02 (fig. S4A, B). For genotyping we divided the hits into six bins according to their classification score (fig. S4C): The top bin represented a cutoff at which we found *ATG5*^{-/-} to be strongly enriched in our test dataset, whereas the second bin corresponded to unstimulated wildtype cells. Bins 3 – 6 contained the remaining potential hits with a roughly equal number of cells per bin. Zooming in on the 8th CNN layer featurization of the LC3 distribution in the potential hits revealed that cells in bins 1 & 2 clustered separately from bins 3 - 6 (fig. S4D). This indicated that they contained different phenotypic variants with regard to their LC3 distribution, potentially corresponding to stronger defects in autophagosome formation. Indeed, we observed the fewest LC3 puncta in cells from bins 1 & 2 (fig. S4E).

For the second genome-wide screen batch we refined our classifier by more stringently selecting training examples of autophagy-on and -off cells, thereby further improving its overall performance (fig. S5). Using this new classifier 2.1 we obtained similar results from the second batch compared to 2.0 on the first screen batch: 1.40% of cells were classified as autophagy-off with a score above 0.98 and in their 8th CNN layer featurization these cells again clustered separately from their autophagy-on counterparts with a score < 0.02 (fig. 4A, B). We therefore applied the same binning strategy to these

bioRxiv preprint doi: <https://doi.org/10.1101/2023.06.01.542416>; this version posted June 1, 2023. The copyright holder for this preprint (which was not certified by peer review) is the author/funder, who has granted bioRxiv a license to display the preprint in perpetuity. It is made available under aCC-BY-NC-ND 4.0 International license.

images (fig. 4C), and, upon zooming in on their 8th CNN layer featurization using parametric UMAP, found the separation of cells in bin 1 & 2 to be even more apparent than in the first batch (fig. 4D, E). We then isolated a total of 395,173 nuclei across both screen batches and sequenced their sgRNAs. Given their similarity on the phenotypic level we analyzed the genetic data of both batches together. All bins showed a marked enrichment of targeting over non-targeting sgRNAs and enrichment scores up to 600-fold, promising the identification of autophagy relevant genes (fig. 4F). In line with our FDR calculation (fig. 3G, fig. S5B) and our conclusions from the featurization of individual images (fig. 4D, fig. S4D), sgRNAs targeting genes known to be involved in autophagosome formation were most strongly enriched in bins 1 & 2 (fig. 4F). On the gene level *ATG5*, which our classifier was trained to identify, was among the most highly enriched genes in several bins, validating our supervised classification approach in the context of this large-scale screen (fig. 4G). The Brunello library targets each gene in the human genome with four sgRNAs. While in the higher score bins 1 & 2, genes with a high mean enrichment score had several sgRNAs enriched, in lower bins genes with a relatively high mean enrichment score often only had a single highly enriched sgRNA, indicating potential off-target effects. This prompted us to evaluate the number of sgRNAs enriched per gene as an alternative metric to score screening hits. Here we again found the strongest hits to contain mainly autophagy-related genes (fig. 4H). Taken together, these results establish that SPARCS is highly effective for large scale genetic screens on spatial phenotypes. Furthermore, despite the inherent complexity of image-based phenotypes, our supervised classifier facilitated the enrichment of a very small subset of individual cells with a genetically defined phenotype from a diverse genome-wide library of 40 million cells.

EI24 reorganizes membranes for autophagy

The power of SPARCS became even more apparent when we evaluated our screen from the perspective of the investigated biological process: Remarkably, this single screen recovered almost all known essential genes of the starvation-induced macroautophagy pathway. This included the complete ULK1 complex and LC3 lipidation cascade (fig. 5A). Closer inspection of individual hits revealed that the most strongly enriched gene that is not a canonical macroautophagy gene was *EI24*, a gene coding for an ER-resident transmembrane protein (37) (fig. 5B). *EI24*^{-/-} cells have previously been described as autophagy-defective, but with a phenotype resulting in spontaneous LC3-puncta formation (38). This finding is not in line with the 82-fold enrichment of *EI24* in our screen, given that our classifier was trained to recognize cells with impaired rather than increased autophagosome formation. To investigate why we found *EI24* KOs enriched among cells classified as autophagy-off, we generated individual *EI24*^{-/-} clones. Consistent with the previously reported spontaneous LC3 puncta formation, *EI24*-deficient cells have been described to exhibit increased lipidation of LC3 under steady state conditions (38), a phenotype we confirmed in *EI24*^{-/-} clones (fig. 5C). However, in contrast to previous results we found LC3 puncta formation in response to Torin-1 to be largely abolished in *EI24*-deficient cells (fig. 5D). Instead, these cells formed a single mCherry-LC3-positive speck that became more pronounced

3.2 SPARCS, a platform for genome-scale CRISPR screening for spatial cellular phenotypes

bioRxiv preprint doi: <https://doi.org/10.1101/2023.06.01.542416>; this version posted June 1, 2023. The copyright holder for this preprint (which was not certified by peer review) is the author/funder, who has granted bioRxiv a license to display the preprint in perpetuity. It is made available under aCC-BY-NC-ND 4.0 International license.

with Torin-1 stimulation, indicating a general defect in membrane traffic or autophagosome formation (fig. 5E). These results explain why our classifier picked up *EI24* knockouts and demonstrate again that even supervised image classification is capable of identifying previously undescribed phenotypes. Our results further indicate that *EI24* is required for autophagosome formation and has a function beyond its recently described LC3 puncta promoting role in maintaining Ca^{2+} homeostasis across the ER membrane (39) that remains to be investigated.

Discussion

We present SPARCS, a platform that enables unbiased exploration of the genetic basis of subcellular spatial features in forward genetic screens. At the core of the SPARCS methodology, we have adapted and refined laser microdissection technology to unprecedented throughput to facilitate genetic screening applications. We have improved the precision and efficiency of isolating single nuclei from cell cultures, while automating the extraction of several hundred thousand nuclei into distinct bins. By integrating a deep learning-based classifier, our genome-wide SPARCS screen successfully identified nearly all known genes related to macroautophagy and revealed a novel phenotype associated with the *EI24* gene.

SPARCS offers a unique combination of features (table S2) that make it a powerful forward genetic screening platform. It can be seamlessly integrated with any state-of-the-art microscope for *in situ* cell imaging. The screening library size is not constrained, except by the imaging microscope's throughput. Consequently, microscopy-based genome-wide perturbation screens can now achieve exceptional coverage. Besides the method described here, which involves isolating cells based on predefined classes, SPARCS is also compatible with the identification of individual cells exhibiting entirely novel or unexpected phenotypes. This is achieved through unbiased clustering and anomaly detection applied to the entire image dataset. Furthermore, we discovered that samples can be stored long-term, allowing for the reanalysis of archived SPARCS screens using newer algorithms. This facilitates the exploration of new biological insights within existing data. To streamline the process of translating the identification of individual cells with subcellular spatial phenotypes into a cutting map for LMD we have developed *py-lmd*, an open-source Python library for laser microdissection on arbitrary sample types that is available on GitHub. We hope that the accessible design of SPARCS, compatible with standard microscopes and sequencing workflows, will encourage its adoption by the scientific community.

Our screen uncovered a potential role in macroautophagy for *EI24*. This gene had previously been implicated in autophagy based on a *C. elegans* screen in 2010, but its mechanism of action had remained unclear (38). Beyond the original observation that *EI24* deficiency leads to pronounced formation of non-functional autophagosomes even under steady state conditions, it was recently suggested that spontaneous Ca^{2+} fluxes across the ER membrane initiated autophagy in *EI24* deficient cells (39). How

3 Publications

bioRxiv preprint doi: <https://doi.org/10.1101/2023.06.01.542416>; this version posted June 1, 2023. The copyright holder for this preprint (which was not certified by peer review) is the author/funder, who has granted bioRxiv a license to display the preprint in perpetuity. It is made available under a [CC-BY-NC-ND 4.0 International license](#).

spontaneous induction of autophagosome formation in *EI24*^{-/-} cells can be reconciled with a defect in autophagy remained unclear. The results from our screen and the following live cell imaging experiments, in which we found *EI24*^{-/-} cells to form fewer autophagosomes than wildtype cells, now suggest that EI24 plays a – potentially additional – role in autophagosome formation.

Systems biology is increasingly driven by large-scale artificial intelligence models that set new standards for reconstructing and predicting cellular behavior, but require enormous amounts of data to train. In light of this development, comprehensive, unbiased data acquisition approaches that can generate large datasets across modalities have become highly desirable. In this context, SPARCS, with its focus on open and accessible design and the ability to screen large libraries, can make a valuable contribution to understanding biology from the molecular to the organismic scale.

3.2 SPARCS, a platform for genome-scale CRISPR screening for spatial cellular phenotypes

bioRxiv preprint doi: <https://doi.org/10.1101/2023.06.01.542416>; this version posted June 1, 2023. The copyright holder for this preprint (which was not certified by peer review) is the author/funder, who has granted bioRxiv a license to display the preprint in perpetuity. It is made available under a [CC-BY-NC-ND 4.0 International license](#).

Acknowledgements

We would like to thank Larissa Hansbauer for outstanding technical support; Jochen Rech and the BioSysM Liquid Handling Unit for excellent support with robotics; Claudia Ludwig and the BioSysM FACS Core Facility for great support with cell sorting; Mario Oroshi and the computing centre of the Max Planck Institute of Biochemistry for computational support and IT infrastructure; the Imaging Facility of the MPI of Biochemistry and the Center for Advanced Light Microscopy (CALM) for support with light microscopy; Rin Ho Kim and the Sequencing Facility of the MPI of Biochemistry as well as Stefan Krebs and the Genomics unit of the Laboratory for Functional Genome Analysis (LAFUGA) for sequencing; and Falk Schlaudraff, Christoph Greb and Florian Hoffmann from Leica Microsystems for technical support.

Funding

S.C.M. is a PhD fellow of the Boehringer-Ingelheim Fonds. This study was supported by the Max-Planck Society for Advancement of Science. This project was funded by European Research Council grant ERC-2020-ADG ENGINES (101018672 to V.H.).

Author Contributions

Conceptualization: N.A.S., S.C.M.; Formal Analysis: N.A.S., S.C.M., G.W.; Funding Acquisition: M.M., V.H.; Investigation: N.A.S., S.C.M., G.W., A.M., M.B., H.H.; Resources: H.H., H.L., M.M., V.H.; Software: N.A.S., S.C.M., G.W.; Visualization: N.A.S., S.C.M., G.W.; Writing – original draft: N.A.S., S.C.M., M.M., V.H.; Writing – review & editing: N.A.S., S.C.M., G.W., A.M., M.B., H.H., H.L., M.M., V.H.

Competing Interests

The authors declare no competing interests.

Data and materials availability

Code to recreate the figure manuscripts is available on GitHub (https://github.com/MannLabs/SPARCS_pub_figures).

The code described in this manuscript is available from the following GitHub repositories:

The py-lmd python library provides code to direct excision of defined regions on a Leica LMD7 laser microdissection microscope (<https://github.com/MannLabs/py-lmd>).

3 Publications

bioRxiv preprint doi: <https://doi.org/10.1101/2023.06.01.542416>; this version posted June 1, 2023. The copyright holder for this preprint (which was not certified by peer review) is the author/funder, who has granted bioRxiv a license to display the preprint in perpetuity. It is made available under a [CC-BY-NC-ND 4.0 International license](#).

The SPARCStools python library provides code to rename TIF image files generated by the PerkinElmer Harmony software and stitch these into WSIs (<https://github.com/MannLabs/SPARCStools>).

The SPARCSpy python library contains the autophagy classifiers, as well as code to segment and extract single-cell images from entire fields of view up to WSIs (<https://github.com/MannLabs/SPARCSpy>).

All other data are available from the authors upon request.

3.2 SPARCS, a platform for genome-scale CRISPR screening for spatial cellular phenotypes

bioRxiv preprint doi: <https://doi.org/10.1101/2023.06.01.542416>; this version posted June 1, 2023. The copyright holder for this preprint (which was not certified by peer review) is the author/funder, who has granted bioRxiv a license to display the preprint in perpetuity. It is made available under aCC-BY-NC-ND 4.0 International license.

Methods

Cell culture

U2OS cells were cultured in DMEM supplemented with 10 % fetal calf serum (FCS), penicillin/streptomycin and 1 mM sodium pyruvate and split every 2-3 days. PPS membrane slides were sterilized for 30 minutes under the UV light of a cell culture hood with their cavity side down. Cells were then plated onto these slides cavity down in 4-well plates with 5 mL DMEM per well.

Genome engineering

U2OS cells stably expressing Cas9, mCherry-LC3 and mNeon tagged N-terminally with the lipidation sequence of Lck (LckLip-mNeon, the original plasmid was a gift from Dorus Gadella (Addgene plasmid # 98821, (40))) were generated via lentiviral transduction. Briefly, HEK-293T cells were transfected with transfer plasmids for Cas9 or mCherry-LC3 and 3rd generation lentiviral particle production plasmids pMDLg and pRSV as wells as a VSV G-protein pseudotyping plasmid 18 hrs after plating. Eight hrs later, the medium was exchanged and cells were washed once in PBS. After 48 hrs supernatants containing viral particles were harvested and transferred onto U2OS cells plated 18 hrs before. 48 hrs later U2OS cells were washed. Cells were selected for Blasticidin resistance with 10 µg/mL Blasticidin or FACS-sorted for high fluorescent protein expression and single clones generated by limiting dilution cloning. A bright clone with a visible reaction to 600 nM Torin-1 was selected, expanded and used for all experiments. Lentiviral particles for the expression of individual sgRNAs from LentiGUIDE-Puro were generated analogously. Cells were selected for sgRNA expression with 5 µg/mL puromycin for 48 hrs. Of note, the cell line used for the autophagy screens did not yet stably express Cas9 but was instead transduced with a LentiCRISPRv2, a vector driving expression of both Cas9 and an sgRNA.

Laser microdissection

Cutting paths for laser microdissection of selected cells were generated using our open-source python library py-lmd (<https://github.com/MannLabs/py-lmd>) with the configurations specified in the “screen config” file. Each shape was dilated to ensure that the cutting line did not go through or damage the nucleus. Laser microdissection was carried out on a Leica LMD7 at 40 x magnification using the software version 8.3.0.8275. The microscope was equipped with the Okolab LMD climate chamber (H201-ENCLOSURE-LMD and H201-LEICA-LMD) to ensure stable temperatures throughout the cutting process. Slides were equilibrated in the microscope to 34.5 °C before cutting to ensure focus stability. Cutting contours were imported from the XML files generated with py-lmd after reference point alignment and cut with the following settings: power 60, aperture 1, speed 100, head current 46 % - 51 %, pulse frequency 1128 and offset 185. Autofocus adjustment was performed every 30 shapes. Shapes were sorted into 48-well plates. During cutting a custom-built wind protection was used around

bioRxiv preprint doi: <https://doi.org/10.1101/2023.06.01.542416>; this version posted June 1, 2023. The copyright holder for this preprint (which was not certified by peer review) is the author/funder, who has granted bioRxiv a license to display the preprint in perpetuity. It is made available under a [CC-BY-NC-ND 4.0 International license](#).

the collection plate to ensure collection of excised shapes into the center of the well and prevent wind disturbances. After cutting, samples were stored at 4 °C before lysis and library generation.

CNN-based image classifier training

Neural networks with 9 randomly initialized convolutional layers and 3 (classifiers 1, P) or 4 (classifiers 2.1 & 2.2) linear layers were trained to classify segmented single cell images as autophagy-on or autophagy-off (table S1). The training datasets were based on several biological replicates of mCherry-LC3 expressing U2OS cells with and without autophagosomes. The autophagy-off class consisted of images from unstimulated wildtype cells (pre-filtered to remove cells showing spontaneous autophagosome formation for 2.1 and 2.2) and two different *ATG5*^{-/-} clones. Where applicable, pre-filtering was performed with classifier P. The autophagy-on class consisted of single-cell images from stimulated wildtype cells, where applicable pre-filtered with classifier P to remove non-responding cells. To increase variability captured in the training data, the training slides were plated at an angle to include varying cell densities on one slide. 500 k, 1 million or 1.2 million single-cell images respectively were randomly selected from each class for training while ensuring balanced sampling from each test slide. An additional 50 k cells from each class were used for testing and validation during training. Training data were augmented by Gaussian blur, addition of Gaussian noise and random rotations in 90° steps. Training was performed using single-gradient descent with a learning rate of 1×10^{-3} . Gradient clipping was set to 0.5. Training was performed over a total of 20, 30 or 40 epochs. Classifier performance was tested on a biologically independent set of unstimulated wildtype cells, Torin-1 stimulated wildtype cells and *ATG5*^{-/-} cells. Models were built and trained using PyTorch (41).

Segmentation of individual cells

Images were flat-field corrected during image acquisition using the Perkin Elmer Harmony software (v4.9) and intensity rescaled to the 1 % and 99 % quantile. Extremely bright regions (pixel values greater than 40000) were set to 0 before determining the normalization quantiles. Stitching of image tiles was performed using the ashlar python API (42) in our open-source python library SPARCStools (<https://github.com/MannLabs/SPARCStools>).

Stitched whole slide images were segmented using our open-source SPARCSpy python library (<https://github.com/MannLabs/SPARCSpy>) with the parameters defined in “config_screen” or “config_training” respectively. A nucleus segmentation mask was generated using a local median thresholding approach and the cytosol segmentation mask was calculated using fast marching from nuclear centroids with WGA staining as a potential map.

Single cell images were extracted based on nuclear and cytosolic segmentation masks. The masked area was extended using a Gaussian filter with a sigma of 5 to extract information from each of the imaged channels and saved to hdf5 files as individual 128 × 128 px images.

3.2 SPARCS, a platform for genome-scale CRISPR screening for spatial cellular phenotypes

bioRxiv preprint doi: <https://doi.org/10.1101/2023.06.01.542416>; this version posted June 1, 2023. The copyright holder for this preprint (which was not certified by peer review) is the author/funder, who has granted bioRxiv a license to display the preprint in perpetuity. It is made available under a [CC-BY-NC-ND 4.0 International license](#).

Sample preparation and imaging of autophagy

After stimulation with 600nM Torin-1, PPS slides were washed 1x in PBS in a Coplin jar and then stained with 10 µg/mL WGA-Alexa488 in PBS for 10 minutes at 37 °C. After washing 1 x with PBS slides were fixed for 10 minutes at room temperature in 4 % MeOH-free PFA in PBS in 4-well plates. After washing 3 x in PBS, slides were stained with 10 µg/mL Hoechst-33342 in PBS at 37 °C for at least 30 minutes. After washing 3 x in PBS, slides were dried in a centrifuge at 3,400 g for 1 minute. Cells in ibidi microwell slides and plates were stained according to the same protocol but imaged in PBS. Imaging was done on a Nikon Eclipse Ti2 spinning disk confocal microscope or an Opera Phenix high-content imager as indicated.

Genetic screening for autophagy regulators

We conducted our screen in mCherry-LC3 expressing U2OS cells using the Brunello human CRISPR KO library in the LentiCRISPRv2 backbone. The Brunello library was a gift from David Root and John Doench (Addgene #73178) and amplified according to their protocol (33). U2OS cells were transduced with lentiviral particles produced as described above at an MOI of approximately 0.2. After 48 hrs, successfully transduced cells were selected with 5 µg/mL puromycin for two days and then expanded for three days. We then plated 50 million cells on a total of 109 slides in 4 well plates, and in addition included unstimulated and wildtype controls on separate slides with every screening batch for classifier training. The day after plating, cells were stimulated with 600 nM Torin-1 for 14 hrs. Slides were then prepared for microscopy as described above and imaged on an Opera Phenix high content imager at 20 x resolution. Where applicable slides were stored at -20 °C and brought to 4 °C the day before laser microdissection. Cells from each bin were excised into multiple wells. Nuclei were then lysed in 48-well plates using the arcturus PicoPure™ DNA extraction kit. 120 µL of lysis buffer was added to each well and incubated at 65 °C for 4 hrs. Proteinase K was inactivated at 95 °C for 15 mins. Cooled samples were transferred to PCR tubes and the emptied wells were rinsed with 40 µL of ddH₂O. Amplification of sgRNAs was performed as described previously (43) but in a single step PCR (33) over 36 cycles with no added water. Sequencing was performed on an Illumina NextSeq with 500 reads per nucleus on average. An sgRNA read count table was generated for each sequencing library. Low quality sgRNAs were removed by applying a minimum number of reads per sgRNA threshold that was set based on the distribution of read counts per sgRNA in the sample. The non-targeting sgRNA with the sequence TACGTCATTAAGAGTTCAAC was excluded from sequencing results of approximately 40 % of cells from bins 3 - 6 of batch 2 of the genome-wide screen due to a contamination of the sequencing library leading to abnormally high read counts of this specific sequence. For further analysis only sgRNAs with at least a fraction of reads corresponding to a single cell per well were used. sgRNA read fractions of individual wells were then aggregated per bin by multiplying with the fraction of excised cells in that well over all excised cells in the bin. The per-bin aggregated sequencing results

3 Publications

bioRxiv preprint doi: <https://doi.org/10.1101/2023.06.01.542416>; this version posted June 1, 2023. The copyright holder for this preprint (which was not certified by peer review) is the author/funder, who has granted bioRxiv a license to display the preprint in perpetuity. It is made available under a [CC-BY-NC-ND 4.0 International license](#).

were used for all further data analysis. Enrichment values were determined by normalizing the aggregated fraction of reads per sgRNA to the fraction of reads per sgRNA in the input cell library.

Immunoblotting

20,000 U2OS cells were plated per 96-well. 18 hrs after plating, cells were stimulated and then harvested in 1 x Lämmli buffer. 3 wells were pooled per condition. Lysates were boiled at 95 °C for 5 min. and then run on 16 % TRIS-glycine polyacrylamide gels before immunoblotting onto 0.2 µm nitrocellulose membrane for 90 minutes. Membranes were blocked in 5 % milk in PBST for 1 hr and incubated with primary antibody at 4 °C overnight. After washing 3 x in PBST for a total of 15 min. membranes were incubated with HRP-labelled secondary antibody for 2 hrs at room temperature. After washing 3 x in PBST for a total of 15 min. membranes were covered in luminescent HRP substrate and immediately imaged.

3.2 SPARCS, a platform for genome-scale CRISPR screening for spatial cellular phenotypes

bioRxiv preprint doi: <https://doi.org/10.1101/2023.06.01.542416>; this version posted June 1, 2023. The copyright holder for this preprint (which was not certified by peer review) is the author/funder, who has granted bioRxiv a license to display the preprint in perpetuity. It is made available under aCC-BY-NC-ND 4.0 International license.

References

1. S. Brenner, The genetics of *Caenorhabditis elegans*. *Genetics* **77**, 71-94 (1974).
2. C. Nusslein-Volhard, E. Wieschaus, Mutations affecting segment number and polarity in *Drosophila*. *Nature* **287**, 795-801 (1980).
3. N. Kayagaki *et al.*, Caspase-11 cleaves gasdermin D for non-canonical inflammasome signalling. *Nature* **526**, 666-671 (2015).
4. J. Y. Wang, J. A. Doudna, CRISPR technology: A decade of genome editing is only the beginning. *Science* **379**, eadd8643 (2023).
5. O. Shalem, N. E. Sanjana, F. Zhang, High-throughput functional genomics using CRISPR-Cas9. *Nat. Rev. Genet.* **16**, 299-311 (2015).
6. B. Adamson *et al.*, A Multiplexed Single-Cell CRISPR Screening Platform Enables Systematic Dissection of the Unfolded Protein Response. *Cell* **167**, 1867-1882 e1821 (2016).
7. D. A. Jaitin *et al.*, Dissecting Immune Circuits by Linking CRISPR-Pooled Screens with Single-Cell RNA-Seq. *Cell* **167**, 1883-1896 e1815 (2016).
8. A. Dixit *et al.*, Perturb-Seq: Dissecting Molecular Circuits with Scalable Single-Cell RNA Profiling of Pooled Genetic Screens. *Cell* **167**, 1853-1866 e1817 (2016).
9. P. Datlinger *et al.*, Pooled CRISPR screening with single-cell transcriptome readout. *Nat Methods* **14**, 297-301 (2017).
10. J. M. Replogle *et al.*, Mapping information-rich genotype-phenotype landscapes with genome-scale Perturb-seq. *Cell* **185**, 2559-2575 e2528 (2022).
11. A. Wroblewska *et al.*, Protein Barcodes Enable High-Dimensional Single-Cell CRISPR Screens. *Cell* **175**, 1141-1155 e1116 (2018).
12. M. Lawson, J. Elf, Imaging-based screens of pool-synthesized cell libraries. *Nat Methods* **18**, 358-365 (2021).
13. A. J. Rubin *et al.*, Coupled Single-Cell CRISPR Screening and Epigenomic Profiling Reveals Causal Gene Regulatory Networks. *Cell* **176**, 361-376 e317 (2019).
14. O. Parnas *et al.*, A Genome-wide CRISPR Screen in Primary Immune Cells to Dissect Regulatory Networks. *Cell* **162**, 675-686 (2015).
15. O. Shalem *et al.*, Genome-scale CRISPR-Cas9 knockout screening in human cells. *Science* **343**, 84-87 (2014).
16. T. Wang, J. J. Wei, D. M. Sabatini, E. S. Lander, Genetic screens in human cells using the CRISPR-Cas9 system. *Science* **343**, 80-84 (2014).
17. M. M. Gaidt *et al.*, The DNA Inflammasome in Human Myeloid Cells Is Initiated by a STING-Cell Death Program Upstream of NLRP3. *Cell* **171**, 1110-1124.e1118 (2017).
18. M. Boutros, F. Heigwer, C. Laufer, Microscopy-Based High-Content Screening. *Cell* **163**, 1314-1325 (2015).
19. D. Feldman *et al.*, Optical Pooled Screens in Human Cells. *Cell* **179**, 787-799 e717 (2019).
20. L. Funk *et al.*, The phenotypic landscape of essential human genes. *Cell* **185**, 4634-4653 e4622 (2022).
21. R. J. Carlson, M. D. Leiken, A. Guna, N. Hacohen, P. C. Blainey, A genome-wide optical pooled screen reveals regulators of cellular antiviral responses. *Proc Natl Acad Sci U S A* **120**, e2210623120 (2023).
22. N. Nitta *et al.*, Intelligent Image-Activated Cell Sorting. *Cell* **175**, 266-276 e213 (2018).

3 Publications

bioRxiv preprint doi: <https://doi.org/10.1101/2023.06.01.542416>; this version posted June 1, 2023. The copyright holder for this preprint (which was not certified by peer review) is the author/funder, who has granted bioRxiv a license to display the preprint in perpetuity. It is made available under a [CC-BY-NC-ND 4.0 International license](#).

23. D. Schraivogel *et al.*, High-speed fluorescence image-enabled cell sorting. *Science* **375**, 315-320 (2022).
24. G. D. Victora *et al.*, Germinal center dynamics revealed by multiphoton microscopy with a photoactivatable fluorescent reporter. *Cell* **143**, 592-605 (2010).
25. G. Kanfer *et al.*, Image-based pooled whole-genome CRISPRi screening for subcellular phenotypes. *J Cell Biol* **220**, (2021).
26. X. Yan *et al.*, High-content imaging-based pooled CRISPR screens in mammalian cells. *J Cell Biol* **220**, (2021).
27. J. Lee *et al.*, Versatile phenotype-activated cell sorting. *Sci Adv* **6**, (2020).
28. N. Hasle *et al.*, High-throughput, microscope-based sorting to dissect cellular heterogeneity. *Mol Syst Biol* **16**, e9442 (2020).
29. L. F. Waanders *et al.*, Quantitative proteomic analysis of single pancreatic islets. *Proc Natl Acad Sci U S A* **106**, 18902-18907 (2009).
30. F. Coscia *et al.*, A streamlined mass spectrometry-based proteomics workflow for large-scale FFPE tissue analysis. *J Pathol* **251**, 100-112 (2020).
31. A. Mund *et al.*, Deep Visual Proteomics defines single-cell identity and heterogeneity. *Nat Biotechnol* **40**, 1231-1240 (2022).
32. F. A. Rosenberger *et al.*, Spatial single-cell mass spectrometry defines zonation of the hepatocyte proteome. *bioRxiv*, 2022.2012.2003.518957 (2022).
33. J. G. Doench *et al.*, Optimized sgRNA design to maximize activity and minimize off-target effects of CRISPR-Cas9. *Nature ...* **34**, 184-191 (2016).
34. I. Dikic, Z. Elazar, Mechanism and medical implications of mammalian autophagy. *Nat Rev Mol Cell Biol* **19**, 349-364 (2018).
35. H. Yamamoto, S. Zhang, N. Mizushima, Autophagy genes in biology and disease. *Nat Rev Genet*, 1-19 (2023).
36. T. Sainburg, L. McInnes, T. Q. Gentner, Parametric UMAP embeddings for representation and semi-supervised learning. 2020 (10.48550/arXiv.2009.12981).
37. P. J. Thul *et al.*, A subcellular map of the human proteome. *Science* **356**, (2017).
38. Y. Tian *et al.*, *C. elegans* screen identifies autophagy genes specific to multicellular organisms. *Cell* **141**, 1042-1055 (2010).
39. Q. Zheng *et al.*, Calcium transients on the ER surface trigger liquid-liquid phase separation of FIP200 to specify autophagosome initiation sites. *Cell* **185**, 4082-4098 e4022 (2022).
40. A. O. Chertkova *et al.*, Robust and Bright Genetically Encoded Fluorescent Markers for Highlighting Structures and Compartments in Mammalian Cells. *bioRxiv*, 160374 (2020).
41. A. Paszke *et al.*, PyTorch: An Imperative Style, High-Performance Deep Learning Library. 2019 (10.48550/arXiv.1912.01703).
42. J. L. Muhlich *et al.*, Stitching and registering highly multiplexed whole-slide images of tissues and tumors using ASHLAR. *Bioinformatics* **38**, 4613-4621 (2022).
43. T. Schmidt, J. L. Schmid-Burgk, V. Hornung, Synthesis of an arrayed sgRNA library targeting the human genome. *Scientific Reports* **5**, 14987 (2015).

3.2 SPARCS, a platform for genome-scale CRISPR screening for spatial cellular phenotypes

bioRxiv preprint doi: <https://doi.org/10.1101/2023.06.01.542416>; this version posted June 1, 2023. The copyright holder for this preprint (which was not certified by peer review) is the author/funder, who has granted bioRxiv a license to display the preprint in perpetuity. It is made available under aCC-BY-NC-ND 4.0 International license.

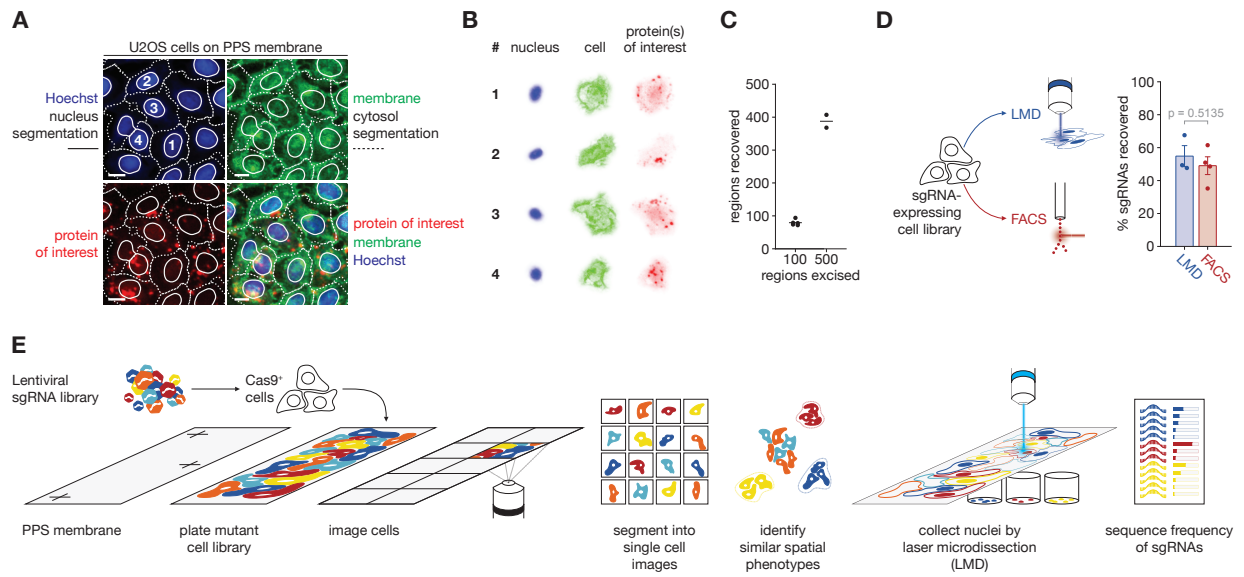


Figure 1

bioRxiv preprint doi: <https://doi.org/10.1101/2023.06.01.542416>; this version posted June 1, 2023. The copyright holder for this preprint (which was not certified by peer review) is the author/funder, who has granted bioRxiv a license to display the preprint in perpetuity. It is made available under a [CC-BY-NC-ND 4.0 International license](#).

Figure 1 | SPARCS enables genome-wide CRISPR screening for spatial phenotypes in human cells

(A) Example images of U2OS cells on PPS membranes in several channels. Solid lines indicate nuclear segmentation based on Hoechst DNA staining; dotted lines indicate cytosol segmentation based on fast marching from nuclear centroids with wheat germ agglutinin (WGA)-Alexa 488 staining as a potential map. Numbers correspond to images of individual cells shown in (B). Images were acquired on an Opera Phenix microscope in confocal mode with 20 x magnification. Scalebars represent 15 μm . PPS: polyphenylene sulfide.

(B) Post-segmentation images of individual mCherry-LC3 expressing U2OS cells. Numbers correspond to cells shown in (A).

(C) 100 or 500 regions were excised from U2OS cells grown on a PPS membrane slide and subsequently counted. Five and two technical replicates were excised from one slide, respectively.

(D) Comparison of sgRNA recovery after isolation of sgRNA-expressing fixed cells from one library either by laser microdissection (Leica LMD7, 1,000 nuclei per replicate, 3 independent biological replicates) or FACS (technical replicates). Bars indicate mean % sgRNAs recovered, error bars indicate SEM. p-value was calculated with an unpaired two-tailed t-test.

(E) Overview of genome-wide CRISPR screening for microscopy-based spatial phenotypes with the SPARCS pipeline. Laser microdissection of individual nuclei on a Leica LMD7 has been optimized to isolate 1,000 nuclei/hr. Instructions for laser microdissection of selected cells are generated using our open-source python library py-lmd. PPS: polyphenylene sulfide.

3.2 SPARCS, a platform for genome-scale CRISPR screening for spatial cellular phenotypes

bioRxiv preprint doi: <https://doi.org/10.1101/2023.06.01.542416>; this version posted June 1, 2023. The copyright holder for this preprint (which was not certified by peer review) is the author/funder, who has granted bioRxiv a license to display the preprint in perpetuity. It is made available under aCC-BY-NC-ND 4.0 International license.

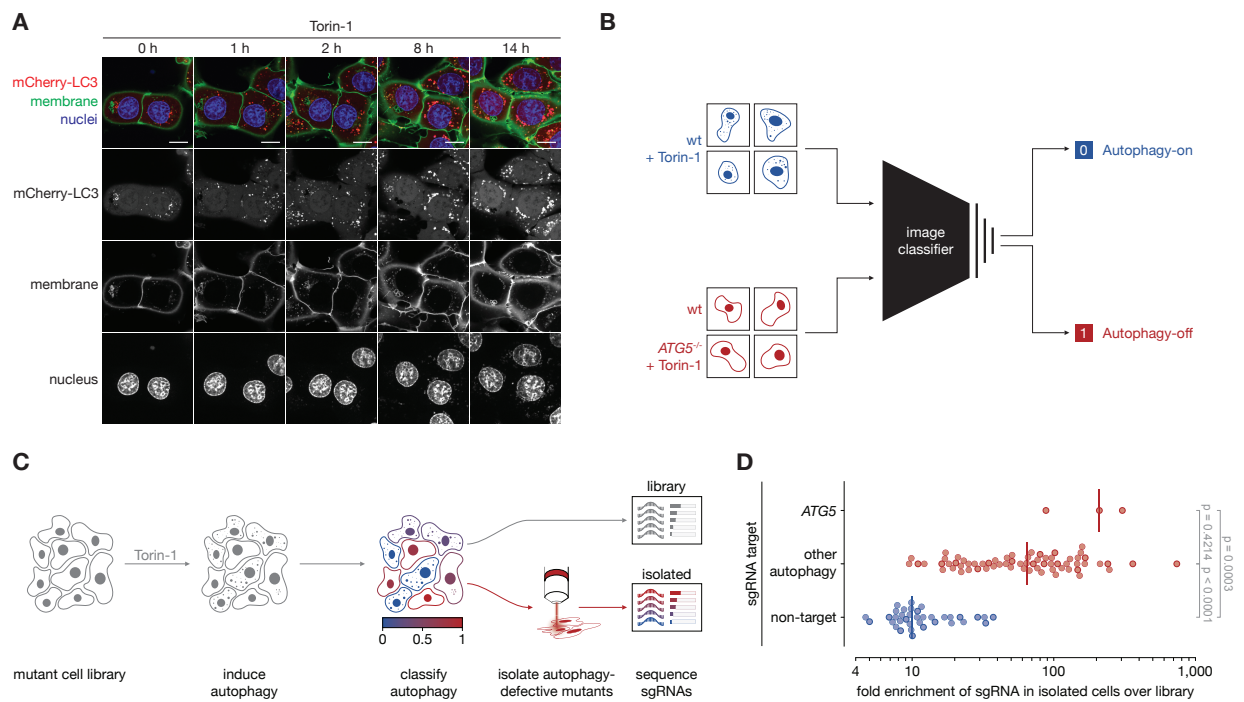


Figure 2

bioRxiv preprint doi: <https://doi.org/10.1101/2023.06.01.542416>; this version posted June 1, 2023. The copyright holder for this preprint (which was not certified by peer review) is the author/funder, who has granted bioRxiv a license to display the preprint in perpetuity. It is made available under a [CC-BY-NC-ND 4.0 International license](#).

Figure 2 | SPARCS achieves strong enrichment of spatial phenotypes in a forward genetic screen

(A) U2OS cells expressing mCherry-LC3 and mNeon tagged with the lipidation signal of Lck at the N-terminus (membrane marker) were stimulated with Torin-1 and imaged live once per hour on a Nikon Eclipse Ti2 confocal microscope with 100 x magnification. Scalebars represent 15 μm . One representative of three independent experiments.

(B) Schematic describing the training of a convolutional neural network-based image classifier for the identification of individual autophagy-defective cells.

(C) Overview of SPARCS screening for autophagy.

(D) Results from a SPARCS screen for autophagosome formation on 1.2 million U2OS cells. The top 0.1 % of cells classified as autophagy-off with a score above 0.94 by classifier 1.0 were isolated by laser microdissection (LMD) and their sgRNAs sequenced to determine their enrichment relative to the input library. p-values were calculated with a Kruskal-Wallis test followed by Tukey's test.

3.2 SPARCS, a platform for genome-scale CRISPR screening for spatial cellular phenotypes

bioRxiv preprint doi: <https://doi.org/10.1101/2023.06.01.542416>; this version posted June 1, 2023. The copyright holder for this preprint (which was not certified by peer review) is the author/funder, who has granted bioRxiv a license to display the preprint in perpetuity. It is made available under aCC-BY-NC-ND 4.0 International license.

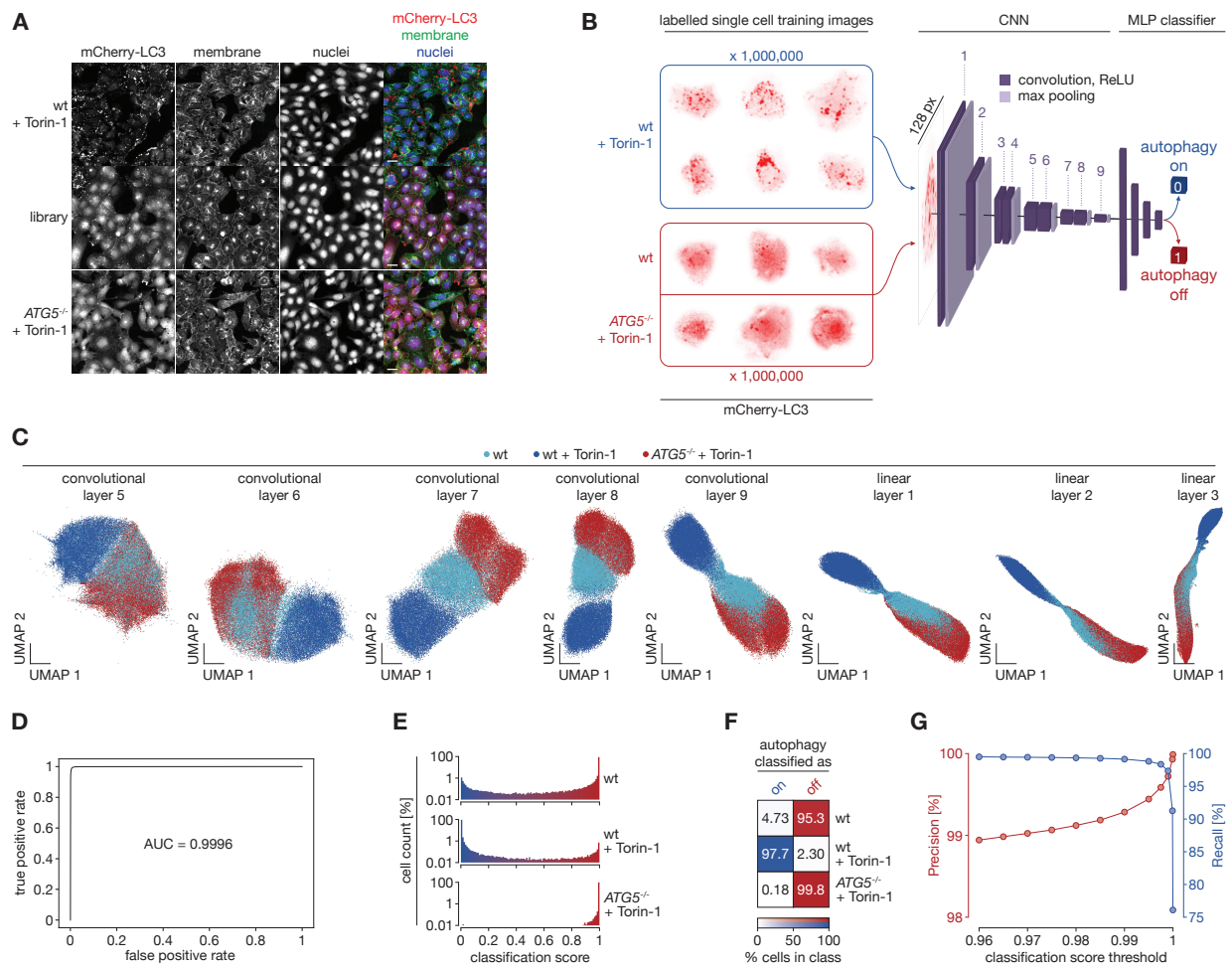


Figure 3

bioRxiv preprint doi: <https://doi.org/10.1101/2023.06.01.542416>; this version posted June 1, 2023. The copyright holder for this preprint (which was not certified by peer review) is the author/funder, who has granted bioRxiv a license to display the preprint in perpetuity. It is made available under a [CC-BY-NC-ND 4.0 International license](#).

Figure 3 | Deep learning accurately identifies autophagy-defective cells

(A) Unsegmented images that were used for training autophagy classifier 2.0 after segmentation. Membranes were stained with WGA-Alexa488. “Library” refers to cells transduced with the Brunello CRISPR KO library. Images were acquired on an Opera Phenix microscope in confocal mode with 20 x magnification. Scale bars represent 30 μm .

(B) Overview of the architecture and training paradigm of the convolutional neural network-based classifier 2.0 for autophagic or non-autophagic distribution of mCherry-LC3 in single U2OS cells. 1 million 128×128 px single cell images from several biological replicates were used in each training class. The autophagy-on class consisted of images of wildtype cells stimulated with Torin-1 pre-filtered for responsive cells. The autophagy-off class consisted of images of unstimulated wildtype cells pre-filtered to remove cells showing spontaneous autophagosome formation and images from two different *ATG5^{-/-}* clones. Images were acquired on an Opera Phenix microscope in confocal mode with 20 x magnification. CNN: convolutional neural network. MLP: multilayer perceptron.

(C) UMAPs of mCherry-LC3 images of single U2OS cells featurized through the autophagy classifier 2.0 illustrated in (B) up to the indicated layers. Colors depict the indicated genotypes and treatments. 20,000 cells are shown for each genotype and treatment.

(D) Receiver Operating Characteristic (ROC) curve of the autophagy classifier 2.0. AUC: Area under the curve.

(E) Histograms of images of mCherry-LC3 expressing U2OS cells of the indicated genotypes treated as indicated after autophagy classification with our classifier 2.0 as illustrated in (B).

(F) Heatmap showing the percentage of cells in e classified as autophagy-on or autophagy-off with a classification score threshold of 0.5.

(G) Precision (Percent *ATG5^{-/-}* among cells classified as autophagy-off from an equal mix of Torin-1 stimulated wildtype cells and *ATG5^{-/-}* cells) and recall (Percent *ATG5^{-/-}* cells classified as autophagy-off) of our autophagy classifier at different thresholds for classifying cells as “autophagy-defective”.

The data used for (C) – (G) come from an independent test dataset that was not used during training of the autophagy classifier.

3.2 SPARCS, a platform for genome-scale CRISPR screening for spatial cellular phenotypes

bioRxiv preprint doi: <https://doi.org/10.1101/2023.06.01.542416>; this version posted June 1, 2023. The copyright holder for this preprint (which was not certified by peer review) is the author/funder, who has granted bioRxiv a license to display the preprint in perpetuity. It is made available under aCC-BY-NC-ND 4.0 International license.

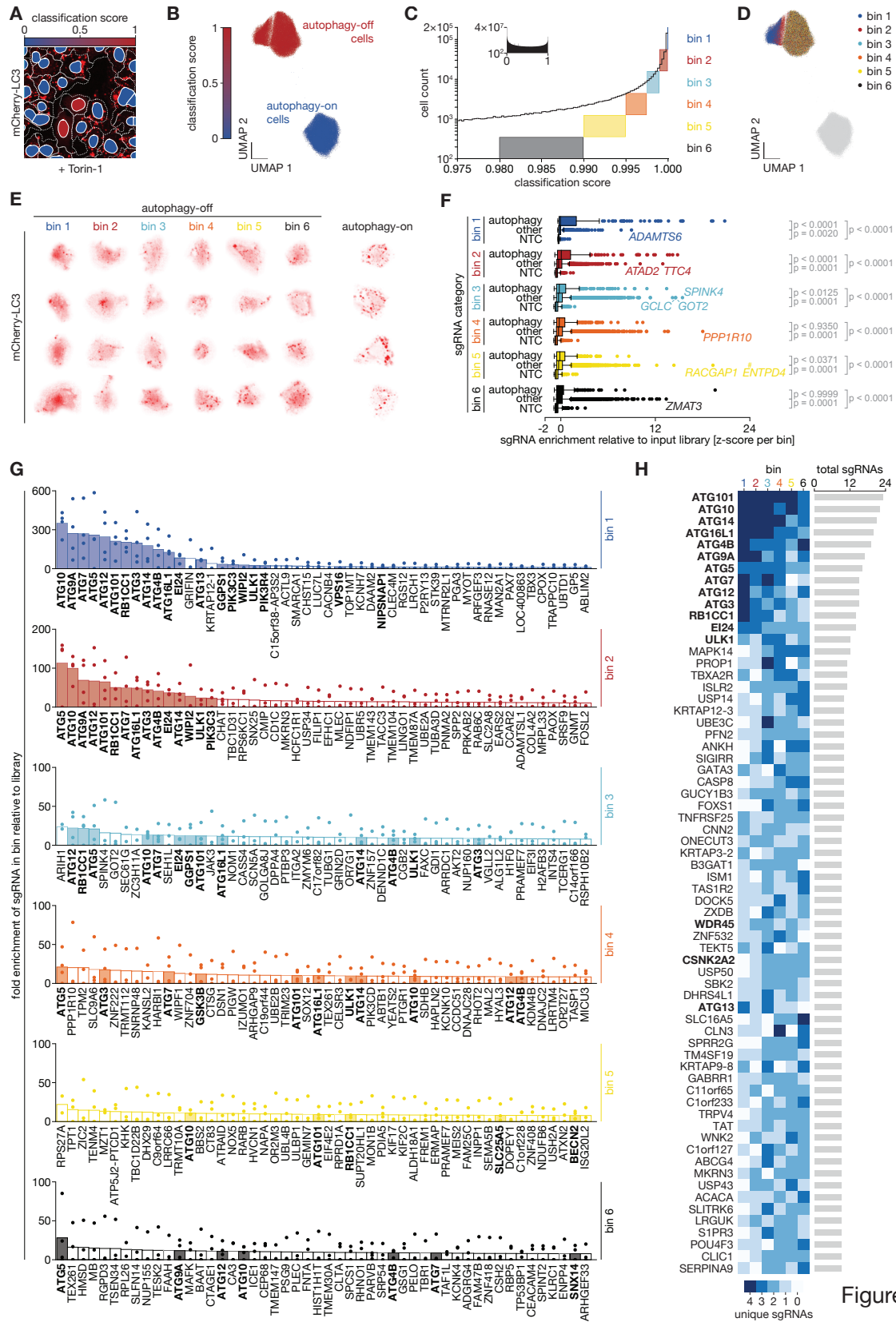


Figure 4

bioRxiv preprint doi: <https://doi.org/10.1101/2023.06.01.542416>; this version posted June 1, 2023. The copyright holder for this preprint (which was not certified by peer review) is the author/funder, who has granted bioRxiv a license to display the preprint in perpetuity. It is made available under a [CC-BY-NC-ND 4.0 International license](#).

Figure 4 | Genome-wide CRISPR screening for autophagosome formation in 40 million U2OS cells using SPARCS

(A) Example region from a genome-wide SPARCS CRISPR knockout screen on autophagosome formation in mCherry-LC3 expressing U2OS cells after Torin-1 stimulation for 14 hrs. Colors in nuclei indicate the result of binary autophagy classification with the classifier 2.1, dotted lines indicate cytosol segmentation. Images were acquired on an Opera Phenix microscope in confocal mode with 20 x magnification.

(B) Histogram of autophagy classification scores in the genome-wide CRISPR KO library batch 2 (inset) zoomed in on cells classified as autophagy-off with a score above 0.975. Colored boxes illustrate the binning strategy we used to isolate cells for sgRNA sequencing.

(C) UMAP representation of single cell images from all cells in screen batch 2 with a classification score ≥ 0.98 (dark blue) or < 0.02 (light blue) featurized through the first 8 convolutional layers of autophagy classifier 2.1. 91,320 images are depicted for each category.

(D) As C but colored according to our binning strategy along different autophagy classification thresholds as outlined in (B). 15,220 images are depicted per bin. Right panel shows a magnification of the UMAP region containing the putative screening hits.

(E) Images of individual cells from each bin in screen batch 2.

(F) z-scored enrichments of individual sgRNAs in each bin from batches 1 & 2. Vertical lines depict median, boxes depict interquartile range (IQR) and whiskers depict $1.5 \times \text{IQR}$. #: One sgRNA targeting the gene *ENTPD4* with a z-score of 42.1 in bin 5 is not depicted. p-values were calculated with a Kruskal-Wallis test followed by Dunn's test. NTC: non-targeting control.

(G) sgRNA sequencing results of the top 50 genes in each of the six bins filtered for genes for which we found at least two different sgRNAs in the respective bin in batches 1 & 2. Enrichment is calculated as the fraction of reads for an sgRNA in the respective bin divided by the fraction of reads of that sgRNA in the entire library. Bars indicate average enrichment per gene calculated from the enrichment of individual sgRNAs indicated as dots. Filled bars depict autophagy-related genes highlighted in bold.

(H) Number of different sgRNAs per gene in each bin for all genes with at least 9 total sgRNAs across all bins. sgRNAs were counted if they were sequenced with a read fraction in the top 50 % per bin.

3.2 SPARCS, a platform for genome-scale CRISPR screening for spatial cellular phenotypes

bioRxiv preprint doi: <https://doi.org/10.1101/2023.06.01.542416>; this version posted June 1, 2023. The copyright holder for this preprint (which was not certified by peer review) is the author/funder, who has granted bioRxiv a license to display the preprint in perpetuity. It is made available under aCC-BY-NC-ND 4.0 International license.

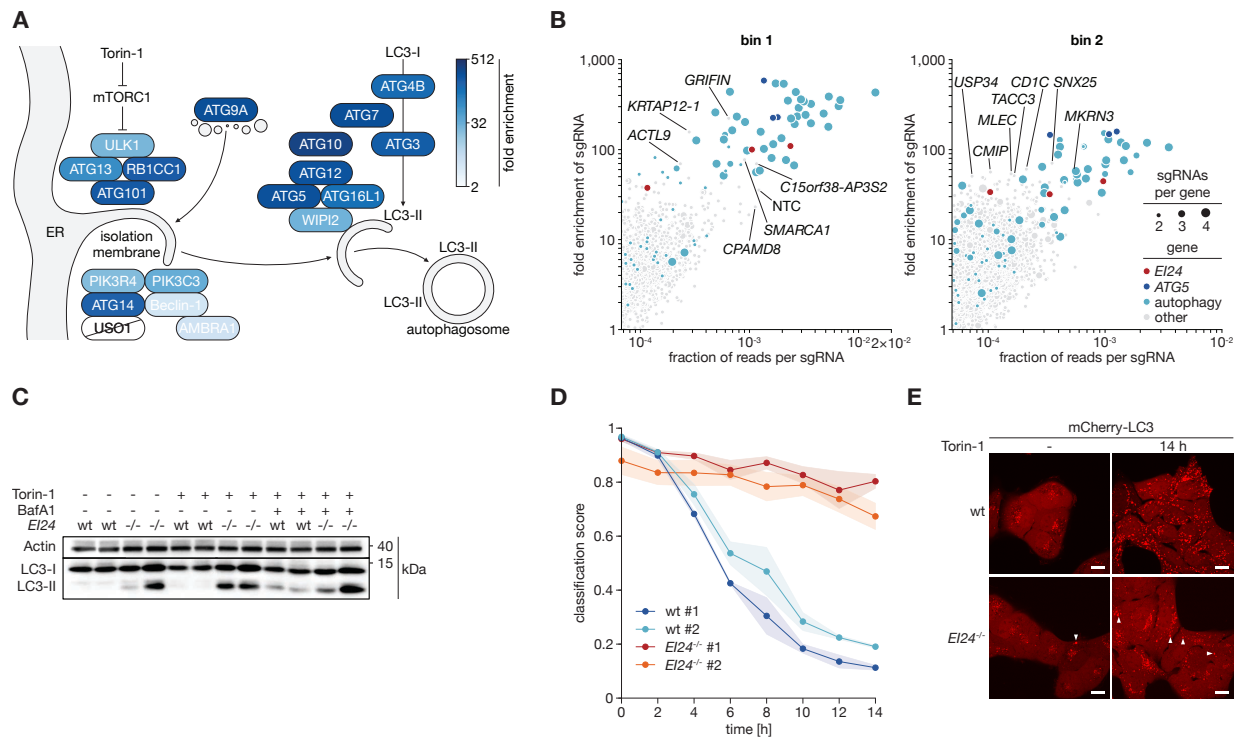


Figure 5

bioRxiv preprint doi: <https://doi.org/10.1101/2023.06.01.542416>; this version posted June 1, 2023. The copyright holder for this preprint (which was not certified by peer review) is the author/funder, who has granted bioRxiv a license to display the preprint in perpetuity. It is made available under a [CC-BY-NC-ND 4.0 International license](#).

Figure 5 | Analysis of hits from genome-wide SPARCS screen

(A) Overview of the canonical macroautophagy pathway. Colors indicate the highest enrichment value we found for a given gene in any bin. *USO1* was not found with at least two different sgRNAs in any single bin.

(B) Enrichment vs read count for individual sgRNAs in the top two bins for genes where we found at least two different sgRNAs in the respective bin. Circle sizes indicate the total number of different sgRNAs we found for a given gene, colors indicate different groups of genes. Individual sgRNAs from the “other” group are annotated. NTC: non-targeting control.

(C) Immunoblot of endogenous LC3 lipidation in wildtype and *EI24*^{-/-} mCherry-LC3 and LckLip-mNeon expressing U2OS cell. Two clones are shown per genotype. One representative of three independent experiments.

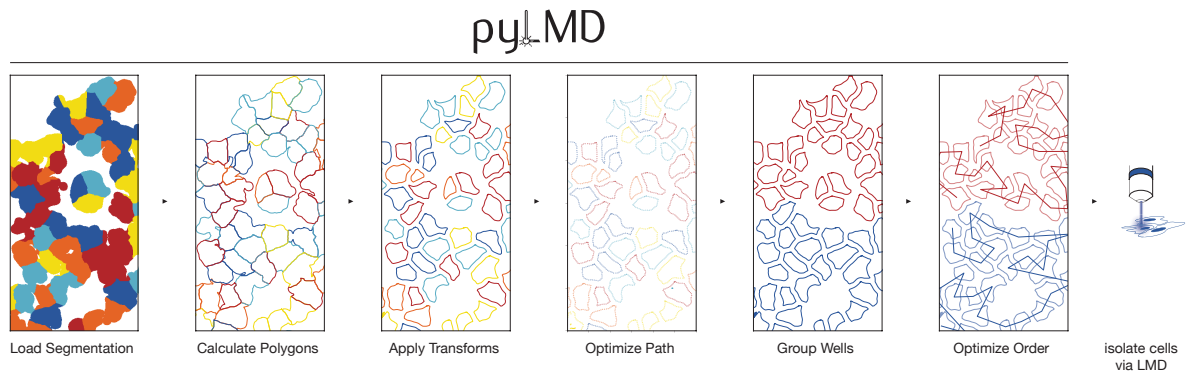
(D) Time course analysis of autophagy classification in clones of wildtype and *EI24*^{-/-} mCherry-LC3 and LckLip-mNeon expressing U2OS cells. Cells were treated with Torin-1 for up to 14 hrs. Dots represent average classifier scores from cells in 15 fields of view per timepoint and clone from three independent experiments, shaded areas represent SEM. Images were acquired on an Opera Phenix microscope in confocal mode with 20 x magnification.

(E) Images of live mCherry-LC3 and LckLip-mNeon expressing wildtype and *EI24*^{-/-} U2OS cells after 14 hrs of Torin-1 stimulation. Arrowheads indicate larger mCherry-LC3 aggregates. Images were acquired on a Nikon Eclipse Ti2 confocal microscope with 100 x magnification. Scalebars represent 15µm. One representative of three independent experiments.

3.2 SPARCS, a platform for genome-scale CRISPR screening for spatial cellular phenotypes

bioRxiv preprint doi: <https://doi.org/10.1101/2023.06.01.542416>; this version posted June 1, 2023. The copyright holder for this preprint (which was not certified by peer review) is the author/funder, who has granted bioRxiv a license to display the preprint in perpetuity. It is made available under a [CC-BY-NC-ND 4.0 International license](#).

A



B

```
from lmd.lib import Collection
from lmd import tools

my_collection = Collection()

my_collection.join(
    tools.makeCross([20, 20], [50, 30, 30, 50], 1, 10)
)

my_collection.join(
    tools.glyph('A', offset=(-50, 130))
)

my_collection.join(
    tools.text('283', offset=(130, 20))
)
```



Figure S1

3 Publications

bioRxiv preprint doi: <https://doi.org/10.1101/2023.06.01.542416>; this version posted June 1, 2023. The copyright holder for this preprint (which was not certified by peer review) is the author/funder, who has granted bioRxiv a license to display the preprint in perpetuity. It is made available under a [CC-BY-NC-ND 4.0 International license](#).

Figure S1 | The py-lmd python library generates cutting paths for automated laser microdissection

(A) Overview of cutting path generation with py-lmd.

(B) py-lmd allows the generation of arbitrary shapes such as calibration crosses.

3.2 SPARCS, a platform for genome-scale CRISPR screening for spatial cellular phenotypes

bioRxiv preprint doi: <https://doi.org/10.1101/2023.06.01.542416>; this version posted June 1, 2023. The copyright holder for this preprint (which was not certified by peer review) is the author/funder, who has granted bioRxiv a license to display the preprint in perpetuity. It is made available under aCC-BY-NC-ND 4.0 International license.

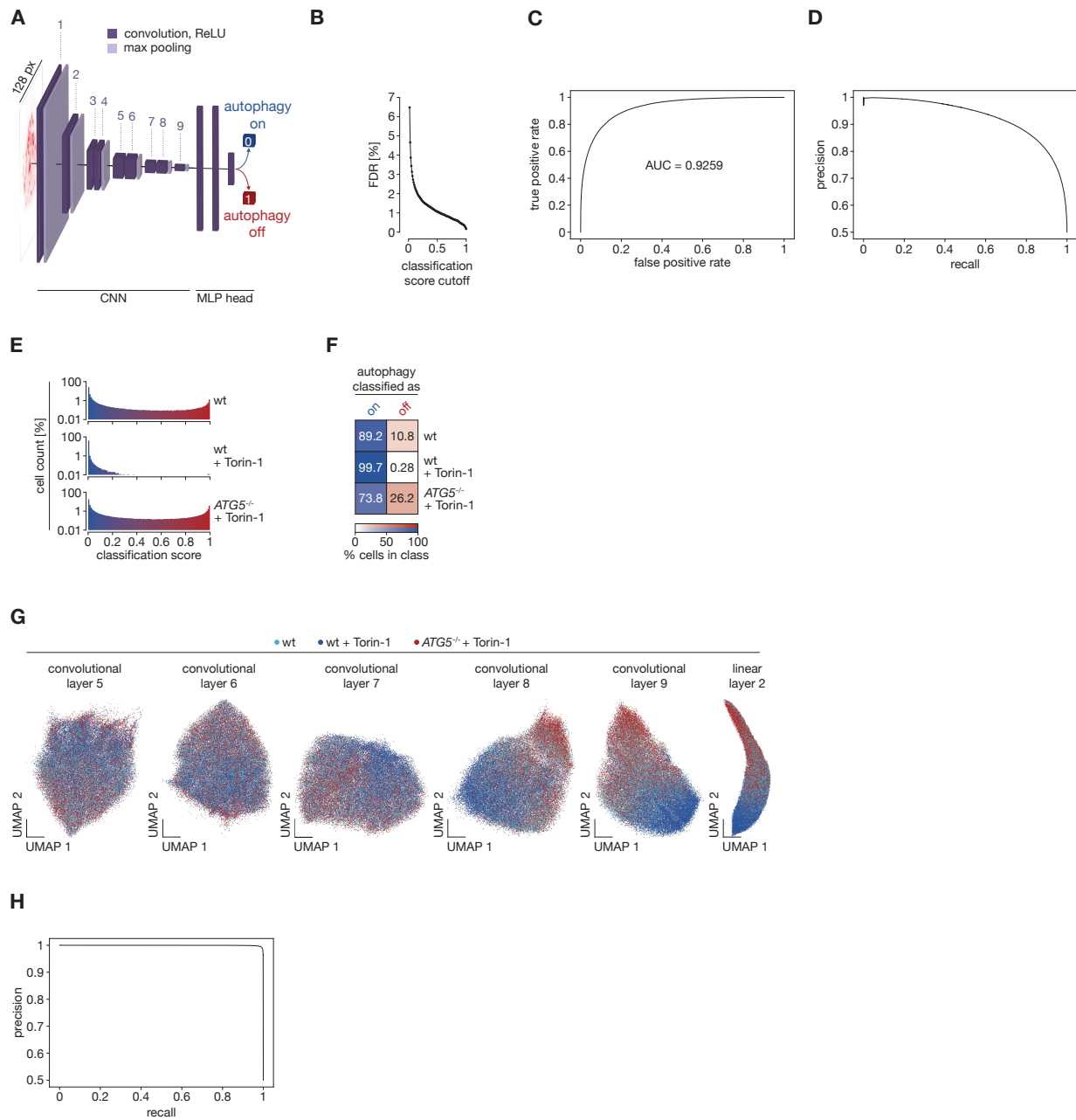


Figure S2

bioRxiv preprint doi: <https://doi.org/10.1101/2023.06.01.542416>; this version posted June 1, 2023. The copyright holder for this preprint (which was not certified by peer review) is the author/funder, who has granted bioRxiv a license to display the preprint in perpetuity. It is made available under a [CC-BY-NC-ND 4.0 International license](#).

Figure S2 | Performance of LC3 image-based autophagy classifiers

(A) Overview of the architecture and training paradigm of our convolutional neural network-based classifier 1.0 for autophagic or non-autophagic distribution of mCherry-LC3 in single U2OS cells. 500,000 128×128 px single cell images from several biological replicates were used in each training class. The autophagy-on class consisted of images of wildtype cells stimulated with Torin-1. The autophagy-off class consisted of images of unstimulated wildtype cells and images from two different *ATG5^{-/-}* clones. CNN: convolutional neural network. MLP: multilayer perceptron.

(B) False discovery rates (FDR) of the autophagy classifier 1.0 at different classification score cutoffs.

(C) Receiver Operating Characteristic (ROC) curve for autophagy classifier 1.0. AUC: area under the curve.

(D) Precision-Recall curve for our autophagy classifier 1.0.

(E) Histograms of images of mCherry-LC3 expressing U2OS cells of the indicated genotypes treated as indicated after autophagy classification with classifier 1.0 as illustrated in (A).

(F) Heatmap showing the percentage of cells in d classified as autophagy-on or autophagy-off with a classification score threshold of 0.5.

(G) Parametric UMAPs of mCherry-LC3 images of single U2OS cells featurized through our autophagy classifier 1.0 illustrated in (A) up to the indicated layers. Colors depict the indicated genotypes and treatments. 20,000 cells are shown for each genotype and treatment.

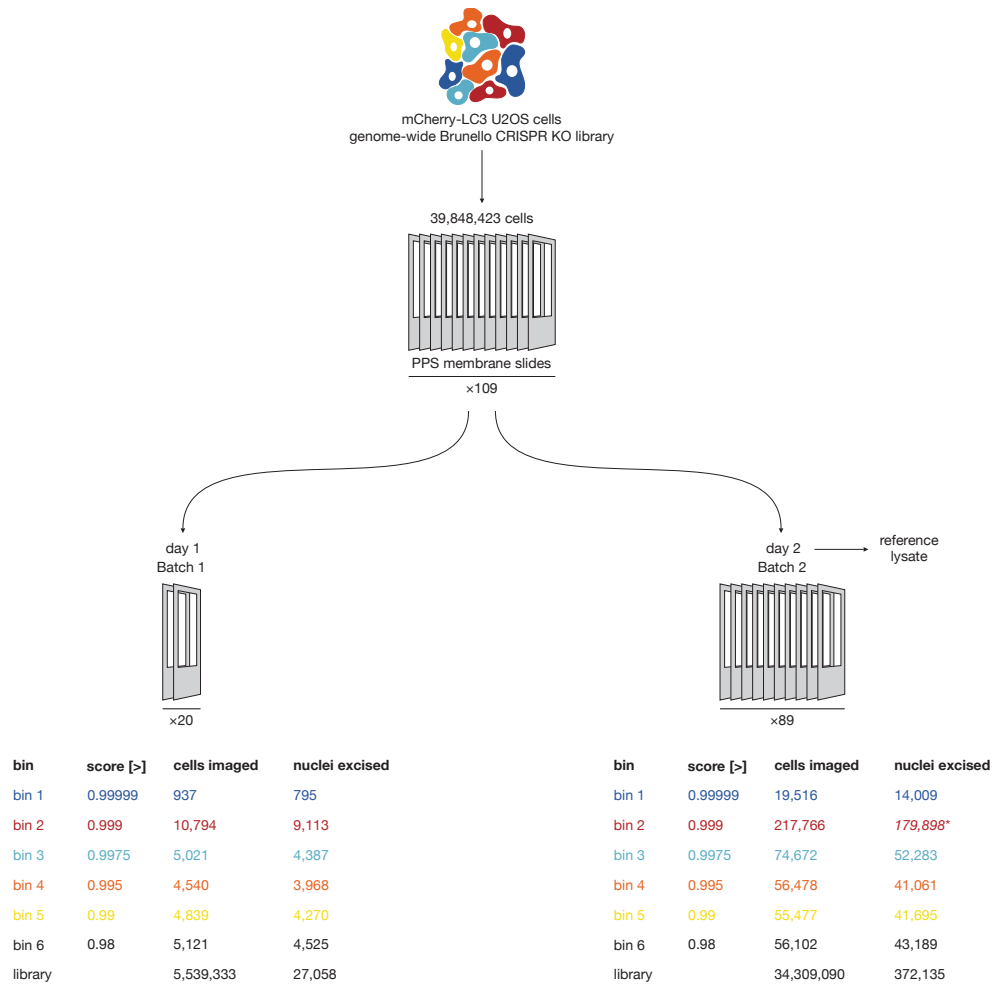
(H) Precision-Recall curve of classifier 2.0.

(B) – (H) were calculated on independent test datasets for the respective classifiers

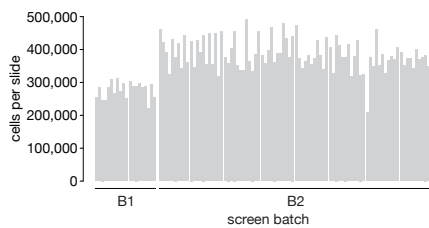
3.2 SPARCS, a platform for genome-scale CRISPR screening for spatial cellular phenotypes

bioRxiv preprint doi: <https://doi.org/10.1101/2023.06.01.542416>; this version posted June 1, 2023. The copyright holder for this preprint (which was not certified by peer review) is the author/funder, who has granted bioRxiv a license to display the preprint in perpetuity. It is made available under aCC-BY-NC-ND 4.0 International license.

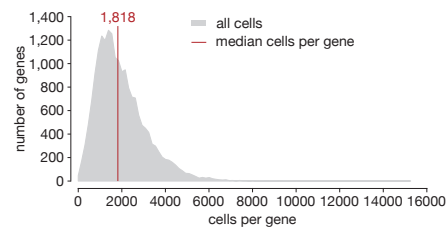
A



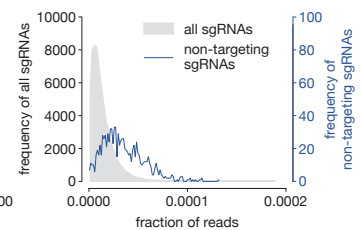
B



C



D



E

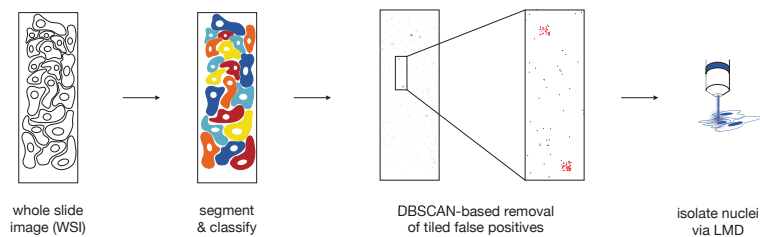


Figure S3

bioRxiv preprint doi: <https://doi.org/10.1101/2023.06.01.542416>; this version posted June 1, 2023. The copyright holder for this preprint (which was not certified by peer review) is the author/funder, who has granted bioRxiv a license to display the preprint in perpetuity. It is made available under a [CC-BY-NC-ND 4.0 International license](#).

Figure S3 | Overview of genome-wide SPARCS screening for autophagy

(A) Batching and binning strategy for screening autophagosome formation in 40 million mCherry-LC3 expressing U2OS cells. We dissected fewer cells than we imaged for a given bin due to the quality control step outlined in e. *The efficiency of the PCR on bin 2 from batch 2 had decreased dramatically, presumably due to the high density of membrane fragments in the reaction, leading to a loss of sgRNAs for sequencing. PPS: polyphenylene sulfide.

(B) Number of cells segmented per screen slide.

(C) Distribution of human genes targeted in the screen across cells in the library as determined by deep sequencing.

(D) Distribution of non-targeting and targeting sgRNAs in the reference library as determined by deep sequencing.

(E) Quality control strategy for false positives arising from out-of-focus images. When we spatially clustered hits using DBSCAN, we found clusters above a certain size to correspond to entire out-of-focus imaging tiles and removed these clusters before nuclei excision.

3.2 SPARCS, a platform for genome-scale CRISPR screening for spatial cellular phenotypes

bioRxiv preprint doi: <https://doi.org/10.1101/2023.06.01.542416>; this version posted June 1, 2023. The copyright holder for this preprint (which was not certified by peer review) is the author/funder, who has granted bioRxiv a license to display the preprint in perpetuity. It is made available under aCC-BY-NC-ND 4.0 International license.

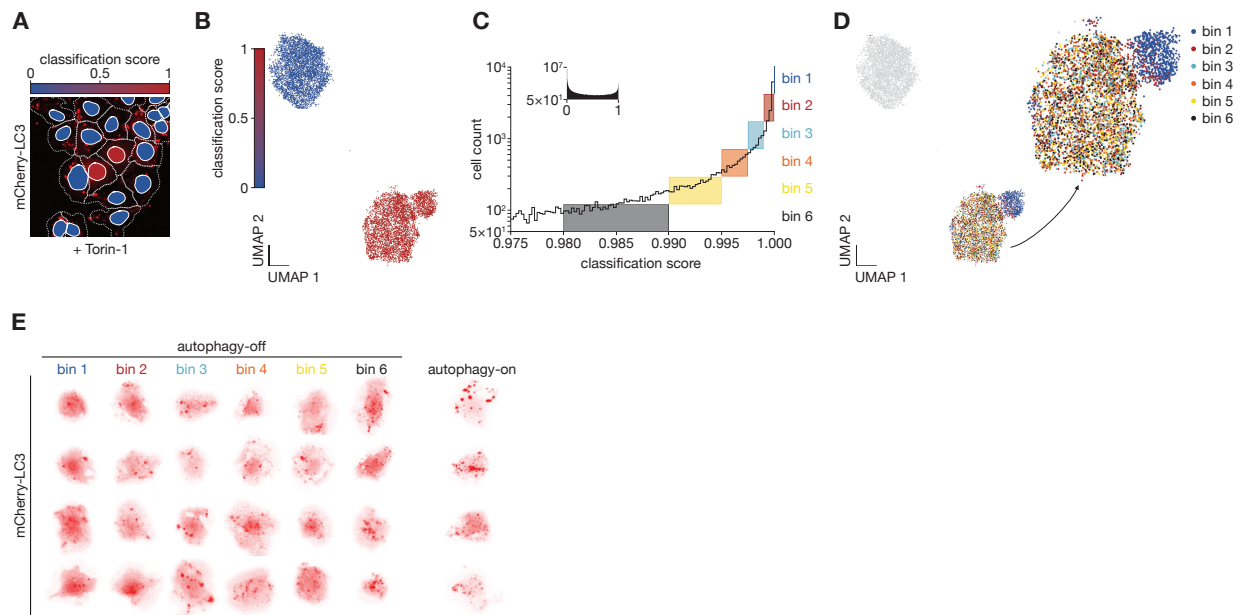


Figure S4

bioRxiv preprint doi: <https://doi.org/10.1101/2023.06.01.542416>; this version posted June 1, 2023. The copyright holder for this preprint (which was not certified by peer review) is the author/funder, who has granted bioRxiv a license to display the preprint in perpetuity. It is made available under a [CC-BY-NC-ND 4.0 International license](#).

Figure S4 | Results from genome-wide autophagy screen batch 1

(A) Example region from a genome-wide SPARCS CRISPR knockout screen on autophagosome formation in mCherry-LC3 expressing U2OS cells after Torin-1 stimulation for 14 hrs. Colors in nuclei indicate the result of binary autophagy classification with classifier 2.0, dotted lines indicate cytosol segmentation. Images were acquired on an Opera Phenix microscope in confocal mode with 20 x magnification.

(B) UMAP representation of single cell images from all cells in screen batch 1 with a classification score ≥ 0.98 (dark blue) or < 0.02 (light blue) featurized through the first 8 convolutional layers of autophagy classifier 2.0. 4,806 cells are depicted per category.

(C) Histogram of autophagy classification scores in the genome-wide CRISPR KO library batch 1 (inset) zoomed in on cells classified as autophagy-off with a score above 0.975. Colored boxes illustrate the binning strategy we used to isolate cells for sgRNA sequencing.

(D) As (B) but colored by screening bin. 801 cells shown per bin.

(E) Images of individual cells from each bin in screen batch 1.

3.2 SPARCS, a platform for genome-scale CRISPR screening for spatial cellular phenotypes

bioRxiv preprint doi: <https://doi.org/10.1101/2023.06.01.542416>; this version posted June 1, 2023. The copyright holder for this preprint (which was not certified by peer review) is the author/funder, who has granted bioRxiv a license to display the preprint in perpetuity. It is made available under aCC-BY-NC-ND 4.0 International license.

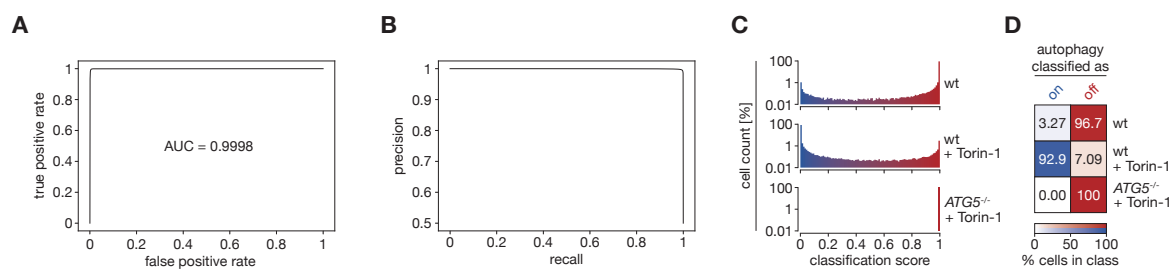


Figure S5

bioRxiv preprint doi: <https://doi.org/10.1101/2023.06.01.542416>; this version posted June 1, 2023. The copyright holder for this preprint (which was not certified by peer review) is the author/funder, who has granted bioRxiv a license to display the preprint in perpetuity. It is made available under a [CC-BY-NC-ND 4.0 International license](#).

Figure S5 | Performance metrics of classifier 2.1

(A) Receiver Operating Characteristic (ROC) curve for autophagy classifier 2.1. AUC: area under the curve.

(B) Precision-Recall curve for our autophagy classifier 2.1.

(C) Histograms of images of mCherry-LC3 expressing U2OS cells of the indicated genotypes treated as indicated after autophagy classification with classifier 2.1.

(D) Heatmap showing the percentage of cells in (C) classified as autophagy-on or autophagy-off with a classification score threshold of 0.5.

(A) – (D) were calculated on an independent test dataset.

3.2 SPARCS, a platform for genome-scale CRISPR screening for spatial cellular phenotypes

bioRxiv preprint doi: <https://doi.org/10.1101/2023.06.01.542416>; this version posted June 1, 2023. The copyright holder for this preprint (which was not certified by peer review) is the author/funder, who has granted bioRxiv a license to display the preprint in perpetuity. It is made available under a [CC-BY-NC-ND 4.0 International license](#).

Table S1 | Overview of CNN-based image classifiers trained in this study

All classifiers were trained on 128×128 px single cell images using PyTorch lightning. Unstimulated control slides containing library cells plated in parallel with the screen slides were included during training to capture possible batch effects introduced during plating and staining of the screening library. Cells were pre-filtered according to their autophagy score using classifier version P where indicated.

Table S1

Classifier Version	Description	Architecture	Number of trainable parameters	Training data	Training Epochs	Number of cells per class	Fig.	Used to classify dataset	Independent Test Dataset	AUC ROC Curve
1.0	Trained on initial staining protocol. Used to classify pilot screen	As in Fig. 2b but classifier head only consists of 3 fully connected linear layers	17,882,244	2 slides unstimulated wt 2 slides wt + Torin-1 1 slide <i>ATG5</i> ^{-/-} clone 1 1 slide <i>ATG5</i> ^{-/-} clone 2	40	500,000	2, S2	A 1.2 million cells	1 slide <i>ATG5</i> ^{-/-} cells clone 1 1 slide unstimulated wt cells 1 slide wt cells + Torin-1	0.925879
P	Only used to pre-filter cells for training 2.0 & 2.1	As in first classifier	17,882,244	3 slides wt + Torin-1 3 slides <i>ATG5</i> ^{-/-} mixed clones 1 slide <i>ATG5</i> ^{-/-} clone 1 1 slide <i>ATG5</i> ^{-/-} clone 2	30	1,200,000			1 slide <i>ATG5</i> ^{-/-} cells clone 1 1 slide unstimulated wt cells 1 slide wt cells + Torin-1	
2.0	Used on initial batch of genome-wide screen	As shown in Fig. 2b	14,340,484	1 slide <i>ATG5</i> ^{-/-} clone 1 1 slide <i>ATG5</i> ^{-/-} clone 2 3 slides <i>ATG5</i> ^{-/-} mixed clones 2 slides unstimulated screen cells score > 0.9 (autophagy-off) 3 slides wt + Torin-1 score < 0.1 (autophagy-on)	20	1,000,000	3, S4	Screen batch 1 5 million cells	1 slide <i>ATG5</i> ^{-/-} cells clone 1 1 slide unstimulated wt cells 1 slide wt cells + Torin-1	0.999649

3.2 SPARCS, a platform for genome-scale CRISPR screening for spatial cellular phenotypes

2.1	Refined for largest part of genome-wide screen	As shown in Fig. 2b	14,340,484	1 slide <i>ATG5^{-/-}</i> clone 1 1 slide <i>ATG5^{-/-}</i> clone 2 3 slides <i>ATG5^{-/-}</i> mixed clones 2 slides unstimulated screen cells score > 0.999 (autophagy-off) 3 slides wt + Torin-1 score < 0.001 (autophagy-on)	20	1,000,000	4, S5	Screen batch 2 35 million cells	1 slide <i>ATG5^{-/-}</i> cells clone 1 1 slide unstimulated wt cells 1 slide wt cells + Torin-1	0.999772
-----	--	---------------------	------------	---	----	-----------	-------	------------------------------------	--	----------

bioRxiv preprint doi: <https://doi.org/10.1101/2023.06.01.542416>; this version posted June 1, 2023. The copyright holder for this preprint (which was not certified by peer review) is the author/funder, who has granted bioRxiv a license to display the preprint in perpetuity. It is made available under a [CC-BY-NC-ND 4.0 International license](#).

Table S2 | Comparison of high-throughput methods for combined spatial phenotyping and genotyping

Search space: library size that can be screened for phenotypes. Target space: Proportion of library that can be analyzed. Phenotypic variants that can be discriminated: The maximum number of different phenotypes that can be recovered from a single screen. Real time decision for genotyping necessary: Whether a decision has to be made for a given image in real time during screening (“yes”) or whether entire single cell datasets can be analyzed after imaging before a decision on which cells to genotype has to be made (“no”).

*A genome-wide screen using in situ-seq has recently been reported (ref 21) with a small library of 10 million cells in which the number of screened and successfully sequenced cells and sgRNA representation remain unclear.

°These technologies have low costs per screened cell, but require the use of instruments often provided by core facilities such as a laser dissection microscope for SPARCS, an imaging sorter device for imaging flow cytometry or an imaging setup equipped with a fluorescence recovery after photobleaching (FRAP) laser for pA-mCherry.

3.2 SPARCS, a platform for genome-scale CRISPR screening for spatial cellular phenotypes

bioRxiv preprint doi: <https://doi.org/10.1101/2023.06.01.542416>; this version posted June 1, 2023. The copyright holder for this preprint (which was not certified by peer review) is the author/funder, who has granted bioRxiv a license to display the preprint in perpetuity. It is made available under aCC-BY-NC-ND 4.0 International license.

Table S2

	SPARCS	In situ seq	Imaging flow cytometry	pA-mCherry
References	This study	19, 20, 21	22, 23	25, 26, 27
Search space	large	medium	large	large
Target space	small	medium	large	small
Phenotypic variants that can be discriminated	microtiter plate	unlimited	microtiter plate	4 per fluorophore
Image quality	confocal	confocal	flow-based	confocal
Real time decision for genotyping necessary	No	No	Yes	Yes
Discovery of new phenotypes after screen by reanalysis with new computational model possible	Yes	Yes	No	No
Largest library size	40 million	31 million	12 million	12.6 million
Genes targeted	19,114	5,072*	18,408	18,905
Special equipment required	Laser microdissection microscope	Ultrafast imaging setup and precise stage for sequencing cycles	Imaging flow sorter	FRAP laser or equivalent
Cost per cell in library	Low°	High	Low°	Low°

Acknowledgements

First and foremost I would like to thank my mentor and advisor Veit Hornung. You created the environment that helped me become the scientist I am now and in which I was able to conduct this work. I tremendously enjoyed the countless fruitful discussions we have had over the almost ten years we have been working together now and I hope there will be many more to come in the future.

I would also like to thank all my colleagues and friends who worked with me over the years, especially everyone from the Hornung lab. You have taught me, comforted me, and kept me on my toes throughout this adventure.

I am grateful to my family, particularly Karin, Martin, and Gundula, for always being interested in my work and looking forward to this conclusion even more than I did.

Finally I would like to thank my partner Sophia for supporting me wherever you could and enduring me where you could not. Your dedication has moved — first my own and then our joint — work forward so reliably.

Bibliography

- Ablasser, A. et al. (2013). “cGAS produces a 2'-5'-linked cyclic dinucleotide second messenger that activates STING.” eng. In: *Nature* 498.7454, pp. 380–384. ISSN: 1476-4687 (Electronic); 0028-0836 (Print); 0028-0836 (Linking). DOI: [10.1038/nature12306](https://doi.org/10.1038/nature12306).
- Abudayyeh, O. O. et al. (2016). “C2c2 is a single-component programmable RNA-guided RNA-targeting CRISPR effector.” eng. In: *Science* 353.6299, aaf5573. ISSN: 1095-9203 (Electronic); 0036-8075 (Print); 0036-8075 (Linking). DOI: [10.1126/science.aaf5573](https://doi.org/10.1126/science.aaf5573).
- Ahn, J., D. Gutman, S. Saijo, and G. N. Barber (2012). “STING manifests self DNA-dependent inflammatory disease”. In: *Proceedings of the National Academy of Sciences* 109.47, pp. 19386–19391. DOI: [10.1073/pnas.1215006109](https://doi.org/10.1073/pnas.1215006109).
- Akkaya, M., K. Kwak, and S. K. Pierce (2020). “B cell memory: building two walls of protection against pathogens”. In: *Nature Reviews Immunology* 20.4, pp. 229–238. DOI: [10.1038/s41577-019-0244-2](https://doi.org/10.1038/s41577-019-0244-2).
- Alberts, B., J. Wilson, and T. Hunt (2008). *Molecular biology of the cell*. 5th ed. New York: Garland Science New York. ISBN: 9780815341055; 0815341059; 0815341067; 9780815341062; 0815341105; 9780815341109; 0815341113; 9780815341116.
- Alexopoulou, L., A. C. Holt, R. Medzhitov, and R. A. Flavell (2001). “Recognition of double-stranded RNA and activation of NF- κ B by Toll-like receptor 3”. In: *Nature* 413.6857, pp. 732–738. DOI: [10.1038/35099560](https://doi.org/10.1038/35099560).
- Andrade, W. A. et al. (2013). “Combined action of nucleic acid-sensing Toll-like receptors and TLR11/TLR12 heterodimers imparts resistance to *Toxoplasma gondii* in mice.” eng. In: *Cell Host Microbe* 13.1, pp. 42–53. ISSN: 1934-6069 (Electronic); 1931-3128 (Print); 1931-3128 (Linking). DOI: [10.1016/j.chom.2012.12.003](https://doi.org/10.1016/j.chom.2012.12.003).
- Andreeva, L. et al. (2021). “NLRP3 cages revealed by full-length mouse NLRP3 structure control pathway activation.” eng. In: *Cell* 184.26, pp. 6299–6312. ISSN: 1097-4172 (Electronic); 0092-8674 (Print); 0092-8674 (Linking). DOI: [10.1016/j.cell.2021.11.011](https://doi.org/10.1016/j.cell.2021.11.011).

- Anzalone, A. V. et al. (2019). “Search-and-replace genome editing without double-strand breaks or donor DNA”. In: *Nature* 576.7785, pp. 149–157. DOI: [10.1038/s41586-019-1711-4](https://doi.org/10.1038/s41586-019-1711-4).
- Ashkenazi, A. and V. M. Dixit (1999). “Apoptosis control by death and decoy receptors.” eng. In: *Curr Opin Cell Biol* 11.2, pp. 255–260. ISSN: 0955-0674 (Print); 0955-0674 (Linking). DOI: [10.1016/s0955-0674\(99\)80034-9](https://doi.org/10.1016/s0955-0674(99)80034-9).
- Avery, O. T., C. M. Macleod, and M. McCarty (1944). “Studies on the chemical nature of the substance inducing transformation of pneumococcal types : induction of transformation by a desoxyribonucleic acid fraction isolated from pneumococcus type III.” eng. In: *J Exp Med* 79.2, pp. 137–158. ISSN: 0022-1007 (Print); 1540-9538 (Electronic); 0022-1007 (Linking). DOI: [10.1084/jem.79.2.137](https://doi.org/10.1084/jem.79.2.137).
- Baek, M. et al. (2021). “Accurate prediction of protein structures and interactions using a three-track neural network”. In: *Science* 373.6557, pp. 871–876. DOI: [10.1126/science.abj8754](https://doi.org/10.1126/science.abj8754).
- Baral, P., S. Udit, and I. M. Chiu (2019). “Pain and immunity: implications for host defence.” eng. In: *Nat Rev Immunol* 19.7, pp. 433–447. ISSN: 1474-1741 (Electronic); 1474-1733 (Print); 1474-1733 (Linking). DOI: [10.1038/s41577-019-0147-2](https://doi.org/10.1038/s41577-019-0147-2).
- Bauernfried, S. et al. (2021). “Human NLRP1 is a sensor for double-stranded RNA.” eng. In: *Science* 371.6528. ISSN: 1095-9203 (Electronic); 0036-8075 (Linking). DOI: [10.1126/science.abd0811](https://doi.org/10.1126/science.abd0811).
- Berke, I. C. and Y. Modis (2012). “MDA5 cooperatively forms dimers and ATP-sensitive filaments upon binding double-stranded RNA.” eng. In: *EMBO J* 31.7, pp. 1714–1726. ISSN: 1460-2075 (Electronic); 0261-4189 (Print); 0261-4189 (Linking). DOI: [10.1038/emboj.2012.19](https://doi.org/10.1038/emboj.2012.19).
- Bertheloot, D. and E. Latz (2017). “HMGB1, IL-1 α , IL-33 and S100 proteins: dual-function alarmins”. In: *Cellular & Molecular Immunology* 14.1, pp. 43–64. DOI: [10.1038/cmi.2016.34](https://doi.org/10.1038/cmi.2016.34).
- Bertheloot, D., E. Latz, and B. S. Franklin (2021). “Necroptosis, pyroptosis and apoptosis: an intricate game of cell death”. In: *Cellular & Molecular Immunology* 18.5, pp. 1106–1121. DOI: [10.1038/s41423-020-00630-3](https://doi.org/10.1038/s41423-020-00630-3).
- Bock, C. et al. (2022). “High-content CRISPR screening”. In: *Nature Reviews Methods Primers* 2.1, p. 8. DOI: [10.1038/s43586-021-00093-4](https://doi.org/10.1038/s43586-021-00093-4).
- Boehm, T., N. McCurley, et al. (2012). “VLR-based adaptive immunity.” eng. In: *Annu Rev Immunol* 30, pp. 203–220. ISSN: 1545-3278 (Electronic); 0732-0582 (Print); 0732-0582 (Linking). DOI: [10.1146/annurev-immunol-020711-075038](https://doi.org/10.1146/annurev-immunol-020711-075038).

- Boehm, T. and J. B. Swann (2014). “Origin and Evolution of Adaptive Immunity”. In: *Annual Review of Animal Biosciences* 2.1. PMID: 25384143, pp. 259–283. DOI: [10.1146/annurev-animal-022513-114201](https://doi.org/10.1146/annurev-animal-022513-114201).
- Boyer, J. A. et al. (2020). “Structural basis of nucleosome-dependent cGAS inhibition.” eng. In: *Science* 370.6515, pp. 450–454. ISSN: 1095-9203 (Electronic); 0036-8075 (Print); 0036-8075 (Linking). DOI: [10.1126/science.abd0609](https://doi.org/10.1126/science.abd0609).
- Boyle, W. S. and G. E. Smith (1970). “Charge Coupled Semiconductor Devices”. In: *Bell System Technical Journal* 49.4, pp. 587–593. DOI: <https://doi.org/10.1002/j.1538-7305.1970.tb01790.x>.
- Brenner, S. (1974). “The genetics of *Caenorhabditis elegans*.” eng. In: *Genetics* 77.1, pp. 71–94. ISSN: 0016-6731 (Print); 0016-6731 (Linking). DOI: [10.1093/genetics/77.1.71](https://doi.org/10.1093/genetics/77.1.71).
- Broz, P. and V. M. Dixit (2016). “Inflammasomes: mechanism of assembly, regulation and signalling”. In: *Nature Reviews Immunology* 16.7, pp. 407–420. DOI: [10.1038/nri.2016.58](https://doi.org/10.1038/nri.2016.58).
- Broz, P., P. Pelegrín, and F. Shao (2020). “The gasdermins, a protein family executing cell death and inflammation.” eng. In: *Nat Rev Immunol* 20.3, pp. 143–157. ISSN: 1474-1741 (Electronic); 1474-1733 (Linking). DOI: [10.1038/s41577-019-0228-2](https://doi.org/10.1038/s41577-019-0228-2).
- Bürckstümmer, T. et al. (2009). “An orthogonal proteomic-genomic screen identifies AIM2 as a cytoplasmic DNA sensor for the inflammasome.” eng. In: *Nat Immunol* 10.3, pp. 266–272. ISSN: 1529-2916 (Electronic); 1529-2908 (Linking). DOI: [10.1038/ni.1702](https://doi.org/10.1038/ni.1702).
- Burdette, D. L. et al. (2011). “STING is a direct innate immune sensor of cyclic di-GMP.” eng. In: *Nature* 478.7370, pp. 515–518. ISSN: 1476-4687 (Electronic); 0028-0836 (Print); 0028-0836 (Linking). DOI: [10.1038/nature10429](https://doi.org/10.1038/nature10429).
- Cabeza-Cabrerizo, M. et al. (2021). “Dendritic Cells Revisited”. In: *Annual Review of Immunology* 39.1. PMID: 33481643, pp. 131–166. DOI: [10.1146/annurev-immunol-061020-053707](https://doi.org/10.1146/annurev-immunol-061020-053707).
- Cao, D. et al. (2020). “Structural basis for nucleosome-mediated inhibition of cGAS activity.” eng. In: *Cell Res* 30.12, pp. 1088–1097. ISSN: 1748-7838 (Electronic); 1001-0602 (Print); 1001-0602 (Linking). DOI: [10.1038/s41422-020-00422-4](https://doi.org/10.1038/s41422-020-00422-4).
- Cao, Z. et al. (1996). “TRAF6 is a signal transducer for interleukin-1.” eng. In: *Nature* 383.6599, pp. 443–446. ISSN: 0028-0836 (Print); 0028-0836 (Linking). DOI: [10.1038/383443a0](https://doi.org/10.1038/383443a0).
- Carette, J. E. et al. (2009). “Haploid genetic screens in human cells identify host factors used by pathogens.” eng. In: *Science* 326.5957, pp. 1231–1235. ISSN: 1095-9203 (Electronic); 0036-8075 (Linking). DOI: [10.1126/science.1178955](https://doi.org/10.1126/science.1178955).

- Carswell, E. A. et al. (1975). “An endotoxin-induced serum factor that causes necrosis of tumors.” eng. In: *Proc Natl Acad Sci U S A* 72.9, pp. 3666–3670. ISSN: 0027-8424 (Print); 1091-6490 (Electronic); 0027-8424 (Linking). DOI: [10.1073/pnas.72.9.3666](https://doi.org/10.1073/pnas.72.9.3666).
- Caruso, R., N. Warner, N. Inohara, and G. Núñez (2014). “NOD1 and NOD2: signaling, host defense, and inflammatory disease.” eng. In: *Immunity* 41.6, pp. 898–908. ISSN: 1097-4180 (Electronic); 1074-7613 (Print); 1074-7613 (Linking). DOI: [10.1016/j.immuni.2014.12.010](https://doi.org/10.1016/j.immuni.2014.12.010).
- Chang, H. H. Y., N. R. Pannunzio, N. Adachi, and M. R. Lieber (2017). “Non-homologous DNA end joining and alternative pathways to double-strand break repair”. In: *Nature Reviews Molecular Cell Biology* 18.8, pp. 495–506. DOI: [10.1038/nrm.2017.48](https://doi.org/10.1038/nrm.2017.48).
- Chen, J. and Z. J. Chen (2018). “PtdIns4P on dispersed trans-Golgi network mediates NLRP3 inflammasome activation.” eng. In: *Nature* 564.7734, pp. 71–76. ISSN: 1476-4687 (Electronic); 0028-0836 (Print); 0028-0836 (Linking). DOI: [10.1038/s41586-018-0761-3](https://doi.org/10.1038/s41586-018-0761-3).
- Chen, S. et al. (2015). “Genome-wide CRISPR screen in a mouse model of tumor growth and metastasis.” eng. In: *Cell* 160.6, pp. 1246–1260. ISSN: 1097-4172 (Electronic); 0092-8674 (Print); 0092-8674 (Linking). DOI: [10.1016/j.cell.2015.02.038](https://doi.org/10.1016/j.cell.2015.02.038).
- Chui, A. J. et al. (2019). “N-terminal degradation activates the NLRP1B inflammasome”. In: *Science* 364.6435, pp. 82–85. DOI: [10.1126/science.aau1208](https://doi.org/10.1126/science.aau1208).
- Cong, L. et al. (2013). “Multiplex Genome Engineering Using CRISPR/Cas Systems”. In: *Science* 339.6121, pp. 819–823. DOI: [10.1126/science.1231143](https://doi.org/10.1126/science.1231143).
- Crow, Y. J. et al. (2006). “Mutations in the gene encoding the 3’-5’DNA exonuclease TREX1 cause Aicardi-Goutières syndrome at the AGS1 locus”. In: *Nature Genetics* 38.8, pp. 917–920. DOI: [10.1038/ng1845](https://doi.org/10.1038/ng1845).
- Cui, S. et al. (2008). “The C-terminal regulatory domain is the RNA 5’-triphosphate sensor of RIG-I.” eng. In: *Mol Cell* 29.2, pp. 169–179. ISSN: 1097-2765 (Print); 1097-2765 (Linking). DOI: [10.1016/j.molcel.2007.10.032](https://doi.org/10.1016/j.molcel.2007.10.032).
- Dangl, J. L. and J. D. Jones (2001). “Plant pathogens and integrated defence responses to infection.” eng. In: *Nature* 411.6839, pp. 826–833. ISSN: 0028-0836 (Print); 0028-0836 (Linking). DOI: [10.1038/35081161](https://doi.org/10.1038/35081161).
- Datlinger, P. et al. (2017). “Pooled CRISPR screening with single-cell transcriptome readout.” eng. In: *Nat Methods* 14.3, pp. 297–301. ISSN: 1548-7105 (Electronic); 1548-7091 (Print); 1548-7091 (Linking). DOI: [10.1038/nmeth.4177](https://doi.org/10.1038/nmeth.4177).
- David, L. et al. (2023). “NINJ1 mediates plasma membrane rupture through formation of nanodisc-like rings”. In: *bioRxiv*. DOI: [10.1101/2023.06.01.543231](https://doi.org/10.1101/2023.06.01.543231).

- de Duve, C. et al. (1955). “Tissue fractionation studies. 6. Intracellular distribution patterns of enzymes in rat-liver tissue.” eng. In: *Biochem J* 60.4, pp. 604–617. ISSN: 0264-6021 (Print); 1470-8728 (Electronic); 0264-6021 (Linking). DOI: [10.1042/bj0600604](https://doi.org/10.1042/bj0600604).
- Decout, A., J. D. Katz, S. Venkatraman, and A. Ablasser (2021). “The cGAS–STING pathway as a therapeutic target in inflammatory diseases”. In: *Nature Reviews Immunology* 21.9, pp. 548–569. DOI: [10.1038/s41577-021-00524-z](https://doi.org/10.1038/s41577-021-00524-z).
- Degen, M. et al. (2023). “Structural basis of NINJ1-mediated plasma membrane rupture in cell death”. In: *Nature* 618.7967, pp. 1065–1071. DOI: [10.1038/s41586-023-05991-z](https://doi.org/10.1038/s41586-023-05991-z).
- Deng, W. et al. (2022). “Streptococcal pyrogenic exotoxin B cleaves GSDMA and triggers pyroptosis.” eng. In: *Nature* 602.7897, pp. 496–502. ISSN: 1476-4687 (Electronic); 0028-0836 (Print); 0028-0836 (Linking). DOI: [10.1038/s41586-021-04384-4](https://doi.org/10.1038/s41586-021-04384-4).
- Devant, P. and J. C. Kagan (2023). “Molecular mechanisms of gasdermin D pore-forming activity”. In: *Nature Immunology* 24.7, pp. 1064–1075. DOI: [10.1038/s41590-023-01526-w](https://doi.org/10.1038/s41590-023-01526-w).
- Diebold, S. S. et al. (2004). “Innate Antiviral Responses by Means of TLR7-Mediated Recognition of Single-Stranded RNA”. In: *Science* 303.5663, pp. 1529–1531. DOI: [10.1126/science.1093616](https://doi.org/10.1126/science.1093616).
- Diez, E. et al. (2003). “Birc1e is the gene within the Lgn1 locus associated with resistance to Legionella pneumophila.” eng. In: *Nat Genet* 33.1, pp. 55–60. ISSN: 1061-4036 (Print); 1061-4036 (Linking). DOI: [10.1038/ng1065](https://doi.org/10.1038/ng1065).
- Dixit, A. et al. (2016). “Perturb-Seq: Dissecting Molecular Circuits with Scalable Single-Cell RNA Profiling of Pooled Genetic Screens.” eng. In: *Cell* 167.7, pp. 1853–1866. ISSN: 1097-4172 (Electronic); 0092-8674 (Print); 0092-8674 (Linking). DOI: [10.1016/j.cell.2016.11.038](https://doi.org/10.1016/j.cell.2016.11.038).
- Doitsh, G. et al. (2014). “Cell death by pyroptosis drives CD4 T-cell depletion in HIV-1 infection”. In: *Nature* 505.7484, pp. 509–514. DOI: [10.1038/nature12940](https://doi.org/10.1038/nature12940).
- Doran, A. C., A. Yurdagul, and I. Tabas (2020). “Efferocytosis in health and disease”. In: *Nature Reviews Immunology* 20.4, pp. 254–267. DOI: [10.1038/s41577-019-0240-6](https://doi.org/10.1038/s41577-019-0240-6).
- Dostert, C. et al. (2008). “Innate Immune Activation Through Nalp3 Inflammasome Sensing of Asbestos and Silica”. In: *Science* 320.5876, pp. 674–677. DOI: [10.1126/science.1156995](https://doi.org/10.1126/science.1156995).
- Duncan-Lowey, B. and P. J. Kranzusch (2022). “CBASS phage defense and evolution of antiviral nucleotide signaling”. In: *Current Opinion in Immunology* 74, pp. 156–163. ISSN: 0952-7915. DOI: <https://doi.org/10.1016/j.coi.2022.01.002>.

- Duncan, J. A. et al. (2007). “Cryopyrin/NALP3 binds ATP/dATP, is an ATPase, and requires ATP binding to mediate inflammatory signaling”. In: *Proceedings of the National Academy of Sciences* 104.19, pp. 8041–8046. DOI: [10.1073/pnas.0611496104](https://doi.org/10.1073/pnas.0611496104).
- Everts, B. et al. (2014). “TLR-driven early glycolytic reprogramming via the kinases TBK1-IKKe supports the anabolic demands of dendritic cell activation.” eng. In: *Nat Immunol* 15.4, pp. 323–332. ISSN: 1529-2916 (Electronic); 1529-2908 (Print); 1529-2908 (Linking). DOI: [10.1038/ni.2833](https://doi.org/10.1038/ni.2833).
- Farber, D. L., N. A. Yudanin, and N. P. Restifo (2014). “Human memory T cells: generation, compartmentalization and homeostasis”. In: *Nature Reviews Immunology* 14.1, pp. 24–35. DOI: [10.1038/nri3567](https://doi.org/10.1038/nri3567).
- Feldman, D. et al. (2019). “Optical Pooled Screens in Human Cells”. In: *Cell* 179.3, 787–799.e17. ISSN: 0092-8674. DOI: <https://doi.org/10.1016/j.cell.2019.09.016>.
- Feng, S. et al. (2007). “Cleavage of RIP3 inactivates its caspase-independent apoptosis pathway by removal of kinase domain.” eng. In: *Cell Signal* 19.10, pp. 2056–2067. ISSN: 0898-6568 (Print); 0898-6568 (Linking). DOI: [10.1016/j.cellsig.2007.05.016](https://doi.org/10.1016/j.cellsig.2007.05.016).
- Fernandes-Alnemri, T. et al. (2009). “AIM2 activates the inflammasome and cell death in response to cytoplasmic DNA.” eng. In: *Nature* 458.7237, pp. 509–513. ISSN: 1476-4687 (Electronic); 0028-0836 (Print); 0028-0836 (Linking). DOI: [10.1038/nature07710](https://doi.org/10.1038/nature07710).
- Fessler, E. et al. (2020). “A pathway coordinated by DELE1 relays mitochondrial stress to the cytosol.” eng. In: *Nature* 579.7799, pp. 433–437. ISSN: 1476-4687 (Electronic); 0028-0836 (Print); 0028-0836 (Linking). DOI: [10.1038/s41586-020-2076-4](https://doi.org/10.1038/s41586-020-2076-4).
- Fitzgerald, K. A. and J. C. Kagan (2020). “Toll-like Receptors and the Control of Immunity.” eng. In: *Cell* 180.6, pp. 1044–1066. ISSN: 1097-4172 (Electronic); 0092-8674 (Print); 0092-8674 (Linking). DOI: [10.1016/j.cell.2020.02.041](https://doi.org/10.1016/j.cell.2020.02.041).
- Flajnik, M. F. (2018). “A cold-blooded view of adaptive immunity”. In: *Nature Reviews Immunology* 18.7, pp. 438–453. DOI: [10.1038/s41577-018-0003-9](https://doi.org/10.1038/s41577-018-0003-9).
- Franchi, L. et al. (2006). “Cytosolic flagellin requires Ipaf for activation of caspase-1 and interleukin 1 β in salmonella-infected macrophages”. In: *Nature Immunology* 7.6, pp. 576–582. DOI: [10.1038/ni1346](https://doi.org/10.1038/ni1346).
- Franklin, R. E. and R. G. Gosling (1953). “Molecular Configuration in Sodium Thymonucleate”. In: *Nature* 171.4356, pp. 740–741. DOI: [10.1038/171740a0](https://doi.org/10.1038/171740a0).
- Gaidt, M. M., A. Morrow, et al. (2021). “Self-guarding of MORC3 enables virulence factor-triggered immunity”. In: *Nature* 600.7887, pp. 138–142. DOI: [10.1038/s41586-021-04054-5](https://doi.org/10.1038/s41586-021-04054-5).
- Gaidt, M. M., T. S. Ebert, D. Chauhan, K. Ramshorn, et al. (2017). “The DNA Inflammasome in Human Myeloid Cells Is Initiated by a STING-Cell Death Program

- Upstream of NLRP3.” eng. In: *Cell* 171.5, pp. 1110–1124. ISSN: 1097-4172 (Electronic); 0092-8674 (Print); 0092-8674 (Linking). DOI: [10.1016/j.cell.2017.09.039](https://doi.org/10.1016/j.cell.2017.09.039).
- Gaidt, M. M., T. S. Ebert, D. Chauhan, T. Schmidt, et al. (2016). “Human Monocytes Engage an Alternative Inflammasome Pathway.” eng. In: *Immunity* 44.4, pp. 833–846. ISSN: 1097-4180 (Electronic); 1074-7613 (Linking). DOI: [10.1016/j.immuni.2016.01.012](https://doi.org/10.1016/j.immuni.2016.01.012).
- Ganz, T. (2003). “Defensins: antimicrobial peptides of innate immunity”. In: *Nature Reviews Immunology* 3.9, pp. 710–720. DOI: [10.1038/nri1180](https://doi.org/10.1038/nri1180).
- Gao, P. et al. (2013). “Cyclic [G(2',5')pA(3',5')p] is the metazoan second messenger produced by DNA-activated cyclic GMP-AMP synthase.” eng. In: *Cell* 153.5, pp. 1094–1107. ISSN: 1097-4172 (Electronic); 0092-8674 (Print); 0092-8674 (Linking). DOI: [10.1016/j.cell.2013.04.046](https://doi.org/10.1016/j.cell.2013.04.046).
- Gasiunas, G., R. Barrangou, P. Horvath, and V. Siksnys (2012). “Cas9–crRNA ribonucleoprotein complex mediates specific DNA cleavage for adaptive immunity in bacteria”. In: *Proceedings of the National Academy of Sciences* 109.39, E2579–E2586. DOI: [10.1073/pnas.1208507109](https://doi.org/10.1073/pnas.1208507109).
- Gewirtz, A. T. et al. (2001). “Cutting Edge: Bacterial Flagellin Activates Basolaterally Expressed TLR5 to Induce Epithelial Proinflammatory Gene Expression1”. In: *The Journal of Immunology* 167.4, pp. 1882–1885. ISSN: 0022-1767. DOI: [10.4049/jimmunol.167.4.1882](https://doi.org/10.4049/jimmunol.167.4.1882).
- Gizzi, A. S. et al. (2018). “A naturally occurring antiviral ribonucleotide encoded by the human genome”. In: *Nature* 558.7711, pp. 610–614. DOI: [10.1038/s41586-018-0238-4](https://doi.org/10.1038/s41586-018-0238-4).
- Gordon, S. (2008). “Elie Metchnikoff: Father of natural immunity”. In: *European Journal of Immunology* 38.12, pp. 3257–3264. DOI: <https://doi.org/10.1002/eji.200838855>.
- Greulich, W. et al. (2019). “TLR8 Is a Sensor of RNase T2 Degradation Products”. In: *Cell* 179.6, 1264–1275.e13. ISSN: 0092-8674. DOI: <https://doi.org/10.1016/j.cell.2019.11.001>.
- Groß, C. J. et al. (2016). “K(+) Efflux-Independent NLRP3 Inflammasome Activation by Small Molecules Targeting Mitochondria.” eng. In: *Immunity* 45.4, pp. 761–773. ISSN: 1097-4180 (Electronic); 1074-7613 (Linking). DOI: [10.1016/j.immuni.2016.08.010](https://doi.org/10.1016/j.immuni.2016.08.010).
- Gurcel, L. et al. (2006). “Caspase-1 activation of lipid metabolic pathways in response to bacterial pore-forming toxins promotes cell survival.” eng. In: *Cell* 126.6, pp. 1135–1145. ISSN: 0092-8674 (Print); 0092-8674 (Linking). DOI: [10.1016/j.cell.2006.07.033](https://doi.org/10.1016/j.cell.2006.07.033).

- Halle, A. et al. (2008). “The NALP3 inflammasome is involved in the innate immune response to amyloid-beta.” eng. In: *Nat Immunol* 9.8, pp. 857–865. ISSN: 1529-2916 (Electronic); 1529-2908 (Print); 1529-2908 (Linking). DOI: [10.1038/ni.1636](https://doi.org/10.1038/ni.1636).
- Harton, J. A. et al. (1999). “GTP Binding by Class II Transactivator: Role in Nuclear Import”. In: *Science* 285.5432, pp. 1402–1405. DOI: [10.1126/science.285.5432.1402](https://doi.org/10.1126/science.285.5432.1402).
- Hayashi, F. et al. (2001). “The innate immune response to bacterial flagellin is mediated by Toll-like receptor 5”. In: *Nature* 410.6832, pp. 1099–1103. DOI: [10.1038/35074106](https://doi.org/10.1038/35074106).
- He, Y. et al. (2016). “NEK7 is an essential mediator of NLRP3 activation downstream of potassium efflux”. In: *Nature* 530.7590, pp. 354–357. DOI: [10.1038/nature16959](https://doi.org/10.1038/nature16959).
- Heil, F. et al. (2004). “Species-Specific Recognition of Single-Stranded RNA via Toll-like Receptor 7 and 8”. In: *Science* 303.5663, pp. 1526–1529. DOI: [10.1126/science.1093620](https://doi.org/10.1126/science.1093620).
- Heinz, L. X. et al. (2020). “TASL is the SLC15A4-associated adaptor for IRF5 activation by TLR7-9.” eng. In: *Nature* 581.7808, pp. 316–322. ISSN: 1476-4687 (Electronic); 0028-0836 (Print); 0028-0836 (Linking). DOI: [10.1038/s41586-020-2282-0](https://doi.org/10.1038/s41586-020-2282-0).
- Hemmi, H., T. Kaisho, et al. (2002). “Small anti-viral compounds activate immune cells via the TLR7 MyD88-dependent signaling pathway”. In: *Nature Immunology* 3.2, pp. 196–200. DOI: [10.1038/ni758](https://doi.org/10.1038/ni758).
- Hemmi, H., O. Takeuchi, et al. (2000). “A Toll-like receptor recognizes bacterial DNA”. In: *Nature* 408.6813, pp. 740–745. DOI: [10.1038/35047123](https://doi.org/10.1038/35047123).
- Hidmark, A., A. von Saint Paul, and A. H. Dalpke (2012). “Cutting Edge: TLR13 Is a Receptor for Bacterial RNA”. In: *The Journal of Immunology* 189.6, pp. 2717–2721. ISSN: 0022-1767. DOI: [10.4049/jimmunol.1200898](https://doi.org/10.4049/jimmunol.1200898).
- Hille, F. et al. (2018). “The Biology of CRISPR-Cas: Backward and Forward”. In: *Cell* 172.6, pp. 1239–1259. ISSN: 0092-8674. DOI: <https://doi.org/10.1016/j.cell.2017.11.032>.
- Hochheiser, I. V. et al. (2022). “Structure of the NLRP3 decamer bound to the cytokine release inhibitor CRID3.” eng. In: *Nature* 604.7904, pp. 184–189. ISSN: 1476-4687 (Electronic); 0028-0836 (Linking). DOI: [10.1038/s41586-022-04467-w](https://doi.org/10.1038/s41586-022-04467-w).
- Hoffman, H. M. et al. (2001). “Mutation of a new gene encoding a putative pyrin-like protein causes familial cold autoinflammatory syndrome and Muckle-Wells syndrome.” eng. In: *Nat Genet* 29.3, pp. 301–305. ISSN: 1061-4036 (Print); 1546-1718 (Electronic); 1061-4036 (Linking). DOI: [10.1038/ng756](https://doi.org/10.1038/ng756).
- Hollingsworth, L. R. et al. (2021). “DPP9 sequesters the C terminus of NLRP1 to repress inflammasome activation”. In: *Nature* 592.7856, pp. 778–783. DOI: [10.1038/s41586-021-03350-4](https://doi.org/10.1038/s41586-021-03350-4).

- Hopfner, K.-P. and V. Hornung (2020). “Molecular mechanisms and cellular functions of cGAS–STING signalling”. In: *Nature Reviews Molecular Cell Biology* 21.9, pp. 501–521. DOI: [10.1038/s41580-020-0244-x](https://doi.org/10.1038/s41580-020-0244-x).
- Hornung, V., A. Ablasser, et al. (2009). “AIM2 recognizes cytosolic dsDNA and forms a caspase-1-activating inflammasome with ASC.” eng. In: *Nature* 458.7237, pp. 514–518. ISSN: 1476-4687 (Electronic); 0028-0836 (Print); 0028-0836 (Linking). DOI: [10.1038/nature07725](https://doi.org/10.1038/nature07725).
- Hornung, V., F. Bauernfeind, et al. (2008). “Silica crystals and aluminum salts activate the NALP3 inflammasome through phagosomal destabilization.” eng. In: *Nat Immunol* 9.8, pp. 847–856. ISSN: 1529-2916 (Electronic); 1529-2908 (Print); 1529-2908 (Linking). DOI: [10.1038/ni.1631](https://doi.org/10.1038/ni.1631).
- Hornung, V., J. Ellegast, et al. (2006). “5′-Triphosphate RNA Is the Ligand for RIG-I”. In: *Science* 314.5801, pp. 994–997. DOI: [10.1126/science.1132505](https://doi.org/10.1126/science.1132505).
- Hsu, H., H. B. Shu, M. G. Pan, and D. V. Goeddel (1996). “TRADD-TRAF2 and TRADD-FADD interactions define two distinct TNF receptor 1 signal transduction pathways.” eng. In: *Cell* 84.2, pp. 299–308. ISSN: 0092-8674 (Print); 0092-8674 (Linking). DOI: [10.1016/s0092-8674\(00\)80984-8](https://doi.org/10.1016/s0092-8674(00)80984-8).
- Inohara, N. and G. Nuñez (2003). “NODs: intracellular proteins involved in inflammation and apoptosis”. In: *Nature Reviews Immunology* 3.5, pp. 371–382. DOI: [10.1038/nri1086](https://doi.org/10.1038/nri1086).
- Israël, A. (2010). “The IKK complex, a central regulator of NF-kappaB activation.” eng. In: *Cold Spring Harb Perspect Biol* 2.3, a000158. ISSN: 1943-0264 (Electronic); 1943-0264 (Linking). DOI: [10.1101/cshperspect.a000158](https://doi.org/10.1101/cshperspect.a000158).
- Janeway, C. A. J. (1989). “Approaching the asymptote? Evolution and revolution in immunology.” eng. In: *Cold Spring Harb Symp Quant Biol* 54 Pt 1, pp. 1–13. ISSN: 0091-7451 (Print); 0091-7451 (Linking). DOI: [10.1101/sqb.1989.054.01.003](https://doi.org/10.1101/sqb.1989.054.01.003).
- Jasin, M. and R. Rothstein (2013). “Repair of strand breaks by homologous recombination.” eng. In: *Cold Spring Harb Perspect Biol* 5.11, a012740. ISSN: 1943-0264 (Electronic); 1943-0264 (Linking). DOI: [10.1101/cshperspect.a012740](https://doi.org/10.1101/cshperspect.a012740).
- Jenster, L.-M. et al. (2023). “P38 kinases mediate NLRP1 inflammasome activation after ribotoxic stress response and virus infection.” eng. In: *J Exp Med* 220.1. ISSN: 1540-9538 (Electronic); 0022-1007 (Print); 0022-1007 (Linking). DOI: [10.1084/jem.20220837](https://doi.org/10.1084/jem.20220837).
- Jiao, H. et al. (2022). “ADAR1 averts fatal type I interferon induction by ZBP1”. In: *Nature* 607.7920, pp. 776–783. DOI: [10.1038/s41586-022-04878-9](https://doi.org/10.1038/s41586-022-04878-9).

- Jiménez Fernández, D. and M. Lamkanfi (2015). “Inflammatory caspases: key regulators of inflammation and cell death.” eng. In: *Biol Chem* 396.3, pp. 193–203. ISSN: 1437-4315 (Electronic); 1431-6730 (Linking). DOI: [10.1515/hsz-2014-0253](https://doi.org/10.1515/hsz-2014-0253).
- Jinek, M., K. Chylinski, et al. (2012). “A Programmable Dual-RNA–Guided DNA Endonuclease in Adaptive Bacterial Immunity”. In: *Science* 337.6096, pp. 816–821. DOI: [10.1126/science.1225829](https://doi.org/10.1126/science.1225829).
- Jinek, M., F. Jiang, et al. (2014). “Structures of Cas9 endonucleases reveal RNA-mediated conformational activation.” eng. In: *Science* 343.6176, p. 1247997. ISSN: 1095-9203 (Electronic); 0036-8075 (Print); 0036-8075 (Linking). DOI: [10.1126/science.1247997](https://doi.org/10.1126/science.1247997).
- Joffre, O. P., E. Segura, A. Savina, and S. Amigorena (2012). “Cross-presentation by dendritic cells”. In: *Nature Reviews Immunology* 12.8, pp. 557–569. DOI: [10.1038/nri3254](https://doi.org/10.1038/nri3254).
- Johnson, A. G. et al. (2022). “Bacterial gasdermins reveal an ancient mechanism of cell death.” eng. In: *Science* 375.6577, pp. 221–225. ISSN: 1095-9203 (Electronic); 0036-8075 (Print); 0036-8075 (Linking). DOI: [10.1126/science.abj8432](https://doi.org/10.1126/science.abj8432).
- Jumper, J. et al. (2021). “Highly accurate protein structure prediction with AlphaFold”. In: *Nature* 596.7873, pp. 583–589. DOI: [10.1038/s41586-021-03819-2](https://doi.org/10.1038/s41586-021-03819-2).
- Kane, H. and L. Lynch (2019). “Innate Immune Control of Adipose Tissue Homeostasis.” eng. In: *Trends Immunol* 40.9, pp. 857–872. ISSN: 1471-4981 (Electronic); 1471-4906 (Linking). DOI: [10.1016/j.it.2019.07.006](https://doi.org/10.1016/j.it.2019.07.006).
- Kanfer, G. et al. (2021). “Image-based pooled whole-genome CRISPRi screening for subcellular phenotypes.” eng. In: *J Cell Biol* 220.2. ISSN: 1540-8140 (Electronic); 0021-9525 (Print); 0021-9525 (Linking). DOI: [10.1083/jcb.202006180](https://doi.org/10.1083/jcb.202006180).
- Kato, H. et al. (2006). “Differential roles of MDA5 and RIG-I helicases in the recognition of RNA viruses.” eng. In: *Nature* 441.7089, pp. 101–105. ISSN: 1476-4687 (Electronic); 0028-0836 (Linking). DOI: [10.1038/nature04734](https://doi.org/10.1038/nature04734).
- Katti, A. et al. (2022). “CRISPR in cancer biology and therapy”. In: *Nature Reviews Cancer* 22.5, pp. 259–279. DOI: [10.1038/s41568-022-00441-w](https://doi.org/10.1038/s41568-022-00441-w).
- Kayagaki, N., O. S. Kornfeld, et al. (2021). “NINJ1 mediates plasma membrane rupture during lytic cell death.” eng. In: *Nature* 591.7848, pp. 131–136. ISSN: 1476-4687 (Electronic); 0028-0836 (Linking). DOI: [10.1038/s41586-021-03218-7](https://doi.org/10.1038/s41586-021-03218-7).
- Kayagaki, N., I. B. Stowe, et al. (2015). “Caspase-11 cleaves gasdermin D for non-canonical inflammasome signalling.” eng. In: *Nature* 526.7575, pp. 666–671. ISSN: 1476-4687 (Electronic); 0028-0836 (Linking). DOI: [10.1038/nature15541](https://doi.org/10.1038/nature15541).
- Kayagaki, N., S. Warming, et al. (2011). “Non-canonical inflammasome activation targets caspase-11”. In: *Nature* 479.7371, pp. 117–121. DOI: [10.1038/nature10558](https://doi.org/10.1038/nature10558).

- Ke, F. F. S. et al. (2018). “Embryogenesis and Adult Life in the Absence of Intrinsic Apoptosis Effectors BAX, BAK, and BOK.” eng. In: *Cell* 173.5, pp. 1217–1230. ISSN: 1097-4172 (Electronic); 0092-8674 (Linking). DOI: [10.1016/j.cell.2018.04.036](https://doi.org/10.1016/j.cell.2018.04.036).
- Kerr, J. F., A. H. Wyllie, and A. R. Currie (1972). “Apoptosis: a basic biological phenomenon with wide-ranging implications in tissue kinetics.” eng. In: *Br J Cancer* 26.4, pp. 239–257. ISSN: 0007-0920 (Print); 1532-1827 (Electronic); 0007-0920 (Linking). DOI: [10.1038/bjc.1972.33](https://doi.org/10.1038/bjc.1972.33).
- Kibby, E. M. et al. (2023). “Bacterial NLR-related proteins protect against phage”. In: *Cell* 186.11, 2410–2424.e18. DOI: [10.1016/j.cell.2023.04.015](https://doi.org/10.1016/j.cell.2023.04.015).
- Kim, Y.-M., M. M. Brinkmann, M.-E. Paquet, and H. L. Ploegh (2008). “UNC93B1 delivers nucleotide-sensing toll-like receptors to endolysosomes.” eng. In: *Nature* 452.7184, pp. 234–238. ISSN: 1476-4687 (Electronic); 0028-0836 (Linking). DOI: [10.1038/nature06726](https://doi.org/10.1038/nature06726).
- Koblansky, A. A. et al. (2013). “Recognition of profilin by Toll-like receptor 12 is critical for host resistance to *Toxoplasma gondii*.” eng. In: *Immunity* 38.1, pp. 119–130. ISSN: 1097-4180 (Electronic); 1074-7613 (Print); 1074-7613 (Linking). DOI: [10.1016/j.immuni.2012.09.016](https://doi.org/10.1016/j.immuni.2012.09.016).
- Kofoed, E. M. and R. E. Vance (2011). “Innate immune recognition of bacterial ligands by NAIPs determines inflammasome specificity”. In: *Nature* 477.7366, pp. 592–595. DOI: [10.1038/nature10394](https://doi.org/10.1038/nature10394).
- Kolb, J. P., T. H. Oguin, A. Oberst, and J. Martinez (2017). “Programmed Cell Death and Inflammation: Winter Is Coming”. In: *Trends in Immunology* 38.10. Special Issue: Innate Sensing Across Kingdoms, pp. 705–718. ISSN: 1471-4906. DOI: <https://doi.org/10.1016/j.it.2017.06.009>.
- Kolb, W. P. and G. A. Granger (1968). “Lymphocyte in vitro cytotoxicity: characterization of human lymphotoxin.” eng. In: *Proc Natl Acad Sci U S A* 61.4, pp. 1250–1255. ISSN: 0027-8424 (Print); 1091-6490 (Electronic); 0027-8424 (Linking). DOI: [10.1073/pnas.61.4.1250](https://doi.org/10.1073/pnas.61.4.1250).
- Koropatnick, T. A. et al. (2004). “Microbial Factor-Mediated Development in a Host-Bacterial Mutualism”. In: *Science* 306.5699, pp. 1186–1188. DOI: [10.1126/science.1102218](https://doi.org/10.1126/science.1102218).
- Krawczyk, C. M. et al. (2010). “Toll-like receptor-induced changes in glycolytic metabolism regulate dendritic cell activation.” eng. In: *Blood* 115.23, pp. 4742–4749. ISSN: 1528-0020 (Electronic); 0006-4971 (Print); 0006-4971 (Linking). DOI: [10.1182/blood-2009-10-249540](https://doi.org/10.1182/blood-2009-10-249540).

- Kujirai, T. et al. (2020). “Structural basis for the inhibition of cGAS by nucleosomes.” eng. In: *Science* 370.6515, pp. 455–458. ISSN: 1095-9203 (Electronic); 0036-8075 (Print); 0036-8075 (Linking). DOI: [10.1126/science.abd0237](https://doi.org/10.1126/science.abd0237).
- Lamkanfi, M. and V. M. Dixit (2014). “Mechanisms and functions of inflammasomes.” eng. In: *Cell* 157.5, pp. 1013–1022. ISSN: 1097-4172 (Electronic); 0092-8674 (Linking). DOI: [10.1016/j.cell.2014.04.007](https://doi.org/10.1016/j.cell.2014.04.007).
- Laster, S. M., J. G. Wood, and L. R. Gooding (1988). “Tumor necrosis factor can induce both apoptic and necrotic forms of cell lysis.” eng. In: *J Immunol* 141.8, pp. 2629–2634. ISSN: 0022-1767 (Print); 0022-1767 (Linking).
- LeCun, Y., Y. Bengio, and G. Hinton (2015). “Deep learning”. In: *Nature* 521.7553, pp. 436–444. DOI: [10.1038/nature14539](https://doi.org/10.1038/nature14539).
- Lee, B. L. et al. (2013). “UNC93B1 mediates differential trafficking of endosomal TLRs”. In: *eLife* 2. Ed. by Medzhitov, R., e00291. ISSN: 2050-084X. DOI: [10.7554/eLife.00291](https://doi.org/10.7554/eLife.00291).
- Lee, J. et al. (2020). “Versatile phenotype-activated cell sorting”. In: *Science Advances* 6.43, eabb7438. DOI: [10.1126/sciadv.abb7438](https://doi.org/10.1126/sciadv.abb7438).
- Lemaitre, B. et al. (1996). “The dorsoventral regulatory gene cassette spätzle/Toll/cactus controls the potent antifungal response in *Drosophila* adults.” eng. In: *Cell* 86.6, pp. 973–983. ISSN: 0092-8674 (Print); 0092-8674 (Linking). DOI: [10.1016/s0092-8674\(00\)80172-5](https://doi.org/10.1016/s0092-8674(00)80172-5).
- Li, X.-D. and Z. J. Chen (2012). “Sequence specific detection of bacterial 23S ribosomal RNA by TLR13”. In: *eLife* 1. Ed. by Taniguchi, T., e00102. ISSN: 2050-084X. DOI: [10.7554/eLife.00102](https://doi.org/10.7554/eLife.00102).
- Li, Y. et al. (2023). “cGLRs are a diverse family of pattern recognition receptors in innate immunity.” eng. In: *Cell* 186.15, pp. 3261–3276. ISSN: 1097-4172 (Electronic); 0092-8674 (Linking). DOI: [10.1016/j.cell.2023.05.038](https://doi.org/10.1016/j.cell.2023.05.038).
- Liddicoat, B. J. et al. (2015). “RNA editing by ADAR1 prevents MDA5 sensing of endogenous dsRNA as nonself.” eng. In: *Science* 349.6252, pp. 1115–1120. ISSN: 1095-9203 (Electronic); 0036-8075 (Print); 0036-8075 (Linking). DOI: [10.1126/science.aac7049](https://doi.org/10.1126/science.aac7049).
- Lin, S.-C., Y.-C. Lo, and H. Wu (2010). “Helical assembly in the MyD88-IRAK4-IRAK2 complex in TLR/IL-1R signalling.” eng. In: *Nature* 465.7300, pp. 885–890. ISSN: 1476-4687 (Electronic); 0028-0836 (Print); 0028-0836 (Linking). DOI: [10.1038/nature09121](https://doi.org/10.1038/nature09121).
- Lin, Y., A. Devin, Y. Rodriguez, and Z. G. Liu (1999). “Cleavage of the death domain kinase RIP by caspase-8 prompts TNF-induced apoptosis.” eng. In: *Genes Dev*

- 13.19, pp. 2514–2526. ISSN: 0890-9369 (Print); 0890-9369 (Linking). DOI: [10.1101/gad.13.19.2514](https://doi.org/10.1101/gad.13.19.2514).
- Liu, S. et al. (2015). “Phosphorylation of innate immune adaptor proteins MAVS, STING, and TRIF induces IRF3 activation.” eng. In: *Science* 347.6227, aaa2630. ISSN: 1095-9203 (Electronic); 0036-8075 (Linking). DOI: [10.1126/science.aaa2630](https://doi.org/10.1126/science.aaa2630).
- Liu, X., H. Zou, C. Slaughter, and X. Wang (1997). “DFF, a Heterodimeric Protein That Functions Downstream of Caspase-3 to Trigger DNA Fragmentation during Apoptosis”. In: *Cell* 89.2, pp. 175–184. ISSN: 0092-8674. DOI: [https://doi.org/10.1016/S0092-8674\(00\)80197-X](https://doi.org/10.1016/S0092-8674(00)80197-X).
- Lopatina, A., N. Tal, and R. Sorek (2020). “Abortive Infection: Bacterial Suicide as an Antiviral Immune Strategy”. In: *Annual Review of Virology* 7.1. PMID: 32559405, pp. 371–384. DOI: [10.1146/annurev-virology-011620-040628](https://doi.org/10.1146/annurev-virology-011620-040628).
- Lugrin, J. and F. Martinon (2018). “The AIM2 inflammasome: Sensor of pathogens and cellular perturbations”. In: *Immunological Reviews* 281.1, pp. 99–114. DOI: <https://doi.org/10.1111/imr.12618>.
- Lykke-Andersen, S. and T. H. Jensen (2015). “Nonsense-mediated mRNA decay: an intricate machinery that shapes transcriptomes”. In: *Nature Reviews Molecular Cell Biology* 16.11, pp. 665–677. DOI: [10.1038/nrm4063](https://doi.org/10.1038/nrm4063).
- Majer, O., B. Liu, L. S. M. Kreuk, et al. (2019). “UNC93B1 recruits syntenin-1 to dampen TLR7 signalling and prevent autoimmunity.” eng. In: *Nature* 575.7782, pp. 366–370. ISSN: 1476-4687 (Electronic); 0028-0836 (Print); 0028-0836 (Linking). DOI: [10.1038/s41586-019-1612-6](https://doi.org/10.1038/s41586-019-1612-6).
- Majer, O., B. Liu, B. J. Woo, et al. (2019). “Release from UNC93B1 reinforces the compartmentalized activation of select TLRs.” eng. In: *Nature* 575.7782, pp. 371–374. ISSN: 1476-4687 (Electronic); 0028-0836 (Print); 0028-0836 (Linking). DOI: [10.1038/s41586-019-1611-7](https://doi.org/10.1038/s41586-019-1611-7).
- Mali, P. et al. (2013). “RNA-Guided Human Genome Engineering via Cas9”. In: *Science* 339.6121, pp. 823–826. DOI: [10.1126/science.1232033](https://doi.org/10.1126/science.1232033).
- Mariathasan, S. et al. (2006). “Cryopyrin activates the inflammasome in response to toxins and ATP”. In: *Nature* 440.7081, pp. 228–232. DOI: [10.1038/nature04515](https://doi.org/10.1038/nature04515).
- Martinon, F., K. Hofmann, and J. Tschopp (2001). “The pyrin domain: a possible member of the death domain-fold family implicated in apoptosis and inflammation.” eng. In: *Curr Biol* 11.4, R118–20. ISSN: 0960-9822 (Print); 0960-9822 (Linking). DOI: [10.1016/S0960-9822\(01\)00056-2](https://doi.org/10.1016/S0960-9822(01)00056-2).
- Martinon, F., K. Burns, and J. Tschopp (2002). “The Inflammasome: A Molecular Platform Triggering Activation of Inflammatory Caspases and Processing of proIL-

- β” in: *Molecular Cell* 10.2, pp. 417–426. DOI: [10.1016/S1097-2765\(02\)00599-3](https://doi.org/10.1016/S1097-2765(02)00599-3).
- Martinon, F., V. Pétrilli, et al. (2006). “Gout-associated uric acid crystals activate the NALP3 inflammasome.” eng. In: *Nature* 440.7081, pp. 237–241. ISSN: 1476-4687 (Electronic); 0028-0836 (Linking). DOI: [10.1038/nature04516](https://doi.org/10.1038/nature04516).
- Masumoto, J. et al. (1999). “ASC, a novel 22-kDa protein, aggregates during apoptosis of human promyelocytic leukemia HL-60 cells.” eng. In: *J Biol Chem* 274.48, pp. 33835–33838. ISSN: 0021-9258 (Print); 0021-9258 (Linking). DOI: [10.1074/jbc.274.48.33835](https://doi.org/10.1074/jbc.274.48.33835).
- Matzinger, P. (1994). “Tolerance, Danger, and the Extended Family”. In: *Annual Review of Immunology* 12.1. PMID: 8011301, pp. 991–1045. DOI: [10.1146/annurev.12.040194.005015](https://doi.org/10.1146/annurev.12.040194.005015).
- McKee, C. M. and R. C. Coll (2020). “NLRP3 inflammasome priming: A riddle wrapped in a mystery inside an enigma”. In: *Journal of Leukocyte Biology* 108.3, pp. 937–952. DOI: <https://doi.org/10.1002/JLB.3MR0720-513R>.
- McNab, F. et al. (2015). “Type I interferons in infectious disease”. In: *Nature Reviews Immunology* 15.2, pp. 87–103. DOI: [10.1038/nri3787](https://doi.org/10.1038/nri3787).
- Medzhitov, R. and C. A. Janeway (2002). “Decoding the Patterns of Self and Nonself by the Innate Immune System”. In: *Science* 296.5566, pp. 298–300. DOI: [10.1126/science.1068883](https://doi.org/10.1126/science.1068883).
- Medzhitov, R., P. Preston-Hurlburt, and C. A. Janeway (1997). “A human homologue of the Drosophila Toll protein signals activation of adaptive immunity”. In: *Nature* 388.6640, pp. 394–397. DOI: [10.1038/41131](https://doi.org/10.1038/41131).
- Meizlish, M. L., R. A. Franklin, X. Zhou, and R. Medzhitov (2021). “Tissue Homeostasis and Inflammation”. In: *Annual Review of Immunology* 39.1. PMID: 33651964, pp. 557–581. DOI: [10.1146/annurev-immunol-061020-053734](https://doi.org/10.1146/annurev-immunol-061020-053734).
- Michalski, S. et al. (2020). “Structural basis for sequestration and autoinhibition of cGAS by chromatin.” eng. In: *Nature* 587.7835, pp. 678–682. ISSN: 1476-4687 (Electronic); 0028-0836 (Linking). DOI: [10.1038/s41586-020-2748-0](https://doi.org/10.1038/s41586-020-2748-0).
- Micheau, O. and J. Tschoop (2003). “Induction of TNF receptor I-mediated apoptosis via two sequential signaling complexes.” eng. In: *Cell* 114.2, pp. 181–190. ISSN: 0092-8674 (Print); 0092-8674 (Linking). DOI: [10.1016/s0092-8674\(03\)00521-x](https://doi.org/10.1016/s0092-8674(03)00521-x).
- Monroe, K. M. et al. (2014). “IFI16 DNA Sensor Is Required for Death of Lymphoid CD4 T Cells Abortively Infected with HIV”. In: *Science* 343.6169, pp. 428–432. DOI: [10.1126/science.1243640](https://doi.org/10.1126/science.1243640).
- Moore, C. B. et al. (2008). “NLRX1 is a regulator of mitochondrial antiviral immunity”. In: *Nature* 451.7178, pp. 573–577. DOI: [10.1038/nature06501](https://doi.org/10.1038/nature06501).

- Moore, J. K. and J. E. Haber (1996). “Cell cycle and genetic requirements of two pathways of nonhomologous end-joining repair of double-strand breaks in *Saccharomyces cerevisiae*.” eng. In: *Mol Cell Biol* 16.5, pp. 2164–2173. ISSN: 0270-7306 (Print); 1098-5549 (Electronic); 0270-7306 (Linking). DOI: [10.1128/MCB.16.5.2164](https://doi.org/10.1128/MCB.16.5.2164).
- Motshwene, P. G. et al. (2009). “An oligomeric signaling platform formed by the Toll-like receptor signal transducers MyD88 and IRAK-4.” eng. In: *J Biol Chem* 284.37, pp. 25404–25411. ISSN: 1083-351X (Electronic); 0021-9258 (Print); 0021-9258 (Linking). DOI: [10.1074/jbc.M109.022392](https://doi.org/10.1074/jbc.M109.022392).
- Mujal, A. M., R. B. Delconte, and J. C. Sun (2021). “Natural Killer Cells: From Innate to Adaptive Features”. In: *Annual Review of Immunology* 39.1. PMID: 33902312, pp. 417–447. DOI: [10.1146/annurev-immunol-101819-074948](https://doi.org/10.1146/annurev-immunol-101819-074948).
- Muñoz-Planillo, R. et al. (2013). “K⁺ Efflux Is the Common Trigger of NLRP3 Inflammasome Activation by Bacterial Toxins and Particulate Matter”. In: *Immunity* 38.6, pp. 1142–1153. DOI: [10.1016/j.immuni.2013.05.016](https://doi.org/10.1016/j.immuni.2013.05.016).
- Murphy, K., P. Travers, M. Walport, and C. Janeway (2012). *Janeway’s immunobiology*. 8th ed. New York: Garland Science New York. ISBN: 9780815342434; 0815342438; 9780815345305; 0815345305.
- Neefjes, J., M. L. M. Jongsma, P. Paul, and O. Bakke (2011). “Towards a systems understanding of MHC class I and MHC class II antigen presentation”. In: *Nature Reviews Immunology* 11.12, pp. 823–836. DOI: [10.1038/nri3084](https://doi.org/10.1038/nri3084).
- Netea, M. G. et al. (2020). “Defining trained immunity and its role in health and disease”. In: *Nature Reviews Immunology* 20.6, pp. 375–388. DOI: [10.1038/s41577-020-0285-6](https://doi.org/10.1038/s41577-020-0285-6).
- Newton, K. and G. Manning (2016). “Necroptosis and Inflammation”. In: *Annual Review of Biochemistry* 85.1. PMID: 26865533, pp. 743–763. DOI: [10.1146/annurev-biochem-060815-014830](https://doi.org/10.1146/annurev-biochem-060815-014830).
- Nirenberg, M. W. and J. H. Matthaei (1961). “The dependence of cell-free protein synthesis in *E. coli* upon naturally occurring or synthetic polyribonucleotides.” eng. In: *Proc Natl Acad Sci U S A* 47.10, pp. 1588–1602. ISSN: 0027-8424 (Print); 1091-6490 (Electronic); 0027-8424 (Linking). DOI: [10.1073/pnas.47.10.1588](https://doi.org/10.1073/pnas.47.10.1588).
- Nüsslein-Volhard, C. and E. Wieschaus (1980). “Mutations affecting segment number and polarity in *Drosophila*”. In: *Nature* 287.5785, pp. 795–801. DOI: [10.1038/287795a0](https://doi.org/10.1038/287795a0).
- O’Neill, L. A. J. and A. G. Bowie (2007). “The family of five: TIR-domain-containing adaptors in Toll-like receptor signalling”. In: *Nature Reviews Immunology* 7.5, pp. 353–364. DOI: [10.1038/nri2079](https://doi.org/10.1038/nri2079).

- O'Neill, L. A. J., R. J. Kishton, and J. Rathmell (2016). "A guide to immunometabolism for immunologists". In: *Nature Reviews Immunology* 16.9, pp. 553–565. DOI: [10.1038/nri.2016.70](https://doi.org/10.1038/nri.2016.70).
- Oberst, A. et al. (2011). "Catalytic activity of the caspase-8-FLIP(L) complex inhibits RIPK3-dependent necrosis." eng. In: *Nature* 471.7338, pp. 363–367. ISSN: 1476-4687 (Electronic); 0028-0836 (Print); 0028-0836 (Linking). DOI: [10.1038/nature09852](https://doi.org/10.1038/nature09852).
- Odegard, V. H. and D. G. Schatz (2006). "Targeting of somatic hypermutation". In: *Nature Reviews Immunology* 6.8, pp. 573–583. DOI: [10.1038/nri1896](https://doi.org/10.1038/nri1896).
- Okondo, M. C. et al. (2017). "DPP8 and DPP9 inhibition induces pro-caspase-1-dependent monocyte and macrophage pyroptosis." eng. In: *Nat Chem Biol* 13.1, pp. 46–53. ISSN: 1552-4469 (Electronic); 1552-4450 (Print); 1552-4450 (Linking). DOI: [10.1038/nchembio.2229](https://doi.org/10.1038/nchembio.2229).
- Oldenburg, M. et al. (2012). "TLR13 Recognizes Bacterial 23S rRNA Devoid of Erythromycin Resistance-Forming Modification". In: *Science* 337.6098, pp. 1111–1115. DOI: [10.1126/science.1220363](https://doi.org/10.1126/science.1220363).
- Oosting, M. et al. (2014). "Human TLR10 is an anti-inflammatory pattern-recognition receptor". In: *Proceedings of the National Academy of Sciences* 111.42, E4478–E4484. DOI: [10.1073/pnas.1410293111](https://doi.org/10.1073/pnas.1410293111).
- Pan, G., K. O'Rourke, and V. M. Dixit (1998). "Caspase-9, Bcl-XL, and Apaf-1 Form a Ternary Complex*". In: *Journal of Biological Chemistry* 273.10, pp. 5841–5845. ISSN: 0021-9258. DOI: <https://doi.org/10.1074/jbc.273.10.5841>.
- Pancer, Z. et al. (2004). "Somatic diversification of variable lymphocyte receptors in the agnathan sea lamprey." eng. In: *Nature* 430.6996, pp. 174–180. ISSN: 1476-4687 (Electronic); 0028-0836 (Linking). DOI: [10.1038/nature02740](https://doi.org/10.1038/nature02740).
- Park, Y. H., G. Wood, D. L. Kastner, and J. J. Chae (2016). "Pyrin inflammasome activation and RhoA signaling in the autoinflammatory diseases FMF and HIDS." eng. In: *Nat Immunol* 17.8, pp. 914–921. ISSN: 1529-2916 (Electronic); 1529-2908 (Print); 1529-2908 (Linking). DOI: [10.1038/ni.3457](https://doi.org/10.1038/ni.3457).
- Parnas, O. et al. (2015). "A Genome-wide CRISPR Screen in Primary Immune Cells to Dissect Regulatory Networks." eng. In: *Cell* 162.3, pp. 675–686. ISSN: 1097-4172 (Electronic); 0092-8674 (Print); 0092-8674 (Linking). DOI: [10.1016/j.cell.2015.06.059](https://doi.org/10.1016/j.cell.2015.06.059).
- Pasparakis, M. and P. Vandenabeele (2015). "Necroptosis and its role in inflammation". In: *Nature* 517.7534, pp. 311–320. DOI: [10.1038/nature14191](https://doi.org/10.1038/nature14191).
- Pathare, G. R. et al. (2020). "Structural mechanism of cGAS inhibition by the nucleosome." eng. In: *Nature* 587.7835, pp. 668–672. ISSN: 1476-4687 (Electronic); 0028-0836 (Linking). DOI: [10.1038/s41586-020-2750-6](https://doi.org/10.1038/s41586-020-2750-6).

- Pelka, K. et al. (2018). “The Chaperone UNC93B1 Regulates Toll-like Receptor Stability Independently of Endosomal TLR Transport.” eng. In: *Immunity* 48.5, pp. 911–922. ISSN: 1097-4180 (Electronic); 1074-7613 (Print); 1074-7613 (Linking). DOI: [10.1016/j.immuni.2018.04.011](https://doi.org/10.1016/j.immuni.2018.04.011).
- Perregaux, D. and C. A. Gabel (1994). “Interleukin-1 beta maturation and release in response to ATP and nigericin. Evidence that potassium depletion mediated by these agents is a necessary and common feature of their activity.” eng. In: *J Biol Chem* 269.21, pp. 15195–15203. ISSN: 0021-9258 (Print); 0021-9258 (Linking).
- Pinci, F. et al. (2022). “Tumor necrosis factor is a necroptosis-associated alarmin.” eng. In: *Front Immunol* 13, p. 1074440. ISSN: 1664-3224 (Electronic); 1664-3224 (Linking). DOI: [10.3389/fimmu.2022.1074440](https://doi.org/10.3389/fimmu.2022.1074440).
- Platanias, L. C. (2005). “Mechanisms of type-I- and type-II-interferon-mediated signalling”. In: *Nature Reviews Immunology* 5.5, pp. 375–386. DOI: [10.1038/nri1604](https://doi.org/10.1038/nri1604).
- Pollard, A. J. and E. M. Bijker (2021). “A guide to vaccinology: from basic principles to new developments”. In: *Nature Reviews Immunology* 21.2, pp. 83–100. DOI: [10.1038/s41577-020-00479-7](https://doi.org/10.1038/s41577-020-00479-7).
- Poltorak, A. et al. (1998). “Defective LPS signaling in C3H/HeJ and C57BL/10ScCr mice: mutations in Tlr4 gene.” eng. In: *Science* 282.5396, pp. 2085–2088. ISSN: 0036-8075 (Print); 0036-8075 (Linking). DOI: [10.1126/science.282.5396.2085](https://doi.org/10.1126/science.282.5396.2085).
- Próchnicki, T. et al. (2023). “Mitochondrial damage activates the NLRP10 inflammasome”. In: *Nature Immunology* 24.4, pp. 595–603. DOI: [10.1038/s41590-023-01451-y](https://doi.org/10.1038/s41590-023-01451-y).
- Py, B. F., M.-S. Kim, H. Vakifahmetoglu-Norberg, and J. Yuan (2013). “Deubiquitination of NLRP3 by BRCC3 Critically Regulates Inflammasome Activity”. In: *Molecular Cell* 49.2, pp. 331–338. ISSN: 1097-2765. DOI: <https://doi.org/10.1016/j.molcel.2012.11.009>.
- Qi, Q. et al. (2014). “Diversity and clonal selection in the human T-cell repertoire”. In: *Proceedings of the National Academy of Sciences* 111.36, pp. 13139–13144. DOI: [10.1073/pnas.1409155111](https://doi.org/10.1073/pnas.1409155111).
- Ramirez, M. L. G. and G. S. Salvesen (2018). “A primer on caspase mechanisms”. In: *Seminars in Cell & Developmental Biology* 82. SI: Nuclear positioning, pp. 79–85. ISSN: 1084-9521. DOI: <https://doi.org/10.1016/j.semcdb.2018.01.002>.
- Rao, S. D. et al. (2022). “M24B aminopeptidase inhibitors selectively activate the CARD8 inflammasome.” eng. In: *Nat Chem Biol* 18.5, pp. 565–574. ISSN: 1552-4469 (Electronic); 1552-4450 (Print); 1552-4450 (Linking). DOI: [10.1038/s41589-021-00964-7](https://doi.org/10.1038/s41589-021-00964-7).

- Rathinam, V. A. K. et al. (2010). “The AIM2 inflammasome is essential for host defense against cytosolic bacteria and DNA viruses”. In: *Nature Immunology* 11.5, pp. 395–402. DOI: [10.1038/ni.1864](https://doi.org/10.1038/ni.1864).
- Rebsamen, M. et al. (2011). “NLRX1/NOD5 deficiency does not affect MAVS signalling.” eng. In: *Cell Death Differ* 18.8, p. 1387. ISSN: 1476-5403 (Electronic); 1350-9047 (Print); 1350-9047 (Linking). DOI: [10.1038/cdd.2011.64](https://doi.org/10.1038/cdd.2011.64).
- Rehwinkel, J. and M. U. Gack (2020). “RIG-I-like receptors: their regulation and roles in RNA sensing”. In: *Nature Reviews Immunology* 20.9, pp. 537–551. DOI: [10.1038/s41577-020-0288-3](https://doi.org/10.1038/s41577-020-0288-3).
- Remick, B. C., M. M. Gaidt, and R. E. Vance (2023). “Effector-Triggered Immunity”. In: *Annual Review of Immunology* 41.1. PMID: 36750319, pp. 453–481. DOI: [10.1146/annurev-immunol-101721-031732](https://doi.org/10.1146/annurev-immunol-101721-031732).
- Replogle, J. M. et al. (2022). “Mapping information-rich genotype-phenotype landscapes with genome-scale Perturb-seq.” eng. In: *Cell* 185.14, pp. 2559–2575. ISSN: 1097-4172 (Electronic); 0092-8674 (Print); 0092-8674 (Linking). DOI: [10.1016/j.cell.2022.05.013](https://doi.org/10.1016/j.cell.2022.05.013).
- Reuver, R. de et al. (2022). “ADAR1 prevents autoinflammation by suppressing spontaneous ZBP1 activation.” eng. In: *Nature* 607.7920, pp. 784–789. ISSN: 1476-4687 (Electronic); 0028-0836 (Linking). DOI: [10.1038/s41586-022-04974-w](https://doi.org/10.1038/s41586-022-04974-w).
- Rice, G. I. et al. (2012). “Mutations in ADAR1 cause Aicardi-Goutières syndrome associated with a type I interferon signature.” eng. In: *Nat Genet* 44.11, pp. 1243–1248. ISSN: 1546-1718 (Electronic); 1061-4036 (Print); 1061-4036 (Linking). DOI: [10.1038/ng.2414](https://doi.org/10.1038/ng.2414).
- Ricklin, D., G. Hajishengallis, K. Yang, and J. D. Lambris (2010). “Complement: a key system for immune surveillance and homeostasis”. In: *Nature Immunology* 11.9, pp. 785–797. DOI: [10.1038/ni.1923](https://doi.org/10.1038/ni.1923).
- Robinson, K. S. et al. (2020). “Enteroviral 3C protease activates the human NLRP1 inflammasome in airway epithelia”. In: *Science* 370.6521, eaay2002. DOI: [10.1126/science.aay2002](https://doi.org/10.1126/science.aay2002).
- Rodriguez, K. R., A. M. Bruns, and C. M. Horvath (2014). “MDA5 and LGP2: accomplices and antagonists of antiviral signal transduction.” eng. In: *J Virol* 88.15, pp. 8194–8200. ISSN: 1098-5514 (Electronic); 0022-538X (Print); 0022-538X (Linking). DOI: [10.1128/JVI.00640-14](https://doi.org/10.1128/JVI.00640-14).
- Rothenfusser, S. et al. (2005). “The RNA helicase Lgp2 inhibits TLR-independent sensing of viral replication by retinoic acid-inducible gene-I.” eng. In: *J Immunol* 175.8, pp. 5260–5268. ISSN: 0022-1767 (Print); 0022-1767 (Linking). DOI: [10.4049/jimmunol.175.8.5260](https://doi.org/10.4049/jimmunol.175.8.5260).

- Rowley, M. J. and V. G. Corces (2018). “Organizational principles of 3D genome architecture”. In: *Nature Reviews Genetics* 19.12, pp. 789–800. DOI: [10.1038/s41576-018-0060-8](https://doi.org/10.1038/s41576-018-0060-8).
- Roy, N. et al. (1995). “The gene for neuronal apoptosis inhibitory protein is partially deleted in individuals with spinal muscular atrophy”. In: *Cell* 80.1, pp. 167–178. ISSN: 0092-8674. DOI: [https://doi.org/10.1016/0092-8674\(95\)90461-1](https://doi.org/10.1016/0092-8674(95)90461-1).
- Ruddle, N. H. and B. H. Waksman (1968). “Cytotoxicity mediated by soluble antigen and lymphocytes in delayed hypersensitivity. 3. Analysis of mechanism.” eng. In: *J Exp Med* 128.6, pp. 1267–1279. ISSN: 0022-1007 (Print); 1540-9538 (Electronic); 0022-1007 (Linking). DOI: [10.1084/jem.128.6.1267](https://doi.org/10.1084/jem.128.6.1267).
- Rühl, S. et al. (2018). “ESCRT-dependent membrane repair negatively regulates pyroptosis downstream of GSDMD activation”. In: *Science* 362.6417, pp. 956–960. DOI: [10.1126/science.aar7607](https://doi.org/10.1126/science.aar7607).
- Sáenz, J. et al. (2009). “Golgicide A reveals essential roles for GBF1 in Golgi assembly and function”. In: *Nature Chemical Biology* 5.3, pp. 157–165. DOI: [10.1038/nchembio.144](https://doi.org/10.1038/nchembio.144).
- Sandstrom, A. et al. (2019). “Functional degradation: A mechanism of NLRP1 inflammasome activation by diverse pathogen enzymes.” eng. In: *Science* 364.6435. ISSN: 1095-9203 (Electronic); 0036-8075 (Print); 0036-8075 (Linking). DOI: [10.1126/science.aau1330](https://doi.org/10.1126/science.aau1330).
- Schatz, D. G. and Y. Ji (2011). “Recombination centres and the orchestration of V(D)J recombination”. In: *Nature Reviews Immunology* 11.4, pp. 251–263. DOI: [10.1038/nri2941](https://doi.org/10.1038/nri2941).
- Schmacke, N. A., S. C. Mädler, et al. (2023). “SPARCS, a platform for genome-scale CRISPR screening for spatial cellular phenotypes”. In: *bioRxiv*. DOI: [10.1101/2023.06.01.542416](https://doi.org/10.1101/2023.06.01.542416).
- Schmacke, N. A., F. O’Duill, et al. (2022). “IKK β primes inflammasome formation by recruiting NLRP3 to the trans-Golgi network.” eng. In: *Immunity* 55.12, pp. 2271–2284. ISSN: 1097-4180 (Electronic); 1074-7613 (Print); 1074-7613 (Linking). DOI: [10.1016/j.immuni.2022.10.021](https://doi.org/10.1016/j.immuni.2022.10.021).
- Schmid-Burgk, J. L., D. Chauhan, et al. (2016). “A Genome-wide CRISPR (Clustered Regularly Interspaced Short Palindromic Repeats) Screen Identifies NEK7 as an Essential Component of NLRP3 Inflammasome Activation.” eng. In: *J Biol Chem* 291.1, pp. 103–109. ISSN: 1083-351X (Electronic); 0021-9258 (Print); 0021-9258 (Linking). DOI: [10.1074/jbc.C115.700492](https://doi.org/10.1074/jbc.C115.700492).
- Schmid-Burgk, J. L., M. M. Gaidt, et al. (2015). “Caspase-4 mediates non-canonical activation of the NLRP3 inflammasome in human myeloid cells.” eng. In: *Eur J*

- Immunol* 45.10, pp. 2911–2917. ISSN: 1521-4141 (Electronic); 0014-2980 (Linking). DOI: [10.1002/eji.201545523](https://doi.org/10.1002/eji.201545523).
- Schmid-Burgk, J. L., K. Höning, T. S. Ebert, and V. Hornung (2016). “CRISPaint allows modular base-specific gene tagging using a ligase-4-dependent mechanism.” eng. In: *Nat Commun* 7, p. 12338. ISSN: 2041-1723 (Electronic); 2041-1723 (Linking). DOI: [10.1038/ncomms12338](https://doi.org/10.1038/ncomms12338).
- Schoggins, J. W. et al. (2011). “A diverse range of gene products are effectors of the type I interferon antiviral response.” eng. In: *Nature* 472.7344, pp. 481–485. ISSN: 1476-4687 (Electronic); 0028-0836 (Print); 0028-0836 (Linking). DOI: [10.1038/nature09907](https://doi.org/10.1038/nature09907).
- Schraivogel, D. et al. (2022). “High-speed fluorescence image-enabled cell sorting”. In: *Science* 375.6578, pp. 315–320. DOI: [10.1126/science.abj3013](https://doi.org/10.1126/science.abj3013).
- Scully, R., A. Panday, R. Elango, and N. A. Willis (2019). “DNA double-strand break repair-pathway choice in somatic mammalian cells”. In: *Nature Reviews Molecular Cell Biology* 20.11, pp. 698–714. DOI: [10.1038/s41580-019-0152-0](https://doi.org/10.1038/s41580-019-0152-0).
- Segawa, K. et al. (2014). “Caspase-mediated cleavage of phospholipid flippase for apoptotic phosphatidylserine exposure.” eng. In: *Science* 344.6188, pp. 1164–1168. ISSN: 1095-9203 (Electronic); 0036-8075 (Linking). DOI: [10.1126/science.1252809](https://doi.org/10.1126/science.1252809).
- Seth, R. B., L. Sun, C.-K. Ea, and Z. J. Chen (2005). “Identification and characterization of MAVS, a mitochondrial antiviral signaling protein that activates NF-kappaB and IRF 3.” eng. In: *Cell* 122.5, pp. 669–682. ISSN: 0092-8674 (Print); 0092-8674 (Linking). DOI: [10.1016/j.cell.2005.08.012](https://doi.org/10.1016/j.cell.2005.08.012).
- Shalem, O., N. E. Sanjana, and F. Zhang (2015). “High-throughput functional genomics using CRISPR-Cas9.” eng. In: *Nat Rev Genet* 16.5, pp. 299–311. ISSN: 1471-0064 (Electronic); 1471-0056 (Print); 1471-0056 (Linking). DOI: [10.1038/nrg3899](https://doi.org/10.1038/nrg3899).
- Sharif, H. et al. (2021). “Dipeptidyl peptidase 9 sets a threshold for CARD8 inflammasome formation by sequestering its active C-terminal fragment”. In: *Immunity* 54.7, 1392–1404.e10. ISSN: 1074-7613. DOI: <https://doi.org/10.1016/j.immuni.2021.04.024>.
- Sheehy, A. M., N. C. Gaddis, J. D. Choi, and M. H. Malim (2002). “Isolation of a human gene that inhibits HIV-1 infection and is suppressed by the viral Vif protein.” eng. In: *Nature* 418.6898, pp. 646–650. ISSN: 0028-0836 (Print); 0028-0836 (Linking). DOI: [10.1038/nature00939](https://doi.org/10.1038/nature00939).
- Shi, H. et al. (2016). “NLRP3 activation and mitosis are mutually exclusive events coordinated by NEK7, a new inflammasome component.” eng. In: *Nat Immunol* 17.3, pp. 250–258. ISSN: 1529-2916 (Electronic); 1529-2908 (Print); 1529-2908 (Linking). DOI: [10.1038/ni.3333](https://doi.org/10.1038/ni.3333).

- Shi, J., Y. Zhao, K. Wang, et al. (2015). “Cleavage of GSDMD by inflammatory caspases determines pyroptotic cell death.” eng. In: *Nature* 526.7575, pp. 660–665. ISSN: 1476-4687 (Electronic); 0028-0836 (Linking). DOI: [10.1038/nature15514](https://doi.org/10.1038/nature15514).
- Shi, J., Y. Zhao, Y. Wang, et al. (2014). “Inflammatory caspases are innate immune receptors for intracellular LPS.” eng. In: *Nature* 514.7521, pp. 187–192. ISSN: 1476-4687 (Electronic); 0028-0836 (Linking). DOI: [10.1038/nature13683](https://doi.org/10.1038/nature13683).
- Shimizu, T. (2009). “Lipid Mediators in Health and Disease: Enzymes and Receptors as Therapeutic Targets for the Regulation of Immunity and Inflammation”. In: *Annual Review of Pharmacology and Toxicology* 49.1. PMID: 18834304, pp. 123–150. DOI: [10.1146/annurev.pharmtox.011008.145616](https://doi.org/10.1146/annurev.pharmtox.011008.145616).
- Singh, R., A. Letai, and K. Sarosiek (2019). “Regulation of apoptosis in health and disease: the balancing act of BCL-2 family proteins”. In: *Nature Reviews Molecular Cell Biology* 20.3, pp. 175–193. DOI: [10.1038/s41580-018-0089-8](https://doi.org/10.1038/s41580-018-0089-8).
- Slavik, K. M. and P. J. Kranzusch (2023). “CBASS to cGAS-STING: The Origins and Mechanisms of Nucleotide Second Messenger Immune Signaling”. In: *Annual Review of Virology* 10.1. PMID: 37380187, null. DOI: [10.1146/annurev-virology-111821-115636](https://doi.org/10.1146/annurev-virology-111821-115636).
- Song, N. et al. (2017). “NLRP3 Phosphorylation Is an Essential Priming Event for Inflammasome Activation”. In: *Molecular Cell* 68.1, 185–197.e6. ISSN: 1097-2765. DOI: <https://doi.org/10.1016/j.molcel.2017.08.017>.
- Sorek, R., V. Kunin, and P. Hugenholtz (2008). “CRISPR—a widespread system that provides acquired resistance against phages in bacteria and archaea.” eng. In: *Nat Rev Microbiol* 6.3, pp. 181–186. ISSN: 1740-1534 (Electronic); 1740-1526 (Linking). DOI: [10.1038/nrmicro1793](https://doi.org/10.1038/nrmicro1793).
- Statello, L., C.-J. Guo, L.-L. Chen, and M. Huarte (2021). “Gene regulation by long non-coding RNAs and its biological functions”. In: *Nature Reviews Molecular Cell Biology* 22.2, pp. 96–118. DOI: [10.1038/s41580-020-00315-9](https://doi.org/10.1038/s41580-020-00315-9).
- Steimle, V., L. A. Otten, M. Zufferey, and B. Mach (1993). “Complementation cloning of an MHC class II transactivator mutated in hereditary MHC class II deficiency (or bare lymphocyte syndrome).” eng. In: *Cell* 75.1, pp. 135–146. ISSN: 0092-8674 (Print); 0092-8674 (Linking).
- Steinman, R. M. and Z. A. Cohn (1973). “Identification of a novel cell type in peripheral lymphoid organs of mice. I. Morphology, quantitation, tissue distribution.” eng. In: *J Exp Med* 137.5, pp. 1142–1162. ISSN: 0022-1007 (Print); 1540-9538 (Electronic); 0022-1007 (Linking). DOI: [10.1084/jem.137.5.1142](https://doi.org/10.1084/jem.137.5.1142).

- Stetson, D. B., J. S. Ko, T. Heidmann, and R. Medzhitov (2008). “Trex1 Prevents Cell-Intrinsic Initiation of Autoimmunity”. In: *Cell* 134.4, pp. 587–598. DOI: [10.1016/j.cell.2008.06.032](https://doi.org/10.1016/j.cell.2008.06.032).
- Stutz, A. et al. (2017). “NLRP3 inflammasome assembly is regulated by phosphorylation of the pyrin domain.” eng. In: *J Exp Med* 214.6, pp. 1725–1736. ISSN: 1540-9538 (Electronic); 0022-1007 (Print); 0022-1007 (Linking). DOI: [10.1084/jem.20160933](https://doi.org/10.1084/jem.20160933).
- Sun, L. et al. (2013). “Cyclic GMP-AMP synthase is a cytosolic DNA sensor that activates the type I interferon pathway.” eng. In: *Science* 339.6121, pp. 786–791. ISSN: 1095-9203 (Electronic); 0036-8075 (Print); 0036-8075 (Linking). DOI: [10.1126/science.1232458](https://doi.org/10.1126/science.1232458).
- Suzuki, J. et al. (2013). “Xk-related protein 8 and CED-8 promote phosphatidylserine exposure in apoptotic cells.” eng. In: *Science* 341.6144, pp. 403–406. ISSN: 1095-9203 (Electronic); 0036-8075 (Linking). DOI: [10.1126/science.1236758](https://doi.org/10.1126/science.1236758).
- Suzuki, K. et al. (2016). “In vivo genome editing via CRISPR/Cas9 mediated homology-independent targeted integration.” eng. In: *Nature* 540.7631, pp. 144–149. ISSN: 1476-4687 (Electronic); 0028-0836 (Print); 0028-0836 (Linking). DOI: [10.1038/nature20565](https://doi.org/10.1038/nature20565).
- Swanson, K. V., M. Deng, and J. P.-Y. Ting (2019). “The NLRP3 inflammasome: molecular activation and regulation to therapeutics.” eng. In: *Nat Rev Immunol* 19.8, pp. 477–489. ISSN: 1474-1741 (Electronic); 1474-1733 (Print); 1474-1733 (Linking). DOI: [10.1038/s41577-019-0165-0](https://doi.org/10.1038/s41577-019-0165-0).
- Tabeta, K. et al. (2006). “The Unc93b1 mutation 3d disrupts exogenous antigen presentation and signaling via Toll-like receptors 3, 7 and 9”. In: *Nature Immunology* 7.2, pp. 156–164. DOI: [10.1038/ni1297](https://doi.org/10.1038/ni1297).
- Takeuchi, O. and S. Akira (2010). “Pattern Recognition Receptors and Inflammation”. In: *Cell* 140.6, pp. 805–820. DOI: [10.1016/j.cell.2010.01.022](https://doi.org/10.1016/j.cell.2010.01.022).
- Takeuchi, O., K. Hoshino, et al. (1999). “Differential Roles of TLR2 and TLR4 in Recognition of Gram-Negative and Gram-Positive Bacterial Cell Wall Components”. In: *Immunity* 11.4, pp. 443–451. ISSN: 1074-7613. DOI: [https://doi.org/10.1016/S1074-7613\(00\)80119-3](https://doi.org/10.1016/S1074-7613(00)80119-3).
- Takeuchi, O., T. Kawai, et al. (2001). “Discrimination of bacterial lipoproteins by Toll-like receptor 6”. In: *International Immunology* 13.7, pp. 933–940. ISSN: 0953-8178. DOI: [10.1093/intimm/13.7.933](https://doi.org/10.1093/intimm/13.7.933).
- Takeuchi, O., S. Sato, et al. (2002). “Cutting Edge: Role of Toll-Like Receptor 1 in Mediating Immune Response to Microbial Lipoproteins1”. In: *The Journal of Immunology* 169.1, pp. 10–14. ISSN: 0022-1767. DOI: [10.4049/jimmunol.169.1.10](https://doi.org/10.4049/jimmunol.169.1.10).

- Tenthorey, J. L., M. Emerman, and H. S. Malik (2022). “Evolutionary Landscapes of Host-Virus Arms Races”. In: *Annual Review of Immunology* 40.1. PMID: 35080919, pp. 271–294. DOI: [10.1146/annurev-immunol-072621-084422](https://doi.org/10.1146/annurev-immunol-072621-084422).
- Tsujimoto, Y. (1998). “Role of Bcl-2 family proteins in apoptosis: apoptosomes or mitochondria?” In: *Genes to Cells* 3.11, pp. 697–707. DOI: <https://doi.org/10.1046/j.1365-2443.1998.00223.x>.
- Uggenti, C. et al. (2020). “cGAS-mediated induction of type I interferon due to inborn errors of histone pre-mRNA processing”. In: *Nature Genetics* 52.12, pp. 1364–1372. DOI: [10.1038/s41588-020-00737-3](https://doi.org/10.1038/s41588-020-00737-3).
- Unterholzner, L. et al. (2010). “IFI16 is an innate immune sensor for intracellular DNA”. In: *Nature Immunology* 11.11, pp. 997–1004. DOI: [10.1038/ni.1932](https://doi.org/10.1038/ni.1932).
- Van Opdenbosch, N. and M. Lamkanfi (2019). “Caspases in Cell Death, Inflammation, and Disease.” eng. In: *Immunity* 50.6, pp. 1352–1364. ISSN: 1097-4180 (Electronic); 1074-7613 (Print); 1074-7613 (Linking). DOI: [10.1016/j.immuni.2019.05.020](https://doi.org/10.1016/j.immuni.2019.05.020).
- Vance, R. E. (2015). “The NAIP/NLRC4 inflammasomes.” eng. In: *Curr Opin Immunol* 32, pp. 84–89. ISSN: 1879-0372 (Electronic); 0952-7915 (Print); 0952-7915 (Linking). DOI: [10.1016/j.coi.2015.01.010](https://doi.org/10.1016/j.coi.2015.01.010).
- (2010). “Immunology Taught by Bacteria”. In: *Journal of Clinical Immunology* 30.4, pp. 507–511. DOI: [10.1007/s10875-010-9389-2](https://doi.org/10.1007/s10875-010-9389-2).
- Victoria, G. D. et al. (2010). “Germinal center dynamics revealed by multiphoton microscopy with a photoactivatable fluorescent reporter.” eng. In: *Cell* 143.4, pp. 592–605. ISSN: 1097-4172 (Electronic); 0092-8674 (Print); 0092-8674 (Linking). DOI: [10.1016/j.cell.2010.10.032](https://doi.org/10.1016/j.cell.2010.10.032).
- Vladimer, G. I. et al. (2012). “The NLRP12 inflammasome recognizes *Yersinia pestis*.” eng. In: *Immunity* 37.1, pp. 96–107. ISSN: 1097-4180 (Electronic); 1074-7613 (Print); 1074-7613 (Linking). DOI: [10.1016/j.immuni.2012.07.006](https://doi.org/10.1016/j.immuni.2012.07.006).
- Wang, C. et al. (2001). “TAK1 is a ubiquitin-dependent kinase of MKK and IKK”. In: *Nature* 412.6844, pp. 346–351. DOI: [10.1038/35085597](https://doi.org/10.1038/35085597).
- Wang, J. Y. and J. A. Doudna (2023). “CRISPR technology: A decade of genome editing is only the beginning”. In: *Science* 379.6629, eadd8643. DOI: [10.1126/science.add8643](https://doi.org/10.1126/science.add8643).
- Wang, Q. et al. (2021). “CARD8 is an inflammasome sensor for HIV-1 protease activity”. In: *Science* 371.6535, eabe1707. DOI: [10.1126/science.abe1707](https://doi.org/10.1126/science.abe1707).
- Wang, Y. et al. (2017). “Chemotherapy drugs induce pyroptosis through caspase-3 cleavage of a gasdermin.” eng. In: *Nature* 547.7661, pp. 99–103. ISSN: 1476-4687 (Electronic); 0028-0836 (Linking). DOI: [10.1038/nature22393](https://doi.org/10.1038/nature22393).

- Warburg, O., K. Posener, and E. Negelein (1924). “Über den Stoffwechsel der Tumoren”. In: *Biochemische Zeitschrift* 152.1, pp. 319–344.
- Watson, J. D. and F. H. C. Crick (1953). “Molecular Structure of Nucleic Acids: A Structure for Deoxyribose Nucleic Acid”. In: *Nature* 171.4356, pp. 737–738. DOI: [10.1038/171737a0](https://doi.org/10.1038/171737a0).
- Wein, T. and R. Sorek (2022). “Bacterial origins of human cell-autonomous innate immune mechanisms.” eng. In: *Nat Rev Immunol* 22.10, pp. 629–638. ISSN: 1474-1741 (Electronic); 1474-1733 (Linking). DOI: [10.1038/s41577-022-00705-4](https://doi.org/10.1038/s41577-022-00705-4).
- Weinlich, R., A. Oberst, H. M. Beere, and D. R. Green (2017). “Necroptosis in development, inflammation and disease”. In: *Nature Reviews Molecular Cell Biology* 18.2, pp. 127–136. DOI: [10.1038/nrm.2016.149](https://doi.org/10.1038/nrm.2016.149).
- Wiedenheft, B., S. H. Sternberg, and J. A. Doudna (2012). “RNA-guided genetic silencing systems in bacteria and archaea”. In: *Nature* 482.7385, pp. 331–338. DOI: [10.1038/nature10886](https://doi.org/10.1038/nature10886).
- Wright, E. K. et al. (2003). “Naip5 affects host susceptibility to the intracellular pathogen *Legionella pneumophila*.” eng. In: *Curr Biol* 13.1, pp. 27–36. ISSN: 0960-9822 (Print); 0960-9822 (Linking). DOI: [10.1016/s0960-9822\(02\)01359-3](https://doi.org/10.1016/s0960-9822(02)01359-3).
- Wu, B. et al. (2013). “Structural basis for dsRNA recognition, filament formation, and antiviral signal activation by MDA5.” eng. In: *Cell* 152.1-2, pp. 276–289. ISSN: 1097-4172 (Electronic); 0092-8674 (Linking). DOI: [10.1016/j.cell.2012.11.048](https://doi.org/10.1016/j.cell.2012.11.048).
- Wu, J. et al. (2013). “Cyclic GMP-AMP is an endogenous second messenger in innate immune signaling by cytosolic DNA.” eng. In: *Science* 339.6121, pp. 826–830. ISSN: 1095-9203 (Electronic); 0036-8075 (Print); 0036-8075 (Linking). DOI: [10.1126/science.1229963](https://doi.org/10.1126/science.1229963).
- Xia, S. et al. (2021). “Gasdermin D pore structure reveals preferential release of mature interleukin-1”. In: *Nature* 593.7860, pp. 607–611. DOI: [10.1038/s41586-021-03478-3](https://doi.org/10.1038/s41586-021-03478-3).
- Xiao, L., V. G. Magupalli, and H. Wu (2023). “Cryo-EM structures of the active NLRP3 inflammasome disc.” eng. In: *Nature* 613.7944, pp. 595–600. ISSN: 1476-4687 (Electronic); 0028-0836 (Print); 0028-0836 (Linking). DOI: [10.1038/s41586-022-05570-8](https://doi.org/10.1038/s41586-022-05570-8).
- Xu, H. et al. (2014). “Innate immune sensing of bacterial modifications of Rho GTPases by the Pyrin inflammasome”. In: *Nature* 513.7517, pp. 237–241. DOI: [10.1038/nature13449](https://doi.org/10.1038/nature13449).
- Yan, X. et al. (2021). “High-content imaging-based pooled CRISPR screens in mammalian cells.” eng. In: *J Cell Biol* 220.2. ISSN: 1540-8140 (Electronic); 0021-9525 (Print); 0021-9525 (Linking). DOI: [10.1083/jcb.202008158](https://doi.org/10.1083/jcb.202008158).

- Yarovinsky, F. et al. (2005). “TLR11 Activation of Dendritic Cells by a Protozoan Profilin-Like Protein”. In: *Science* 308.5728, pp. 1626–1629. DOI: [10.1126/science.1109893](https://doi.org/10.1126/science.1109893).
- Zaver, S. A. and J. J. Woodward (2020). “Cyclic dinucleotides at the forefront of innate immunity.” eng. In: *Curr Opin Cell Biol* 63, pp. 49–56. ISSN: 1879-0410 (Electronic); 0955-0674 (Print); 0955-0674 (Linking). DOI: [10.1016/j.ceb.2019.12.004](https://doi.org/10.1016/j.ceb.2019.12.004).
- Zetsche, B. et al. (2015). “Cpf1 is a single RNA-guided endonuclease of a class 2 CRISPR-Cas system.” eng. In: *Cell* 163.3, pp. 759–771. ISSN: 1097-4172 (Electronic); 0092-8674 (Print); 0092-8674 (Linking). DOI: [10.1016/j.cell.2015.09.038](https://doi.org/10.1016/j.cell.2015.09.038).
- Zewinger, S. et al. (2020). “Apolipoprotein C3 induces inflammation and organ damage by alternative inflammasome activation.” eng. In: *Nat Immunol* 21.1, pp. 30–41. ISSN: 1529-2916 (Electronic); 1529-2908 (Linking). DOI: [10.1038/s41590-019-0548-1](https://doi.org/10.1038/s41590-019-0548-1).
- Zhang, L. et al. (2015). “Cryo-EM structure of the activated NAIP2-NLRC4 inflammasome reveals nucleated polymerization”. In: *Science* 350.6259, pp. 404–409. DOI: [10.1126/science.aac5789](https://doi.org/10.1126/science.aac5789).
- Zhang, T., C. Yin, D. F. Boyd, et al. (2020). “Influenza Virus Z-RNAs Induce ZBP1-Mediated Necroptosis”. In: *Cell* 180.6, 1115–1129.e13. DOI: [10.1016/j.cell.2020.02.050](https://doi.org/10.1016/j.cell.2020.02.050).
- Zhang, T., C. Yin, A. Fedorov, et al. (2022). “ADAR1 masks the cancer immunotherapeutic promise of ZBP1-driven necroptosis”. In: *Nature* 606.7914, pp. 594–602. DOI: [10.1038/s41586-022-04753-7](https://doi.org/10.1038/s41586-022-04753-7).
- Zhao, B. et al. (2020). “The molecular basis of tight nuclear tethering and inactivation of cGAS.” eng. In: *Nature* 587.7835, pp. 673–677. ISSN: 1476-4687 (Electronic); 0028-0836 (Print); 0028-0836 (Linking). DOI: [10.1038/s41586-020-2749-z](https://doi.org/10.1038/s41586-020-2749-z).
- Zhao, Y. et al. (2011). “The NLRC4 inflammasome receptors for bacterial flagellin and type III secretion apparatus”. In: *Nature* 477.7366, pp. 596–600. DOI: [10.1038/nature10510](https://doi.org/10.1038/nature10510).
- Zheng, D. et al. (2023). “Epithelial Nlrp10 inflammasome mediates protection against intestinal autoinflammation”. In: *Nature Immunology* 24.4, pp. 585–594. DOI: [10.1038/s41590-023-01450-z](https://doi.org/10.1038/s41590-023-01450-z).
- Zhou, R., A. S. Yazdi, P. Menu, and J. Tschopp (2011). “A role for mitochondria in NLRP3 inflammasome activation”. In: *Nature* 469.7329, pp. 221–225. DOI: [10.1038/nature09663](https://doi.org/10.1038/nature09663).